Low dimensional electron systems out of equilibrium

im Fachbereich Physik
der Freien Universität Berlin
eingereichte

Dissertation

von

Torsten Karzig

16. Mai 2012

Erstgutachter (Betreuer):	Prof. Felix von Oppen, PhD
Zweitgutachter:	Prof. Dr. Piet W. Brouwer
Disputationstermin:	9. Juli 2012

Zusammenfassung

Jüngste experimentelle Fortschritte in der Herstellung von Nanostrukturen werfen vermehrt Fragen zum Nichtgleichgewichtsverhalten niedrigdimensionaler Systeme auf. Von besonderem Interesse sind dabei die stark wechselwirkenden eindimensionalen Elektronensysteme, deren Physik jenseits des thermischen Gleichgewichts man erst langsam zu verstehen beginnt. Die vorliegende Arbeit trägt zu diesem Verständnis bei und diskutiert grundlegende Elementarprozesse in der Nichtgleichgewichtsphysik eindimensionaler Elektronensysteme.

Wenn ein niederenergetisches Elektron in eine eindimensionale Luttingerflüssigkeit tunnelt, werden seine Ladung und Energie in gegenläufige Anregungen aufgeteilt. In dieser Doktorarbeit wird die bisher noch nicht verstandene Energieaufteilung untersucht. Es stellte sich dabei heraus, dass sich Ladung und Energie gänzlich unabhängig voneinander aufteilen und sich sogar gegenläufig ausbreiten können. Ein weiterer wichtiger Unterschied besteht in ihrer experimentellen Zugänglichkeit. Im Gegensatz zur Ladung kann die Energieaufteilung in Gleichstromexperimenten nachgewiesen werden und wir schlagen experimentelle Geometrien zur Steuerung und Messung der Energieaufteilung in eindimensionalen Systemen vor.

Bei höheren Anregungsenergien wird es notwendig den Krümmungseffekt der Elektronendispersion mit in Betracht zu ziehen. Ein weiterer Teil der vorliegenden Arbeit diskutiert die Auswirkung von krümmungsinduzierten Dreiteilchenstreuprozessen auf die Relaxation in Quantendrähten. Dies ist insbesondere deshalb hochinteressant, weil das Standardmodell eindimensionaler Systeme (Luttingermodel) integrabel ist und somit keine Thermalisierung zulässt. In einer wohldefinierten Störungstheorie jenseits des Luttingermodels bestimmt diese Arbeit die Energierelaxationsraten dieser Dreiteilchenstreuprozesse. Dabei stellt sich heraus, dass der Elektronenspin und die langreichweitige Coulombwechselwirkung von zentraler Wichtigkeit für die Relaxation sind. Unter Betrachtung dieser liefern wir eine quantitative Beschreibung eines kürzlich durchgeführten Experiments.

Im weiteren Verlauf der Arbeit werden die Auswirkungen der Dreiteilchenstreuprozesse auf die Energierelaxation in Quanten-Hall Randzuständen untersucht. Dabei wird insbesondere der Effekt einer wechselwirkungsinduzierten Randrekonstruktion betrachtet. Letztere führt zu einer Beschleunigung der Energierelaxation, die insbesondere dann stark ausgeprägt ist, wenn die Rekonstruktion zusätzliche gegenläufige Randzustände erzeugt.

Im abschließenden Teil der Arbeit wird ein weiteres System untersucht, bei dem Nichtgleichgewichtseffekte eine entscheidende Rolle spielen. Die sogenannten nanoelektromechanischen Systeme weisen eine Kopplung von mechanischen und elektronischen Freiheitsgraden auf. Ein elektrischer Strom kann somit die mechanische Bewegung beeinflussen, was eine Reihe von interessanten Anwendungen ermöglicht. Vorangehende theoretische Untersuchungen mit Hilfe von Nichtgleichgewichts-Greenfunktionen haben gezeigt, dass sich die strominduzierten Kräfte letztendlich durch intuitive Streumatrixausdrücke beschreiben lassen. Diese Arbeit gibt nun tiefere Einblicke in diesen Zusammenhang und liefert eine vollständig streutheoretische Beschreibung der strominduzierten Kräfte.

Abstract

Recent advances of experimental nanofabrication techniques draw increasing attention to the non-equilibrium behavior of low dimensional systems. Of particular interest are the strongly interacting one dimensional systems whose description in out of equilibrium situations remains a theoretical challenge. This thesis contributes to the understanding of important elementary processes in the non-equilibrium physics of one dimensional electron systems.

Tunneling of an electron into a Luttinger liquid leads to partitioning of its charge and energy into counter-propagating modes. This thesis studies the partitioning of the energy which had previously remained unexplored. It turns out that energy partitioning is essentially independent of the charge partitioning and one can even reach conditions such that energy and charge propagate in opposite directions. Another important difference is their experimental accessibility. In contrast to the charge, energy partitioning provides a measurable characteristic of the tunneling process even in dc setups and we propose experimental geometries that allow for tuning and detecting energy partitioning.

At higher excitation energies it becomes necessary to include curvature effects of the electron dispersion. Another part of this thesis discusses the consequences of curvature induced three-body collisions on the relaxation in quantum wires. This is particularly interesting due to the integrability of the Luttinger model which does not allow for thermalization within this paradigm of one dimensional systems. In this thesis we derive energy relaxation rates due to three-body processes beyond the Luttinger model within a well-defined perturbative approach. It turns out that the electron spin and the long range Coulomb interaction are important ingredients for a quantitative description of recent experiments which we provide in this thesis.

Furthermore, we study the influence of three-body collisions on the energy relaxation in integer quantum Hall edge states. We specifically address different interaction induced edge reconstruction scenarios and find that edge reconstruction strongly enhances the energy relaxation. This is particularly pronounced when the reconstruction creates additional counter-propagating modes.

Finally, we discuss another system which is crucially controlled by non-equilibrium effects. The so called nanoelectromechanical systems show a coupling between the electronic and mechanical degrees of freedom. The electron current can thus influence the mechanical motion which leads to a number of interesting applications. Previous theoretical studies on the basis of non-equilibrium Green's functions showed that these current induced forces can be expressed in terms of intuitive scattering matrix expressions. This thesis sheds considerable light on this observation by providing a much more satisfactory and concise derivation of the scattering theory of current induced forces.

Contents

1 Introduction

> The process of "model-building", essentially that of discarding all but essentials and focusing on a model simple enough to do the job but not too hard to see all the way through, is possibly the least understood of all the functions of a theoretical physicist.
>
> P. W. Anderson, *"BCS" and Me*, More and Different (2011)

When it comes to the problem of understanding a given system, a well-built minimal model can be much more powerful than a description which aims to be as accurate as possible. This curiosity driven search for an explanation of certain aspects of nature is fascinating and important in its own right. Moreover, an understanding of relevant mechanisms can be a promising starting point for designing new systems with desired properties.

The main challenge for "seeing through" the behavior of a many-body system is to find an effective way of dealing with the interactions between the vast number of (typically 10^{23}) particles. One of our most powerful and intuitive tools for this task is Landau's Fermi liquid theory [Landau (1957)]. It states that, despite the interactions between the electrons, the low energy excitations can be seen as almost free quasi-particles. This allows us to think in an intuitive free particle picture and explains the surprising success of the non interacting electron gas model for the description of metals. The power of the Fermi liquid paradigm is its wide applicability (*e.g.* to essentially all metals). This in turn also stimulates the search for the "rare exceptions" as non-Fermi liquid behavior is often accompanied with new and exciting physics.

One particularly remarkable example is given by the Luttinger model[1] [Luttinger (1963)], describing electrons in one spatial dimension with a linear dispersion. The ground state of this model is a strongly correlated state, which is not compatible with a description in terms of almost free fermionic quasi-particles. In addition the Luttinger model is also an exception in the sense that it is one of the very few examples that allow for an *exact* solution of an *interacting* many-body problem. The latter is possible by mapping the original interacting fermionic system onto that of noninteracting bosons, which describe collective density wave excitations (plasmons).

[1] Also known as Tomonaga-Luttinger model due to related work by Tomonaga (1950).

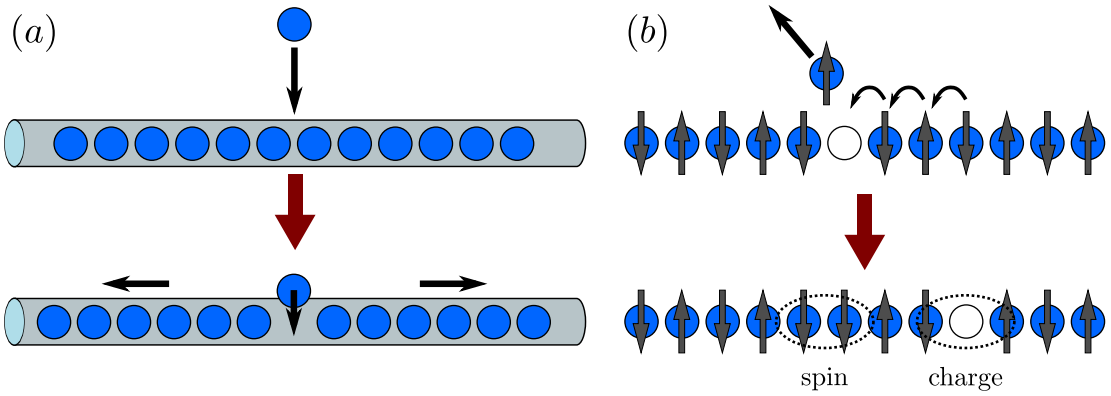

Figure 1.1: Illustration of the peculiarities of one dimensional systems. (a) Zero bias anomaly in a quantum wire. Tunneling is strongly suppressed because it requires a shift of all particles left and right from the injection point. (b) Spin charge separation in an antiferromagnetic chain. Removing a particle from the system creates a hole excitation. Subsequent electron hopping leads to a splitting into separate spin and charge excitations.

Luttinger introduced his model as a mere proof of principle that interactions can lead to a break down of Fermi liquid theory. Interestingly he noted at the beginning of his famous paper:

> "The model is quite unrealistic for two reasons:
> it is one-dimensional and the fermions are massless."

As it turned out, this assessment was premature and the implications of his model were far reaching. In fact, due to its exceptional combination of complexity (strong correlations) and simplicity (exact solubility) Luttinger's model received much theoretical attention. The result is known as Luttinger liquid theory [Haldane (1981)], which describes the low energy behavior of a wide variety of one dimensional systems. Haldane argued that the free bosons of the Luttinger model are essential for the Luttinger liquid in much the same sense as the free electrons are for the Fermi liquid.

A peculiar consequence of the strong correlations in one dimensional systems is that low energy tunneling into a Luttinger liquid is strongly suppressed and the probability of entering the system vanishes as a power law for small bias voltages. This so called zero bias anomaly is caused by the difficulty that accommodating a new particle in a one dimensional system requires to displace essentially all the other particles [see Fig. 1.1a]. Another hallmark of the strong interactions is the separation of spin and charge degrees of freedom. While spin and charge are tied together in a single electron picture, their collective dynamics are completely independent from each other in a Luttinger liquid [see Fig. 1.1b]. In a similar sense it is possible to effectively break up the elementary charge of the electron and to introduce fractional excitations [Pham *et al.* (2000)].

Modern nanofabrication techniques give access to one dimensional systems and have led to an active and still ongoing experimental search for their remarkable properties.

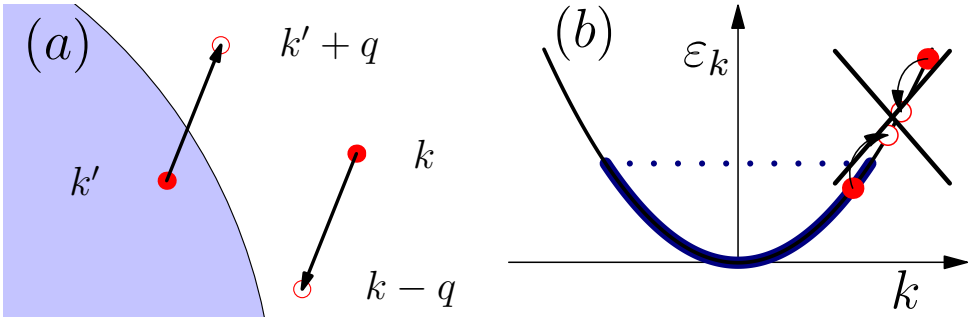

Figure 1.2: Two-body relaxation processes. (a) Typical relaxation process in two or three dimensions by exciting a particle out of the Fermi sea. (b) Two-body relaxation processes are not allowed in one dimension due to a finite curvature of the dispersion.

In this way, it was possible to observe the zero bias anomaly for tunneling into carbon nanotubes [Yao *et al.* (1999); Bockrath *et al.* (1999)], engineered quantum wires [Auslaender *et al.* (2000); Tserkovnyak *et al.* (2003)] and fractional quantum Hall edge states [Chang *et al.* (1996); Grayson *et al.* (1998)]. Spectroscopic measurements provide evidence for spin charge separation in one dimensional $SrCuO_2$ [Kim *et al.* (1996, 2006)], quantum wires [Auslaender *et al.* (2002, 2005); Jompol *et al.* (2009)] and even single-atom gold chains [Segovia *et al.* (1999)].

This experimental availability is drawing more and more attention to the out of equilibrium behavior of these peculiar systems. A theoretical description of non-equilibrium effects of strongly interacting electrons is however highly nontrivial. This becomes already evident in the fundamental question of how a non-equilibrium state relaxes towards thermal equilibrium. The integrable Luttinger model does not provide a mechanism for such thermalization. The reason lies in the lack of interaction between the plasmons which leads to infinite lifetimes of the non-equilibrium state. Addressing relaxation in one dimensional systems requires therefore new theoretical concepts and is an important part of the active and exciting study of out of equilibrium effects in low dimensional systems.

This thesis aims to contribute to the understanding of the non-equilibrium physics of low dimensional systems. The main focus will be on new implications of the Luttinger model in tunneling processes as well as the necessity to go beyond its approximations to describe thermalization in one dimensional systems.

1.1 Relaxation in quantum wires

The unusual relaxation physics in one dimensional systems already shows up in the single particle picture. In higher dimensions, an excited quasi-particle can easily relax towards the Fermi surface by transferring part of its excess energy and momentum to a particle in the Fermi sea [Fig. 1.2a]. This relaxation process is one of the key ingredients of Fermi liquid theory and leads to the famous quasi-particle relaxation rate $1/\tau \propto \varepsilon^2$, where ε is

the excitation energy. In one dimension, such a two-body process is forbidden by energy and momentum conservation [Fig. 1.2b]. Due to the finite curvature, a relaxing particle loses more energy per momentum than the particle from the Fermi sea gains. The only allowed processes have either zero momentum transfer or exchange the involved particles, which does not contribute to the relaxation of the distribution function. This problem is circumvented in higher dimensions via the additional angular degrees of freedom.

It is already clear from this simple argument that relaxation in one dimensional systems is not as effective as in higher dimensions. Moreover, in view of the integrability of the Luttinger model one could even assume the complete absence of thermalization in one dimensional systems. This emphasizes the importance of a series of recent experiments that were able to address relaxation in one dimensional systems.

The key observable in most of these experiments is the non-equilibrium energy distribution function, which could be measured in tunneling spectroscopies of carbon nanotubes [Chen *et al.* (2009)] and quantum Hall edge states [Altimiras *et al.* (2010a,b); le Sueur *et al.* (2010)]. Interestingly, these experiments see clear signs of relaxation and equilibration by studying the evolution of an out of equilibrium excitation of the distribution function to its equilibrium form.

One possible starting point for a theoretical understanding of the underlying relaxation mechanisms is to include curvature effects of the electron dispersion, that break the Luttinger model's integrability. Parts of this thesis show that curvature effects can contribute substantially to the relaxation in quantum wires (chapter 4) and quantum Hall edge states (chapter 5).

In the following we will discuss an inspiring experiment by Barak *et al.* (2010b) that underlines the importance of these curvature effects in the relaxation of quantum wires.

1.1.1 Momentum resolved tunneling spectroscopy

A well-established method to produce extremely clean and atomically precise quantum wires is the so called cleaved edge overgrowth (CEO) method [Pfeiffer *et al.* (1993)]. These wires have a large mean free path ($> 10\,\mu$m) and subband spacing (20 meV) [Yacoby *et al.* (1996)] and are therefore perfectly suited to study the behavior of ballistic one dimensional systems.

The starting point for the fabrication of CEO wires is a two dimensional electron gas (2DEG) which can form in a AlGaAs-GaAs heterostructure [see Fig. 1.3]. The sample is then cleaved with atomic precision perpendicular to the 2DEG and a doped layer of AlGaAs is grown on the cleaved surface. For suitable doping and gate voltages a one dimensional wire forms at the edge of the 2DEG. Maximal confinement is reached by applying a negative voltage to the top gate (which depletes most of the 2DEG) and a strong positive voltage at the side gate which collects all the electrons at the cleaved edge.

Momentum resolved tunneling spectroscopy relies on a similarly produced double quantum wire setup [Fig. 1.4]. With depletion top gates, a part of the upper wire is

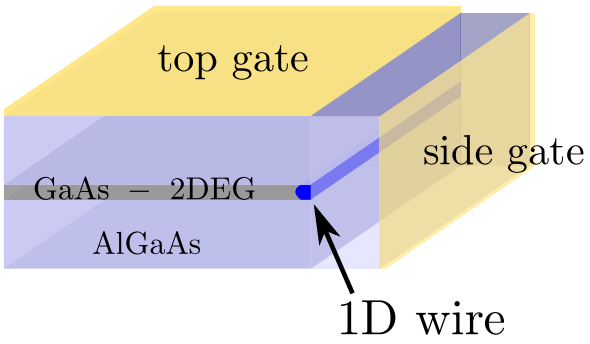

Figure 1.3: Schematic view of the CEO method. The quantum wire (dark blue) forms at the intersection of the 2DEG and the cleaved edge.

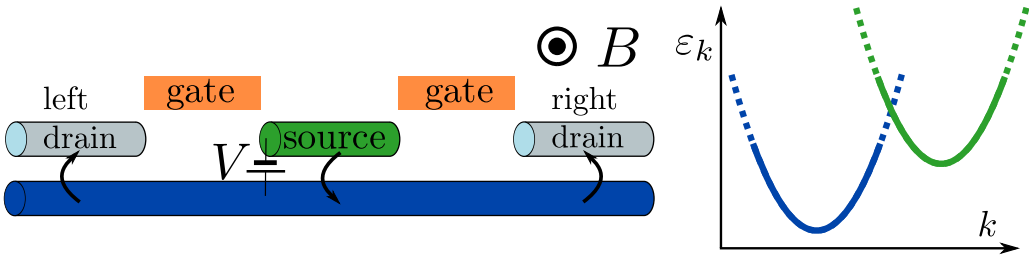

Figure 1.4: (a) Double CEO wire setup of the experiment by Barak *et al.* (2010b). The dispersions of the upper (green) and lower (blue) wire are shifted by magnetic and electric fields. (b) shows the case of injection of hot particles into the lower wire.

separated and used as a source electrode for tunneling into the lower wire. In contrast to local tunneling experiments, the length of this tunneling source is chosen to be long enough (a few μm) that the tunneling can be considered as momentum conserving. By applying a voltage V between the upper and lower wires, the dispersions of the two wires can be shifted by the energy eV relative to each other. With a perpendicular magnetic field B [see Fig. 1.4], the dispersions can also be shifted in momentum by $k = eBd/\hbar$, where d is the distance between the two wires. The complete control over the way the two dispersions overlap allows for the injection or extraction of electrons with specific energy and momentum. This makes momentum resolved tunneling spectroscopies an ideal testbed for the study of excitations in one dimensional electron systems.

Barak *et al.* (2010b) used this setup to address the relaxation of hot particles and holes injected into the quantum wire. They observed that injecting a hot right-moving particle at energy ε above the Fermi energy ε_F leads to an increased number of hot particles at intermediate energies (*e.g.* $\sim \varepsilon_F + \varepsilon/2$) in the right drain. This is a clear signature for the relaxation of the initial hot particle by exciting additional particles from the Fermi sea. Interestingly, there was no similar effect for the injection of hot hole excitations or cold particle and hole excitations injected very close to the Fermi energy. Thus, the experiment implies a relaxation of hot particles into co-propagating excitations while the corresponding holes do not relax on the experimentally observable length scale of a few

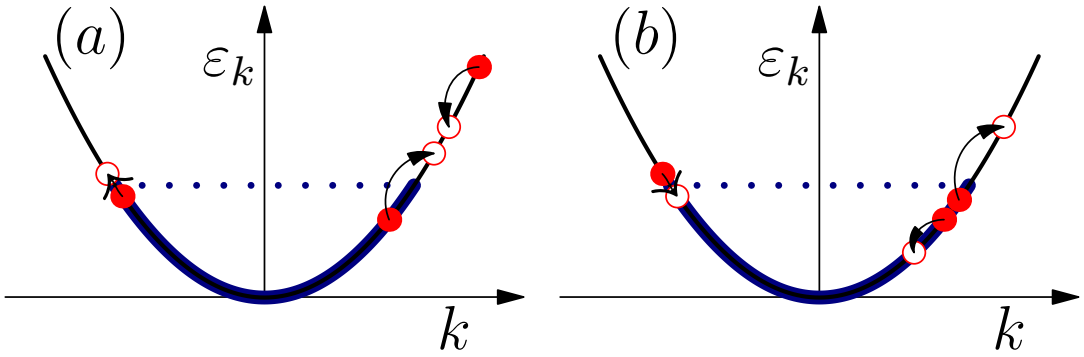

Figure 1.5: Possible three-body process for the relaxation of hot particle (a) and hole (b) excitations.

micrometers.

As we will show in the following, this strong particle-hole asymmetry follows naturally from relaxation effects that include the finite curvature of the electron dispersion.

1.1.2 Relaxation due to curvature effects of the electron dispersion

Already Haldane (1981) realized that a finite curvature introduces interactions between the plasmonic excitations causing them to decay over time. Although this has similarities with the quasi-particles of a Fermi liquid, assigning a plasmon lifetime is highly nontrivial because perturbative approaches run into divergences [Samokhin (1998)]. The reason is that although their interaction becomes weak at low energies, the plasmon velocities become more and more equal, making them interact for much longer times. Thus, developing a perturbative description of curvature effects within the bosonization language is a delicate task [Aristov (2007); Pereira *et al.* (2006, 2007); Teber (2007)].

In order to avoid these difficulties it can be favorable to go back to the fermionic picture when dealing with curvature effects. Indeed, the finite velocity difference Δv of the hot electron and those in the Fermi sea allows for a well-defined single particle picture. In line with the Born approximation of quantum mechanics [Landau and Lifshitz (1977)] the interaction can be treated perturbatively in the limit $V_0 \ll \hbar \Delta v$, where V_0 is the $q = 0$ component of the Fourier transformed interaction potential.

As mentioned above, the corresponding relaxation mechanisms are however quite different from their higher dimensional counterparts due to the absence of two-body processes. As first pointed out by Lunde *et al.* (2007), the curvature induced excess energy of a relaxing hot particle requires the excitation of an additional third particle to fix the energy and momentum conservation laws [Fig. 1.5a].

Note that these three-body processes are indeed strongly particle-hole asymmetric for low temperatures. Since the relaxing hole has a lower velocity than the particles at the Fermi surface that it excites, the curvature induced energy mismatch of a two-particle process has the opposite sign compared to the particle relaxation [see Fig. 1.5b]. Instead of

exciting, the hole relaxation therefore needs to annihilate a counter-propagating particle-hole pair which is impossible at $T = 0$.

Although the existence of this unusual relaxation process is of great conceptual importance one may ask whether it has a practical significance on the experimentally observable relaxation in one dimensional systems. In view of first calculations which resulted in very slow relaxation rates $1/\tau \propto \varepsilon^8$ [Khodas *et al.* (2007)] it was tempting to doubt this significance. However these slow relaxation rates where calculated under the additional assumption of spinless electrons with only short ranged interactions. Chapter 4 of this thesis will focus on the fact that taking into account the electron spin and long range Coulomb interaction is crucial for much faster relaxation rates $1/\tau \propto \varepsilon^2$ [Karzig *et al.* (2010)] which allow us to explain the experiment of Barak *et al.* (2010b) quantitatively.

1.1.3 Alternative approaches for relaxation in one dimensional systems

Although, three-body collisions seem to capture the relaxation of hot particles in clean quantum wires, they might not give the leading contribution in other experimental setups. The above mentioned experimental observation of relaxation indeed led to a flurry of different theoretical proposals. It is therefore beneficial to acquire an overview over other possible sources of relaxation in one dimensional systems.

One class of proposals relies on introducing disorder and thus breaking the translational invariance of the system. Without momentum conservation two-particle relaxation processes are again possible. In the related problem of equilibration between two $\nu = 2$ quantum Hall edge states, Lunde *et al.* (2010) indeed used a perturbative two-body scattering approach to interpret the experimentally observed relaxation. On more general grounds Bagrets *et al.* (2008, 2009) showed in a non-equilibrium bosonization study that disorder introduces relaxation to the Luttinger model, yielding an energy relaxation length of the order of the transport mean free path.

A complementary approach to explain the experimentally observed relaxation of the non-equilibrium distribution function relies on dispersive effects of the plasmons [Kovrizhin and Chalker (2011a,b); Levkivskyi and Sukhorukov (2012)]. The dispersion of the plasmons is not necessarily completely linear. Unscreened Coulomb interactions for example lead to a logarithmic correction to the plasmon velocity. Different plasmon velocities then result in a broadening of the initial electron distribution. An injected non-equilibrium double step distribution function can thus change into a broader single step distribution, which might be interpreted experimentally as equilibration. Note however that purely dispersive effects will never lead to a thermal equilibrium distribution function because the lifetime of the non-equilibrium state is still infinite.

This emphasizes the conceptual importance of the effects of the curvature of the dispersion as they represent the only mechanism for true thermalization in translationally invariant systems. However, the above theories show that there exist a number of possible sources for the experimental observation of relaxation, which have to be checked on a

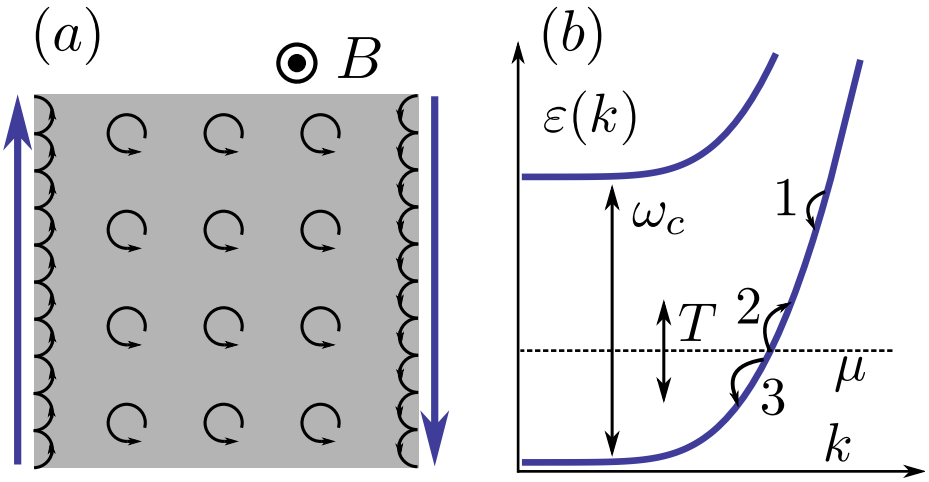

Figure 1.6: Quantum Hall edge states. (a) While the electrons in the bulk are localized, the quantum Hall edge exhibits propagating modes that can be understood in terms of skipping orbits at the sample's edge. (b) Typical dispersion at the edge of the sample, including a possible chiral three-body relaxation process.

case to case basis. As a general trend, three-body collisions will dominate the relaxation of ballistic systems at higher excitation energies.

1.2 Relaxation in quantum Hall edge states

A different class of one dimensional systems appears at the edge of two dimensional electron gases that show the quantum Hall effect [Halperin (1982)]. While the electrons in the bulk of the system are localized by a strong magnetic field, there exist chiral modes that propagate ballistically along the edge of the sample (see Fig 1.6a). It is a well-known fact that the charge transport of the edge modes leads to a quantized Hall conductance in units of e^2/h [v. Klitzing *et al.* (1980), see also the books by Prange and Girvin (1987); Sarma and Pinczuk (2008)]. However, charge transport measurements alone do not provide a full picture of quantum Hall edges.

A closer examination shows that interaction effects can lead to the emergence of neutral (possibly counter) propagating modes which only contribute to energy transport [Kane *et al.* (1994); Lee *et al.* (2007); Levin *et al.* (2007); Grosfeld and Das (2009)]. Measurements of thermal transport properties can therefore give valuable insights into the structure of the quantum Hall edge and have received much experimental attention recently. It was indeed possible to detect neutral edge modes in such measurements [Bid *et al.* (2010); Dolev *et al.* (2011); Altimiras *et al.* (2012)]. Interestingly, thermal transport experiments also show that electrons cool as they propagate along the edge [Granger *et al.* (2009)] which again leads to the question of relaxation and equilibration physics in these one dimensional systems.

A particularly direct observation of relaxation effects was possible in integer quantum Hall systems at Landau level filling factor $\nu = 2$ [Altimiras *et al.* (2010a,b); le Sueur *et al.* (2010)]. These systems host two co-propagating edge states. One of them is driven out of

equilibrium by mixing with a third mode at a quantum point contact. The resulting non-equilibrium distribution function is then probed downstream with a quantum-dot-based energy spectrometer. These experiments show that the initial non-equilibrium distribution relaxes to a stationary form which is close to a thermal distribution.

Motivated by these experimental observations chapter 5 of this thesis studies the effect of three-body collisions on the energy relaxation in integer quantum Hall edge states. The crucial difference to the processes in a quantum wire is that the chirality requires a relaxation process that only involves co-moving particles. For finite temperatures such a relaxation process is possible by exploiting the curvature of the dispersion close to the chemical potential μ [see Fig. 1.6b]. A hot particle (1) can then relax a small amount of its energy by exciting and annihilating a thermal particle-hole pair.

The study of relaxation processes in quantum Hall edge states is made even richer by possible interaction induced reconstruction effects of the edge. Indeed, the simple picture of a spin degenerate, strictly monotonic dispersion [Fig. 1.6b] only holds for a sharp edge [Halperin (1982)]. Smoother confinement potentials were predicted to cause a spin [Dempsey *et al.* (1993); Gelfand *et al.* (1994); Rijkels and Bauer (1994); Stoof and Bauer (1995); Barlas *et al.* (2011)] and charge [de C. Chamon and Wen (1994); Barlas *et al.* (2011)] reconstruction of the edge. Also recent experiments [Barak *et al.* (2010a); Deviatov *et al.* (2011)] point towards an important role of reconstruction effects in the quantum Hall edge.

Accordingly, chapter 5 focuses in particular on the consequences of the different edge reconstruction scenarios for the relaxation of hot electrons injected into quantum Hall edge states.

1.3 Energy and charge partitioning in Luttinger liquids

In the discussions above we considered a tunneling process as a simple source of hot particle excitations. This description only applies in the limit where curvature effects become important ($\hbar\Delta v \gg V_0$, see section 1.1.2). In the low energy regime however, the tunneling leads to a collective excitation of the Luttinger liquid. A full description of the resulting non-equilibrium state is quite complex and requires an out of equilibrium generalization of the bosonization technique [Gutman *et al.* (2010a)]. Chapter 3 of this thesis shows that it is even highly nontrivial to address the simple question of how the excess energy of the injected particle distributes over the system.

This question is inspired by the already known unusual behavior of the charge. Consider injecting a right-moving particle into a Luttinger liquid. The strong correlations then lead to a partitioning of its charge e into two parts $eQ_\pm = e(1 \pm K)/2$ (determined by the Luttinger parameter K) that travel in opposite directions [see Fig. 1.7]. This charge partitioning can be motivated by a relatively simple argument [Deshpande *et al.* (2010)].

The injected electron with momentum $k_F = mv_F$ will lead to excitations of the Luttinger liquid that distribute the charge. The crucial point is that the latter travel with a faster

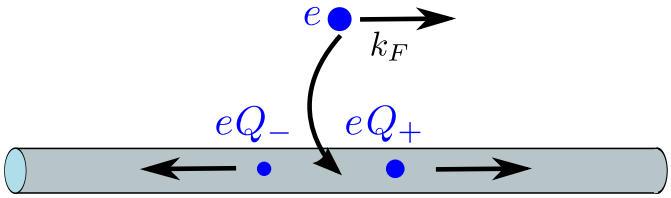

Figure 1.7: Schematic picture of charge partitioning.

velocity $c = v_F/K$ than the original particle [see Section 2.1]. Since the charge transport has to be accompanied by a corresponding mass transport we can use momentum conservation

$$mv_F = Q_+ mc - Q_- mc \tag{1.1}$$

as well as charge conservation ($Q_+ + Q_- = 1$) to determine

$$Q_\pm = \frac{1 \pm K}{2}. \tag{1.2}$$

The Luttinger parameter K varies from 1 (non-interacting) to 0 (infinitely strong interactions) for repulsive interactions. In the non-interacting case the charge would only move in the direction of the injected particle while it is equally distributed in the strongly interacting case.

Although the electron density in a solid is a continuous quantity, the splitting of the injected charge is often called charge fractionalization. The reason for this is the close connection to the fractional excitations [Pham *et al.* (2000)] of the Luttinger liquid. The electrons in the Luttinger model can be decomposed into right and left-moving eigenmodes and one can think of this as if a fraction of the electron is traveling to the right while another one travels to the left. The charge ratio between these fractions is also determined by the ratio Q_+/Q_- and one can interpret charge partitioning as a consequence of the fractionalization of the injected electron.[2]

The study of the corresponding energy partitioning is an important step to complete the understanding of the tunneling process and can also be valuable in the ongoing experimental verification of Luttinger liquid theory. In fact the energy partitioning might even be easier to detect than that of the charge. The reason for this is that the measuring contacts are not Luttinger liquids and that the backscattering at the contacts completely masks any charge partitioning effects in dc measurements. Thinking in the picture of fractionalized excitations, only "full" electrons can enter the weakly interacting contacts. This makes the charge partitioning ratio trivial such that injecting a right-mover into the Luttinger liquid leads to a single electron flowing out of the right contact. The problem of accessing the charge partitioning in dc experiments is the underlying reason why there are currently only indirect experimental signatures of charge partitioning [Steinberg *et al.*

[2]Note that the reverse statement that from the charge partitioning follows fractional behavior is in general not true.

(2008)].

This difficulty is already well-known in the context of conductance measurements. The dc conductance of a Luttinger liquid attached to leads is simply $2e^2/h$, independent of the interaction [Maslov and Stone (1995); Ponomarenko (1995); Safi and Schulz (1995)]. On the other hand, the interaction manifests itself in various thermal transport properties [Kane and Fisher (1996); Fazio *et al.* (1998); Gutman *et al.* (2009)] so that thermal conductance takes the K dependent value $G_T = \pi KT/3\left(1+K^2\right)$. Similarly, also the energy partitioning can be addressed directly by relatively simple spectroscopies and dc measurements.

The corresponding study of the partitioning of excess energies [Karzig *et al.* (2011)] will be discussed in chapter 3 of this thesis. In stark contrast with the Fermi liquid behavior, the energy will in general be partitioned into counter-propagating contributions whose ratio is determined by the interaction as well as the injected excess momentum and energy. With the large degree of control of momentum conserving tunneling experiments [see Section 1.1.1] it would therefore be possible to tune the energy partitioning ratio experimentally.

1.4 Current induced forces in nanoelectromechanical systems

Another area where non-equilibrium effects have recently played a prominent role is that of nanoelectromechanical systems [Craighead (2000); Roukes (2001)]. Beyond being interesting on their own right, these also provide a paradigm for systems in which the electronic degrees of freedom are coupled to other collective modes. A central question in this field concerns the forces exerted by the out of equilibrium electrons on the mechanical mode(s), as well as the backaction on the electronic transport. In chapter 6 of this thesis we address these questions for the case of quantum coherent transport within the framework of a scattering matrix approach to mesoscopic conductors.

For a theoretical description of nanoelectromechanical systems it is important to compare the relevant time scales of the electronic and mechanical motions. One possible limit can be realized in transport through molecular junctions [for a review see Galperin *et al.* (2007)], and considers electrons that stay much longer in the system than the inverse frequency of the mechanical vibrations. In this thesis we will address the opposite case where the mechanical motion is much slower than typical electronic time scales. This limit is well-suited to describe the collective mechanical vibration of nano- and mesoscopic systems. A prominent realization are suspended carbon nanotubes and recent experiments [Steele *et al.* (2009); Lassagne *et al.* (2009)] indeed show that current induced forces [see Fig. 1.8] have profound influences on these systems.

Specifically, these experiments observe that the electrons exert an average force on the nanotube that shifts its vibrational frequency. Moreover, a current flowing through the system leads to a dramatic change in the quality factor of the mechanical mode which is caused by damping forces. The fluctuation-dissipation theorem then also suggests the presence of fluctuating forces such that the equation of motion of the mechanical degree

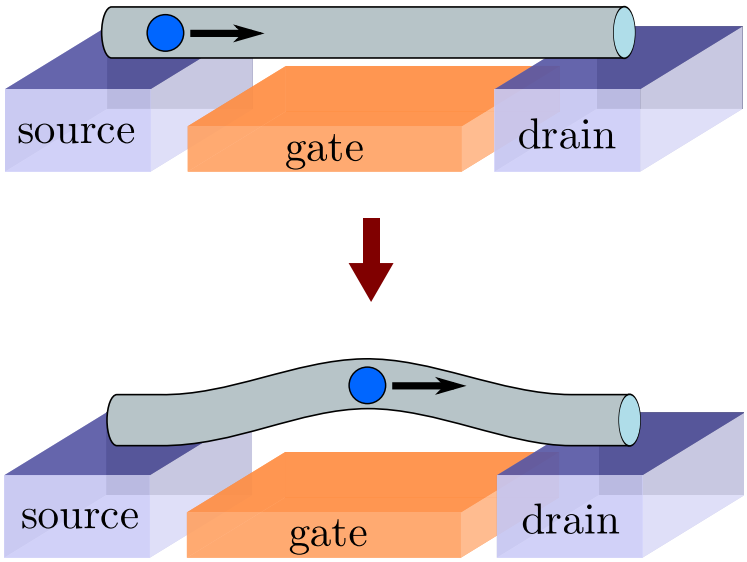

Figure 1.8: Schematic picture of a nanoelectromechanical system out of equilibrium. A charge traveling though a suspended wire is repelled by the electric field of a gate, which leads to a mechanical distortion of the wire.

of freedom X_α can be cast into a Langevin equation

$$M_\alpha \ddot{X}_\alpha + \frac{\partial U}{\partial X_\alpha} = F_\alpha^{(0)} - \sum_\beta \gamma_{\alpha\beta}\dot{X}_\beta + \xi_\alpha \,. \tag{1.3}$$

Here the left hand side of the equation describes the purely mechanical motion and the right hand side includes (from left to right) the average, damping, and fluctuating force that is exerted by the electrons. The corresponding dynamics is especially rich when considering multiple mechanical modes ($\alpha = 1, ..., N$) out of equilibrium [Lü *et al.* (2010); Bode *et al.* (2011, 2012)]. In this case, the electron current can lead to non conservative average forces. Moreover, the asymmetric part of the damping matrix $\gamma_{\alpha\beta}$ gives rise to Lorentz-like forces which stem from the electronic Berry phase [Berry and Robbins (1993)] and can cause cyclic motions of $\mathbf{X}$. Note that also the symmetric part of $\gamma_{\alpha\beta}$ can be qualitatively changed out of equilibrium such that it becomes negative and leads to the possibility of amplifying certain mechanical modes.

Theoretical studies of these forces applied Green's function approaches [Mozyrsky *et al.* (2006); Pistolesi *et al.* (2008); Lü *et al.* (2010)] as well as hybrid Green's functions/scattering theories that derive scattering matrix expressions within the Keldysh technique [Bode *et al.* (2011, 2012)]. The beauty of a scattering approach [*e.g.* the book by [Blanter (2010)] lies in its conceptual simplicity as transport can be described by the intuitive picture of reflection and transmission amplitudes of the electronic waves [Landauer (1957, 1970); Büttiker (1992)]. It also provides a powerful tool to use the symmetries of a system which directly determine the structure of the scattering matrix.

In this spirit it is highly desirable to obtain a scattering theory of current induced forces.

So far scattering descriptions of nanoelectromechanical systems were only applied to special cases [Kindermann and Beenakker (2002); Bennett *et al.* (2010, 2011)]. Chapter 6 of this thesis provides a direct derivation of the general scattering theory of nanoelectromechanical systems eliminating the need to derive this theory via Keldysh Green's functions.

Besides providing a streamlined and more satisfactory derivation of the expressions of Bode *et al.* (2011, 2012) the scattering approach also leads to additional insights into the underlying structure of the theory. In fact, we show that the scattering formalism gives a natural generalization of the well-known derivation of geometric magnetism [Berry and Robbins (1993)] to infinite (gapless) systems. The finite dwell time that an electron spends in the scattering region leads to a well-defined limit for an infinite quantum system which allows for a description of dissipative forces, exerted on the mechanical modes.

1.5 Outline

This thesis will be structured as follows. In chapter 2 we introduce the basic notions of the Luttinger model which represents the standard description of the low energy behavior of one dimensional systems. Building on this, chapter 3 discusses energy partitioning effects in tunneling into a Luttinger liquid. In the following we will then depart from the Luttinger model and address relaxation effects in quantum wires (chapter 4) and quantum Hall edges (chapter 5), which rely crucially on the nonlinearity of the electron dispersion.

Chapter 6 addresses the non-equilibrium behavior of nanoelectromechanical systems and provides a scattering theoretical description of current induced forces.

We conclude our findings in chapter 7 and provide an outlook to further interesting questions that are related to this thesis.

Throughout the main text of the thesis we will set the reduced Planck constant ($\hbar = 1$) and the Boltzmann constant ($k_B = 1$) to unity.

2 The Luttinger model

In this chapter we will discuss basic aspects of the Luttinger model and the bosonization technique which will be needed in the course of the thesis. The literature on Luttinger model is extensive [for reviews see *e.g.* Voit (1995); Giamarchi (2004); Giuliani and Vignale (2005)] and a complete derivation of all the required properties is not within the scope of this thesis. We will therefore concentrate on the central ideas and the properties that will be required in the remaining part of this thesis. The Luttinger model is motivated by the low energy behavior of one dimensional electrons. The latter is essentially controlled by a small region around the two Fermi points, where the electron dispersion is linear to leading order [see Fig. 2.1].

2.1 Luttinger model Hamiltonian

As a starting point we will discuss spinless electrons in one dimension. The corresponding Hamiltonian takes the form

$$H = H_0 + H_{\text{int}} \tag{2.1}$$

$$= \sum_k \varepsilon_k c_k^\dagger c_k + \frac{1}{2L} \sum_{k,k',q\neq 0} V_q c_{k+q}^\dagger c_{k'-q}^\dagger c_{k'} c_k \,, \tag{2.2}$$

where the $q = 0$ term is excluded because it cancels against the positive background in a charge neutral system. The mapping to the Luttinger model can now be performed by

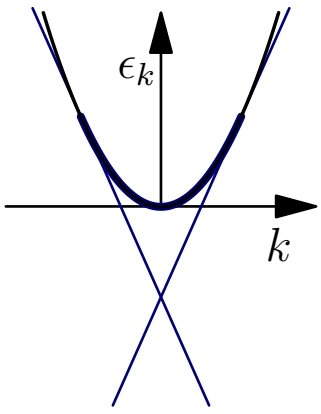

Figure 2.1: Comparison of the Luttinger model dispersion with that of non-interacting one dimensional electrons.

dividing the electrons into independent right and left-moving branches

$$c_k = \Theta(k)\, c_{kR} + \Theta(-k) c_{kL} \tag{2.3}$$

with linear dispersions ($\hbar = 1$)

$$\varepsilon_{k\tau} = v_F(\tau k - k_F)\ . \tag{2.4}$$

Here $\Theta(k)$ is the Heaviside step function and we used $\tau = +1, -1 \mathrel{\widehat{=}} R, L$ for brevity. By this seemingly harmless manipulation one introduces an infinite number of occupied states below the Fermi energy. Although these states do not alter the low energy physics they lead to divergences due to the infinite overall particle number. This problem is a generic feature of relativistic theories and can be circumvented by focusing on deviations from the "vacuum state" as already pointed out by Dirac (1930). In this case the vacuum state is a filled Fermi sea with occupation numbers $\langle c^\dagger_{k,\tau} c_{k,\tau}\rangle_0 = \Theta(k_F - \tau k)$ and one should only discuss the normal ordered Hamiltonian with respect to this vacuum.

Another consequence of the infinite number of particles is that the commutator of two density operators $\rho_{q,\tau} = \sum_k c^\dagger_{k-q,\tau} c_{k,\tau}$ with opposite values of q does not vanish. Interestingly this fact was overlooked by Luttinger (1963) as pointed out by Mattis and Lieb (1965) who provided the first correct solution of Luttinger's model. Indeed, by separating $\rho_{q,\tau}$ into normal ordered and vacuum parts one obtains the important relation

$$\left[\rho_{q,\tau}, \rho_{-q',\tau'}\right] = \frac{\tau L q}{2\pi} \delta_{qq'} \delta_{\tau\tau'}\ . \tag{2.5}$$

Thus, up to a prefactor the density operators obey bosonic commutation relations. This allows one to define boson creation and annihilation operators which take the form

$$b_q \;=\; \sqrt{\frac{2\pi}{L|q|}} \left(\Theta(q)\rho_{q,R} + \Theta(-q)\rho_{q,L}\right)\ . \tag{2.6}$$

It was shown in a beautiful proof by Haldane (1981) that this bosonic basis is complete and can therefore be used instead of the original Fermions. The great advantage of this bosonization is that the interaction part of the Hamiltonian is quadratic in the densities and therefore also in the newly introduced bosons. Moreover, one can also show that $b^\dagger_q(b_q)$ increases (decreases) the energy of an energy eigenstate of H_0 by $\hbar v_F|q|$. This leads to the remarkable result that also the kinetic energy is quadratic in the densities, a result which is true only for the linear dispersion. It is therefore possible to rewrite the complete Hamiltonian in a quadratic form of the boson operators (see Appendix A.1 for details)

$$H = \sum_{q\neq 0} \left[\left(v_F + \frac{V_1(q)}{2\pi}\right)|q| b^\dagger_q b_q + \frac{V_2(q)}{2\pi}|q| \left(b^\dagger_q b^\dagger_{-q} + b_{-q} b_q\right)\right]\ , \tag{2.7}$$

where $V_1(q)$ and $V_2(q)$ depend on the interaction V_q and can be taken as $V_1(q) = V_2(q) =$

$(V_0 - V_{2k_F})/2\pi$ in the case that the Coulomb interaction is screened at some scale and V_0 remains finite (see Appendix A.1).

The quadratic Hamiltonian can then be diagonalized by the canonical transformation

$$\begin{pmatrix} b_q \\ b_{-q}^\dagger \end{pmatrix} = \begin{pmatrix} \cosh\alpha_q & -\sinh\alpha_q \\ -\sinh\alpha_q & \cosh\alpha_q \end{pmatrix} \begin{pmatrix} \beta_q \\ \beta_{-q}^\dagger \end{pmatrix}, \tag{2.8}$$

to

$$H = \sum_{q\neq 0} c_q\,|q|\,\beta_q^\dagger\beta_q\,. \tag{2.9}$$

Here the operators β_q describe free plasmonic energy eigenmodes and we introduced

$$c_q = v_F\sqrt{\left|1+\frac{V_1(q)}{2\pi}\right|^2 - \left|\frac{V_2(q)}{2\pi}\right|^2} \tag{2.10}$$

$$\alpha_q = \frac{1}{4}\ln\left(\frac{2\pi v_F + V_1(q) + V_2(q)}{2\pi v_F + V_1(q) - V_2(q)}\right). \tag{2.11}$$

2.1.1 Displacement and phase field representation

For a real space representation of the Luttinger model Hamiltonian it is convenient to introduce the displacement field

$$\phi(x) = \frac{1}{2\mathrm{i}}\sum_{q\neq 0}\sqrt{\frac{2\pi}{L|q|}}\,\mathrm{sign}\,(q)\,\mathrm{e}^{\mathrm{i}qx}\left(b_q + b_{-q}^\dagger\right) \tag{2.12}$$

and the phase field

$$\theta(x) = \frac{1}{2\mathrm{i}}\sum_{q\neq 0}\sqrt{\frac{2\pi}{L|q|}}\mathrm{e}^{\mathrm{i}qx}\left(b_q - b_{-q}^\dagger\right). \tag{2.13}$$

The advantage of this representation is a close analogy to classical elasticity theory. One can think of the field $\phi(x)$ as the displacement of particles from their equilibrium position. In one dimension, a change of the displacement has a one to one correspondence to a density fluctuation and Eqs. (2.6,2.12,2.13) confirm that

$$\nabla\phi(x) = \pi : \rho(x) := \pi : \rho_R(x) + \rho_L(x) : \tag{2.14}$$

$$\nabla\theta(x) = \pi : \rho_R(x) - \rho_L(x) :, \tag{2.15}$$

where the colons denote normal ordering. While $\nabla\phi$ describes the local density fluctuations $\nabla\theta$ "counts" the difference between right and left-movers and is therefore connected to the current operator. Moreover, $\nabla\theta$ is the canonical conjugate (or generalized momentum) of ϕ in the sense that

$$\left[\phi(x), \nabla\theta(x')\right] = -\mathrm{i}\pi\delta(x-x') \tag{2.16}$$

$$\left[\theta(x), \nabla\phi(x')\right] = -\mathrm{i}\pi\delta(x-x')\,. \tag{2.17}$$

With these definitions one can rewrite the Luttinger Hamiltonian in the form

$$H = \frac{c}{2\pi} \int \mathrm{d}x \left[K \left[\nabla\theta(x) \right]^2 + \frac{1}{K} \left[\nabla\phi(x) \right]^2 \right] , \tag{2.18}$$

where K is the Luttinger parameter. Eq. (2.18) is the classical field theory analog of a harmonic chain consisting only of a kinetic part (momentum squared) and a harmonic potential. For a connection to Eq. (2.9) the long wavelength limit of $c = c_{q=0}$ and $\alpha = \alpha_{q=0}$ was used such that with $V_1(q) = V_2(q) = \left(V_0 - V_{2k_F} \right) / 2\pi$ we obtain

$$c = \frac{v_F}{K} \tag{2.19}$$

$$\frac{1}{K} = \mathrm{e}^{2\alpha} = \sqrt{1 + \frac{V_0 - V_{2k_F}}{\pi}} . \tag{2.20}$$

Note that it is not straight forward to derive Eqs. (2.19,2.20) from the interacting fermionic Hamiltonian (2.2). By assuming a linear dispersion and distinguishing between right- and left-moving electrons, one effectively takes a short-cut to a rigorous renormalization group treatment. The latter projects the low energy behavior of the initial Hamiltonian onto the Luttinger model but also renormalizes the coupling constants. Without knowledge of the details of the renormalization one should regard c and K as phenomenological parameters which should be fixed separately. The form of Eqs. (2.19,2.20) can be fixed by the Pauli principle and Galilean invariance as described by Starykh *et al.* (2000) (see Appendix A.1 for details).

2.1.2 Spin

Most of the arguments in the derivation of the Luttinger Hamiltonian also apply when including the spin degree of freedom. Then the bosonization procedure is carried out starting from spin and charge densities which are defined as asymmetric and symmetric combinations of the spin resolved densities. In the language of the phase and displacement fields one uses

$$\phi_{c/s} = \frac{1}{\sqrt{2}} \left(\phi_\uparrow \pm \phi_\downarrow \right) \tag{2.21}$$

$$\theta_{c/s} = \frac{1}{\sqrt{2}} \left(\theta_\uparrow \pm \theta_\downarrow \right) \tag{2.22}$$

and finds that the spinful Hamiltonian splits up into two independent parts (see Appendix A.1 for details)

$$
\begin{aligned}
H &= H_c + H_s + H_{SG} && (2.23)\\
H_{c/s} &= \frac{v_{c/s}}{2\pi}\int \mathrm{d}x \left[\frac{1}{K_{c/s}}\left(\nabla\phi_{c/s}\right)^2 + K_{c/s}\left(\nabla\theta_{c/s}\right)^2\right] && (2.24)\\
H_{SG} &= \frac{V_{2k_F}\Lambda^2}{2\pi^2}\int \mathrm{d}x \cos\left[2\sqrt{2}\phi_s\right], && (2.25)
\end{aligned}
$$

which is known as spin charge separation. The contribution H_{SG} is known as the sine-Gordon term, where Λ is the UV momentum cutoff of the linear dispersion. The sine-Gordon term follows from backscattering terms of the structure $c^\dagger_{R\uparrow}c_{L\uparrow}c^\dagger_{L\downarrow}c_{R\downarrow}$ which cannot be written as density operators. A renormalization group analysis of the Hamiltonian [see *e.g.* Giamarchi (2004)] shows that the sine-Gordon term is irrelevant for the low energy behavior. In particular, the renormalization group analysis for the spin rotational invariant case yields that the "coupling constant" V_{2k_F} flows to zero which leads to

$$
\begin{aligned}
K_c v_c &= K_s v_s = v_F && (2.26)\\
\frac{1}{K_c} &= \sqrt{1+\frac{2V_0}{\pi v_F}} && (2.27)\\
K_s &= 1\,. && (2.28)
\end{aligned}
$$

2.2 Bosonization of the fermion operators

In this section we discuss how the fermionic field operators $\psi(x) = 1/\sqrt{L}\sum_k \exp(\mathrm{i}kx)c_k$ can be rewritten in terms of the bosonic fields, which is required to calculate fermionic correlation functions within the bosonization technique. The desired relation can be obtained by studying the commutation relation of $\psi(x)$ with the bosonic fields. Using the relations between ϕ, θ and the density operators [Eqs. (2.14,2.15)] it is straight forward to check that

$$
\begin{aligned}
\left[\psi_{R/L}(x), \nabla\phi(x')\right] &= \pi\delta(x-x')\psi_{R/L}(x) && (2.29)\\
\left[\psi_{R/L}(x), \nabla\theta(x')\right] &= \pm\pi\delta(x-x')\psi_{R/L}(x)\,, && (2.30)
\end{aligned}
$$

which is, with a look at the commutation relations of ϕ and θ [Eqs. (2.16,2.17)], solved by $\psi_{R/L}(x) \sim \mathrm{e}^{\mathrm{i}[\theta(x)\pm\phi(x)]}$. This however is still a purely bosonic operator and has to be combined with a unitary operator $U_{R/L}$ that acts on the fermionic Hilbert space and changes the electron number by one. Fixing the prefactors then leads in the thermodynamic limit to

$$
\psi_{R/L}(x) = \sqrt{\frac{\Lambda}{2\pi}}\mathrm{e}^{\pm\mathrm{i}k_F x}\mathrm{e}^{\mathrm{i}[\theta(x)\pm\phi(x)]}U_{R/L}\,, \qquad (2.31)
$$

where Λ is again the UV momentum cutoff of the theory and the Klein factor $U_{R/L}$ is often omitted because it drops out in particle number conserving expressions due to its unitarity. The corresponding field operator in the case of spinful fermions takes the form

$$\psi_{R/L\sigma}(x) = \sqrt{\frac{\Lambda}{2\pi}} e^{\pm \mathrm{i} k_F x} \mathrm{e}^{\frac{\mathrm{i}}{\sqrt{2}}\{[\theta_c(x) \pm \phi_c(x)] + \sigma[\theta_s(x) \pm \phi_s(x)]\}} U_{R/L\sigma} \,. \tag{2.32}$$

2.2.1 Chiral fields

The fields θ and ϕ contain contributions from both, the right- and left-moving eigenmodes β_q. When studying partitioning and fractionalization effects it is beneficial to separate these contributions and introduce chiral fields

$$\theta_\pm(x) = \theta(x) \pm \frac{1}{K}\phi(x) \tag{2.33}$$

which are expressed only in terms of right- or left-moving plasmons, respectively. The corresponding commutation relations read

$$\begin{aligned} \left[\theta_\pm(x), \theta_\pm(x')\right] &= \pm \frac{\mathrm{i}\pi}{K} \mathrm{sign}(x - x') & (2.34) \\ \left[\theta_\pm(x), \theta_\mp(x')\right] &= 0 \,. & (2.35) \end{aligned}$$

Since the plasmons are energy eigenmodes traveling with velocity c the time evolution of the chiral fields is given by $\theta_\pm(x,t) = \theta_\pm(x \mp ct)$.

From its diagonal form in terms of the plasmon operators [Eq. (2.9)] it is clear that also the Hamiltonian can be divided into a right- and left-moving part. Applying Eq. (2.33) to the Hamiltonian of Eq. (2.18) we find

$$H = \frac{v_F}{4\pi} \int \mathrm{d}x \left\{ [\nabla\theta_+(x)]^2 + [\nabla\theta_-(x)]^2 \right\} . \tag{2.36}$$

Current operators

The chiral fields also allow one to separate the current and density operators

$$\begin{aligned} j(x) &= \frac{v_F}{\pi} \nabla\theta(x) & (2.37) \\ \rho(x) &= \frac{1}{\pi} \nabla\phi(x) & (2.38) \end{aligned}$$

into right- and left-moving contributions

$$\begin{aligned} j_\pm(x) &= \frac{v_F}{\pi} \nabla\theta_\pm(x) & (2.39) \\ \rho_\pm(x) &= \pm \frac{K}{2\pi} \nabla\theta_\pm(x) \,. & (2.40) \end{aligned}$$

Similarly one can also derive an expression for the chiral energy current operators from $\partial_t \rho_\pm^E(x) = \mathrm{i}\left[H, \rho_\pm^E(x)\right] = -\nabla j_\pm^E(x)$, with the energy density $\rho_\pm^E = v_F \left[\nabla\theta_\pm\right]^2 / 4\pi$. The result reads

$$j_\pm^E = \pm c\rho_\pm^E(x) = \pm\frac{v_F^2}{4\pi K}\left[\nabla\theta_\pm(x)\right]^2 . \tag{2.41}$$

Fractionalization

Interestingly it is also possible to divide the electron field operators into a right- and left-moving part. By substituting the chiral fields into Eq. (2.31) we obtain

$$\psi_{R/L} \propto \mathrm{e}^{\mathrm{i}Q_\pm\theta_+}\mathrm{e}^{\mathrm{i}Q_\mp\theta_-} , \tag{2.42}$$

with the same coefficients $Q_\pm = (1 \pm K)/2$ that also determine the charge partitioning [see Eq. (1.2)]. This split up of the original electron operator into right- and left-moving eigenmodes leads to the notion of charge fractionalization. These eigenmodes can also be interpreted as free *fermionic* quasi-particles of the Luttinger model which are called holons and spinons (in the spinless case there are only holons). The crucial difference to the quasi-particles in Fermi liquids is however that the overlap of the original electrons and the new quasi-particles vanishes, which reflects itself in a momentum distribution function which is continuous at the Fermi momentum.

2.2.2 Holons and spinons

Holons can be introduced naturally by rescaling the bosonic fields to $\tilde{\phi} = \phi/\sqrt{K}$ and $\tilde{\theta} = \theta\sqrt{K}$ [see *e.g.* Voit (1995)] which leads to a Hamiltonian of the form

$$H = \frac{c}{2\pi}\int \mathrm{d}x \left(\left[\nabla\tilde{\theta}(x)\right]^2 + \left[\nabla\tilde{\phi}(x)\right]^2\right) , \tag{2.43}$$

where we focused on the spin independent problem (spinons can be defined analogously). This Hamiltonian describes a non-interacting ($K = 1$) fermionic systems with $v_F = c$. Reading the bosonization formular [Eq. (2.31)] backwards then leads to the definition of the corresponding free fermions

$$\tilde{\psi}_\pm \propto \mathrm{e}^{\mathrm{i}\left[\tilde{\theta}(x) \pm \tilde{\phi}(x)\right]} = \mathrm{e}^{\mathrm{i}\sqrt{K}\theta_\pm(x)} \tag{2.44}$$

which are called holons. The corresponding density operator can be expressed as

$$:\tilde{\psi}_+^\dagger(x)\tilde{\psi}_+(x): + :\tilde{\psi}_-^\dagger(x)\tilde{\psi}_-(x): := \sqrt{K}\nabla\tilde{\phi}(x). \tag{2.45}$$

The mass and charge of the holons is therefore renormalized by a factor of $\sqrt{K}$. This would lead to a more tedious form of the prefactor in Eq. (2.44) which we circumvent by defining the holons as dimensionless. The original Fermion operator can then be rewritten in terms

of the holons as

$$\psi_{R/L}(x,t) = \sqrt{\frac{\Lambda}{2\pi}} e^{ik_F x} \left[\tilde{\psi}_+(x,t)\right]^{\frac{Q_\pm}{\sqrt{K}}} \left[\tilde{\psi}_-(x,t)\right]^{\frac{Q_\mp}{\sqrt{K}}} \tag{2.46}$$

with $\tilde{\psi}_\pm = e^{i\sqrt{K}\theta_\pm(x)}$ and similarly $Q_{+(-)}/\sqrt{K} = \cosh\alpha(\sinh\alpha)$.

2.2.3 Correlation functions

The advantage of the representation in terms of holons and spinons is that this allows for a fast calculation of correlation functions. The holon Green's functions are simply given by the noninteracting expressions[1]

$$i\tilde{G}^>_\pm(x,t) = \left\langle \tilde{\psi}_\pm(x,t)\tilde{\psi}^\dagger_\pm(0,0)\right\rangle = \left(\frac{i/\Lambda}{\pm x - ct + i/\Lambda}\right) \tag{2.47}$$

$$-i\tilde{G}^<_\pm(x,t) = \left\langle \tilde{\psi}^\dagger_\pm(0,0)\tilde{\psi}_\pm(x,t)\right\rangle = \left(\frac{i/\Lambda}{\mp x + ct + i/\Lambda}\right). \tag{2.48}$$

Here we focus on the $T = 0$ behavior. The finite T expression follows by substituting $(\pm x - ct)$ by $L_T \sinh\left[(\pm x - ct)/L_T\right]$, where $L_T = c/\pi T$ describes the length scale beyond which the correlation functions start to decay exponentially. Using Eq. (2.46) and the fact that $\tilde{\psi}$ with different chiralities commute it is then possible to write the correlation function of the original electrons as

$$G^>_{R/L}(x,t) = -i\frac{\Lambda}{2\pi} e^{\pm ik_F x} \left\langle \tilde{\psi}_\pm(x,t)^{\cosh\alpha}\tilde{\psi}^\dagger_\pm(0,0)^{\cosh\alpha}\right\rangle \left\langle \tilde{\psi}_\mp(x,t)^{\sinh\alpha}\tilde{\psi}^\dagger_\mp(0,0)^{\sinh\alpha}\right\rangle \tag{2.49}$$

Since the fields $\tilde{\psi}$ are exponentials of free bosonic operators we can use the independent boson theorem [for a prove see *e.g.* Giuliani and Vignale (2005)]

$$\left\langle e^{\sum_i \left(x_i\beta_i^\dagger + y_i\beta_i\right)}\right\rangle = e^{\frac{1}{2}\sum_i \left\langle (x_i\beta_i^\dagger + y_i\beta_i)^2\right\rangle} \tag{2.50}$$

to realize that

$$\left\langle \tilde{\psi}^\gamma_\pm \tilde{\psi}^{\dagger\gamma}_\pm\right\rangle = \left\langle \tilde{\psi}_\pm\tilde{\psi}^\dagger_\pm\right\rangle^{\gamma^2}. \tag{2.51}$$

With the known correlation functions of $\tilde{\psi}$ we can then immediately write down

$$G^>_{R/L}(x,t) = \frac{\Lambda}{2\pi} e^{\pm ik_F x} \left(\frac{1/\Lambda}{\pm x - ct + i/\Lambda}\right)^{\cosh^2\alpha} \left(\frac{1/\Lambda}{\pm x + ct - i/\Lambda}\right)^{\sinh^2\alpha}, \tag{2.52}$$

where the lesser Green's function can be obtained from $G^<_{R/L}(x,t) = -G^>_{R/L}(-x,-t)$.

With the knowledge of the Green's function we can derive the spectral function

$$A_{R/L}(x,t) = \frac{1}{2\pi}\left\langle\left\{\psi_{R/L}(x,t), \psi^\dagger_{R/L}(0,0)\right\}\right\rangle = \frac{i}{2\pi}\left(G^>_{R/L}(x,t) - G^<_{R/L}(x,t)\right) \tag{2.53}$$

[1] Note that a missing factor of $\Lambda/2\pi$ is due to the dimensionless definition of $\tilde{\psi}$.

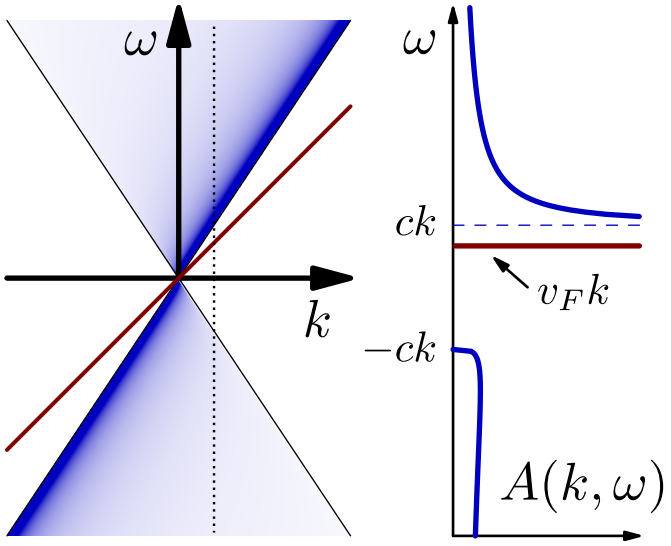

Figure 2.2: Right-mover spectral function (blue) for $\gamma = 0.2$ in comparison with the non-interacting spectral functions (dark red). The right part shows a cut along the dotted line.

as well as its Fourier transform

$$A_{R/L}(k,\omega) = \int \mathrm{d}t \int \mathrm{d}x \mathrm{e}^{\mathrm{i}(\omega t - kx)} A_{R/L}(x,t) \tag{2.54}$$

$$= \frac{1}{\gamma\Gamma(\gamma)^2}\left(\frac{1}{2c\Lambda}\right)^{2\gamma} |\omega \mp ck|^{\gamma-1} |\omega \pm ck|^{\gamma} \Theta\left(|\omega| - c\,|k|\right), \tag{2.55}$$

where Γ denotes the Gamma function and we introduced

$$\gamma = \sinh^2 \alpha = \frac{1}{4}\left(K - 2 + \frac{1}{K}\right). \tag{2.56}$$

A plot of a typical spectral function can be seen in Fig. 2.2. The algebraic behavior of the spectral function differs dramatically from a Lorentzian quasi-particle peak and reflects the strongly interacting nature of the Luttinger model. Integrating over different momenta yields the local tunneling density of states

$$\nu_{R/L}(\omega) = \int \frac{\mathrm{d}k}{2\pi} A_{R/L}(k,\omega) \tag{2.57}$$

$$\nu_{R/L}(\omega) = \frac{1}{2\sqrt{\pi}\gamma\Gamma(\gamma)\Gamma\left(\frac{1}{2}+\gamma\right)c}\left(\frac{|\omega|}{2c\Lambda}\right)^{2\gamma}, \tag{2.58}$$

that (also in contrast to the Fermi liquid) vanishes as $\omega \to 0$. This is known as zero bias anomaly.

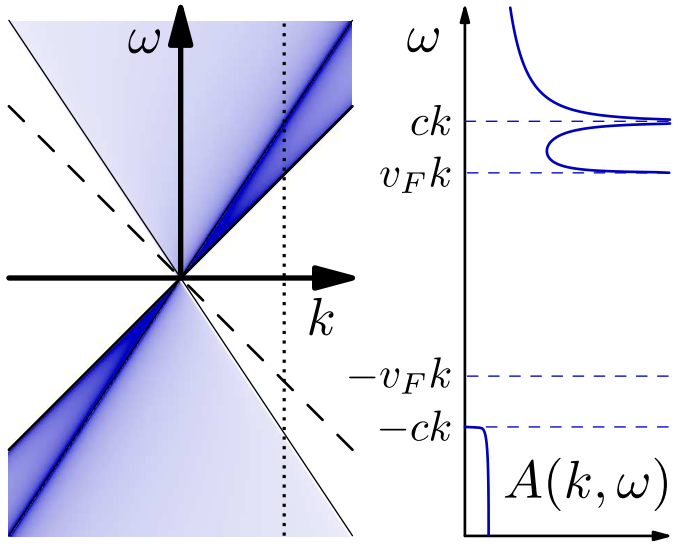

Figure 2.3: Right-mover spectral function (for $\gamma_c = 0.2$) in the spinful case. The right panel shows a cut along the dotted line. Also in the spinful case, the power law structure of the spectral function shows the absence of Fermi liquid like single particle excitations.

Spinful case

For spinful particles in a spin rotation invariant system the spectral function takes the form [Voit (1993)]

$$A_R(k,\omega) \propto \begin{cases} (\omega - v_F k)^{\gamma_c - \frac{1}{2}} \, |\omega - v_c k|^{\frac{\gamma_c - 1}{2}} & , \omega > v_F k \\ (-\omega - v_F k)^{\frac{\gamma_c}{2}} & , \omega < -v_c k \end{cases} \tag{2.59}$$

with $\gamma_c = (K_c - 2 + K_c^{-1})/4$ and we focused at the case $k > 0$. A plot of the typical form of the right-mover spectral function is shown in Fig. 2.3. It exhibits power law singularities along the holon and spinon dispersions which resemble peaks around the right-moving holon and spinon mass shell for not too strong interactions. Note that the spectral function vanishes between the left-moving spinon and holon dispersion. This is a consequence of the spin rotational invariance which leads to $K_s = 1$. One can think of $K_{c/s}$ as determining the ratio of the fractional right- and left-moving holons/spinons that are "contained" in an original right-moving electron [see Eq. (2.46)]. For $K_s = 1$ this simply means that right-moving electrons do not contain left-moving spinons and can therefore only excite holons and right-moving spinons in a tunneling process, which leads to the asymmetric distribution of finite spectral weight.

3 Energy partitioning of tunneling currents into Luttinger liquids

In the Fermi liquid picture of the electron tunneling process one expects that injecting, say, a right-moving particle introduces a right-moving quasi-particle excitation. The latter carries away the excess energy and momentum of the injected electron, while the charge distributes isotropically on the fast plasmon time scale. In one dimension, plasmon excitations and single particle excitations cannot be distinguished. This leads to the collective Luttinger liquid behavior and an unusual charge partitioning which is connected to the fractional excitations of the highly correlated state [see Eqs. (1.2,2.46)]. This chapter discusses that strong interactions also lead to a partitioning of energy currents and is based on Karzig *et al.* (2011).

In contrast to the charge, partitioning of energy can be measured in dc transport setups and spectroscopies which makes it easier to access. The reason for the trivial dc charge partitioning ratios are backscattering effects at the measuring leads, which will be discussed in the following.

3.1 Backscattering at Fermi liquid leads

We start with considering spinless fermions and model the interface between the Luttinger liquid and the Fermi liquid leads by a position dependent Luttinger parameter $K(x)$. It changes at the interface on a length scale w from its Luttinger liquid value $K(x) = K$ to $K(x) = 1$, which describes the weakly interacting lead. This model, was already studied extensively in the literature in the context of the dc conductance [Maslov and Stone (1995); Safi and Schulz (1995)], the thermal transport [Fazio *et al.* (1998)] as well as recently in the out of equilibrium extension of bosonization [Gutman *et al.* (2009, 2010a,b)]. Here we recast some of these results in terms of a simple scattering picture.

3.1.1 Charge currents

In realistic samples w will be much larger than the Fermi wavelength, which is typically of the order of the width of the wire. This leads to an absence of backscattering of individual electrons at the interface and thus conserves the number of right- and left-moving electrons. After a time much larger than L/c (L being the length of the Luttinger liquid and c the holon velocity) the excitations introduced by an injected right-moving electron have left the interacting region. Due to the conservation of the number of right- and left-movers

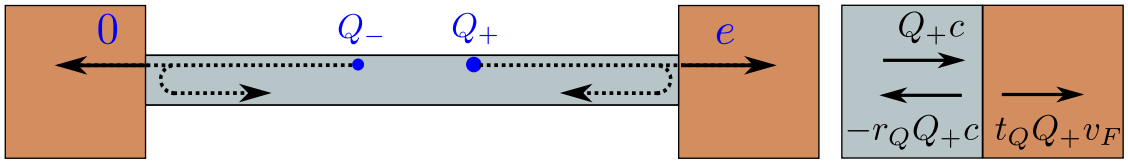

Figure 3.1: Schematic picture of charge backscattering in a Luttinger liquid with leads. (a) shows the resulting trivial charge partitioning in the leads. (b) depicts the Luttinger liquid/lead interface and the corresponding current conservation.

this is only possible when a single right-mover exits into the right lead, yielding the trivial noninteracting charge partitioning ratio [see Fig. 3.1a].

It is instructive to understand this simple argument also in terms of backscattering of the charge carrying eigenmodes (holons) of the interacting system. Consider a corresponding current $Q_+ c$ incident on the interface from the Luttinger liquid side [see Fig. 3.1b]. After scattering at the boundary the current splits up into transmitted and reflected parts $Q_+ t_Q v_F$ and $-Q_+ r_Q c$, respectively. The conservation of the number of right- and left-movers is equivalent to current conservation (before and after hitting the interface) and requires $c = t v_F - r c$. Together with the charge conservation condition $1 = r_Q + t_Q$ we can solve

$$r_Q = -\frac{1-K}{1+K} \tag{3.1}$$

$$t_Q = \frac{2}{1+K}\,. \tag{3.2}$$

The overall charge $Q^0_\pm$ leaving into the right and left leads can be obtained by summing over all possible elementary scattering process which resemble a geometric series of the form

$$Q^0_\pm = (Q_\pm t_Q + Q_\mp r_Q t_Q)\left(1 + r_Q^2 + r_Q^4 + \ldots\right) \tag{3.3}$$

$$Q^0_+ = (Q_\pm + Q_\mp r_Q)\,\frac{t_Q}{1-r_Q^2}\,. \tag{3.4}$$

If we now use the known charge partitioning ratio $Q_\pm = (1 \pm K)/2$ we find

$$Q^0_\pm = \frac{1}{2}\,(1 \pm 1)\,, \tag{3.5}$$

which indeed shows that all the charge will exit into the right lead when injecting a right-moving electron. Note that it is crucial that the reflection amplitude r_Q is negative to cancel the left-moving contributions of the current. This in turn already indicates a crucial difference for the corresponding backscattering of energies. Since there is nothing like a backscattering of negative energies, a nontrivial energy partitioning ratio after the tunneling process will result in nontrivial energy currents exiting into the leads.

3.1.2 Energy currents

The influence of the Fermi liquid leads on energy partitioning can be described in terms of the scattering behavior of the plasmons which carry the energy current. For an interface which is smooth on the plasmon length scale, the plasmons are adiabatically transmitted to the leads and the energy partitioning can be directly probed by measuring the heat currents flowing into the leads. Note however that the plasmons are the low energy excitations in a Luttinger liquid and their typical wavelength is therefore much longer than the Fermi wavelength. Assuming a smooth interface for the plasmons is therefore more demanding than for the electrons. Moreover, since there is no lower bound to the plasmon momentum, there will be plasmons for every given w that behave as if the interface was sharp.

In the low energy limit the interface can therefore be modeled generically as $K(x) = K\Theta(-x) + \Theta(x)$. The abrupt change causes backscattering of plasmons in a similar way to that of photons at an interface between two materials with two different refractive indices. In both cases, free bosons change their velocity abruptly and one can indeed obtain the plasmon transmission and reflection probabilities from the well-known Fresnel equations as we will show in the following.

The interface can be described best in the real space representation of the bosonic fields whose time evolution is governed by the Hamiltonian [see Eq. (2.18)]

$$H = \frac{v_F}{2\pi} \int \mathrm{d}x \left([\nabla\theta(x)]^2 + \frac{1}{K(x)^2} [\nabla\phi(x)]^2 \right) . \tag{3.6}$$

The fields fulfill the commutation relations $[\nabla\theta(x), \phi(x')] = [\nabla\phi(x), \theta(x')] = \mathrm{i}\pi\delta(x - x')$ [see Eqs. (2.16,2.17)] from which we obtain

$$\partial_t \phi(x,t) = \mathrm{i}\,[H, \phi(x,t)] = -v_F \nabla\theta(x,t) \tag{3.7}$$

$$\partial_t \theta(x,t) = \mathrm{i}\,[H, \theta(x,t)] = -\frac{v_F}{K(x)^2} \nabla\phi(x,t)\,, \tag{3.8}$$

where the time dependent fields can be obtained by replacing the operators β_q by $\beta_q(t) = \mathrm{e}^{-\mathrm{i}\omega_q t}\beta_q$ in their definitions [see Eqs. (2.12,2.13)]. Decoupling the equations of motion then yields the wave equations

$$\left(\partial_t^2 - \nabla \left(\frac{v_F}{K(x)} \right)^2 \nabla \right) \phi(x,t) = 0 \tag{3.9}$$

$$\left(\partial_t^2 - \left(\frac{v_F}{K(x)} \right)^2 \nabla^2 \right) \theta(x,t) = 0\,, \tag{3.10}$$

from which we can deduce the behavior of the fields at the interface ($x = 0$). Despite the jump of $K(x)$, the relations above imply that θ, $\nabla\theta$, and ϕ are continuous at $x = 0$, while

$\nabla\phi$ jumps as

$$\frac{\nabla\phi\left(0^{-}\right)}{K^{2}}=\nabla\phi\left(0^{+}\right)\,. \tag{3.11}$$

In the spirit of standard scattering theory, we now use these conditions to match "wavefunctions" left and right of the interface. For a given energy, say $\omega_q = cq$ these "wavefunctions" are formed by the plasmons β_q in the interacting region to the left of the interface. In the Fermi liquid leads however the same energy is reached at higher momenta with corresponding plasmons $b_{q/K}$. For $q > 0$ the incoming waves are given in terms of β_q and $b_{-q/K}$ while the outgoing operators can be obtained by a 2×2 scattering matrix[1] via

$$\begin{aligned}\beta_{-q} &= r\beta_q + tb_{-q/K} &(3.12)\\ b_{q/K} &= t'\beta_q + r'b_{-q/K}\,. &(3.13)\end{aligned}$$

We now use the definition of the fields ϕ and θ [see Eqs. (2.12,2.13)] to determine the reflection and transmission coefficients. The fields can be written as

$$\begin{aligned}\phi(x) &= \Theta(-x)\frac{1}{2\mathrm{i}}\sqrt{\frac{L}{2\pi}}\int_0^\infty \mathrm{d}q\sqrt{\frac{1}{q}}\sqrt{K}\left[\mathrm{e}^{\mathrm{i}qx}\beta_q - \mathrm{e}^{-\mathrm{i}qx}\beta_{-q} - \mathrm{H.c.}\right] &(3.14)\\ &\quad +\Theta(x)\frac{1}{2\mathrm{i}}\sqrt{\frac{L}{2\pi}}\int_0^\infty \mathrm{d}q\sqrt{\frac{1}{q}}\frac{1}{\sqrt{K}}\left[\mathrm{e}^{\mathrm{i}qx/K}b_{q/K} - \mathrm{e}^{-\mathrm{i}qx/K}b_{-q/K} - \mathrm{H.c.}\right]\end{aligned}$$

and

$$\begin{aligned}\theta(x) &= \Theta(-x)\frac{1}{2\mathrm{i}}\sqrt{\frac{L}{2\pi}}\int_0^\infty \mathrm{d}q\sqrt{\frac{1}{q}}\frac{1}{\sqrt{K}}\left[\mathrm{e}^{\mathrm{i}qx}\beta_q + \mathrm{e}^{-\mathrm{i}qx}\beta_{-q} - \mathrm{H.c.}\right] &(3.15)\\ &\quad +\Theta(x)\frac{1}{2\mathrm{i}}\sqrt{\frac{L}{2\pi}}\int_0^\infty \mathrm{d}q\sqrt{\frac{1}{q}}\frac{1}{\sqrt{K}}\left[\mathrm{e}^{\mathrm{i}qx/K}b_{q/K} + \mathrm{e}^{-\mathrm{i}qx/K}b_{-q/K} - \mathrm{H.c.}\right]\,.\end{aligned}$$

From the continuity of ϕ, θ, and $\nabla\theta$, as well as the well-defined jump of $\nabla\phi$, we then find

$$\begin{aligned}r &= -\frac{1-K}{1+K} &(3.16)\\ r' &= \frac{1-K}{1+K} &(3.17)\\ t &= \frac{2}{1+K} &(3.18)\\ t' &= \frac{2K}{1+K}\,. &(3.19)\end{aligned}$$

The fact that $r = r_Q$ and $t = t_Q$ can be understood in the following way. The right- and left-moving (particle) current operator is linear in the bosonic fields, and given by [see Eq. (2.39)] $I_\pm(x) = \frac{v_F}{\pi}\nabla\theta_\pm(x)$. Since an incident plasmon is reflected as $\beta_q = r\beta_{-q} + tb_{q/K}$, the

[1] Note that the scattering matrix in this form is not unitary because the waves corresponding to the boson operators are not normalized to unit flux. Defining the scattering matrix as a transformation between β_q, $\frac{1}{\sqrt{K}}b_{-q/K}$ and β_{-q}, $\frac{1}{\sqrt{K}}b_{\pm q/K}$ then indeed satisfies the unitarity condition.

plasmon reflection and transmission amplitudes directly determine the charge reflection. The energy currents however depend quadratically on the plasmon operators via [see Eq. (2.41)]

$$j_{\pm}^{E}(x) = \pm \frac{v_F^2}{4\pi K(x)} \left[\nabla \theta_{\pm}(x)\right]^2 \tag{3.20}$$

and are therefore determined by the plasmon reflection and transmission probabilities. Thus, reflection and transmission coefficients for the energy current take the form

$$r_E = r^2 = \left(\frac{1-K}{1+K}\right)^2 \tag{3.21}$$

$$t_E = Kt^2 = \frac{4K}{(1+K)^2}, \tag{3.22}$$

which indeed coincides with the Fresnel formulas when setting $v_1 = c$ and $v_2 = v_F$ (or alternatively the refractive indices $n_1 = K$ and $n_2 = 1$). Note that the analogy to optics can even explain the backscattering of negative charges. When going from the Luttinger liquid to the Fermi liquid leads, the refractive index increases from K to 1. In optics this leads to a phase shift of π which yields negative reflection amplitudes that cause the charges to cancel.

However, since r_E is positive this is not possible for the energies and introducing right- and left-moving energy excitations $\varepsilon_{\pm}$ in the Luttinger liquid will lead to an energy flow $\varepsilon_{\pm}^{0}$ into both leads. The latter can be calculated in the same way as for the charges by taking into account all possible multiple reflections [see Eq. (3.4)]. The result reads

$$\varepsilon_{\pm}^{0} = \left(\varepsilon_{\pm} + \varepsilon_{\mp} r_E\right) \frac{1}{1+r_E}, \tag{3.23}$$

and can be used to determine the initial energy partitioning from the heat currents into the Fermi liquid leads.

3.1.3 Thermal conductance of a Luttinger liquid

The above reflection and transmission coefficients are already sufficient to calculate the thermal conductance of a Luttinger liquid in a transparent plasmon scattering picture. As derived in section 2.2.1 the energy current operator of the Luttinger liquid takes the intuitive form $j_{\pm}^{E}(x) = \pm c \rho_{\pm}^{E}(x)$ [see Eq. (2.41)]. The expectation value averaged over a homogeneous system is thus given by

$$\left\langle j_{\pm}^{E} \right\rangle = \pm \frac{1}{L} \sum_{q} c\omega_q \left\langle \beta_q^{\dagger} \beta_q \right\rangle, \tag{3.24}$$

which can be obtained by comparison with the Hamiltonian (2.9) in terms of the plasmon operators β_q. Introducing the Bose distribution function $\left\langle \beta_q^{\dagger} \beta_q \right\rangle = n_B(\omega_q) = \left(\exp(\omega_q/T) - 1\right)^{-1}$ and using the plasmon density of states $L/2\pi c$, we then obtain the

simple relation

$$\left\langle j_{\pm}^{E} \right\rangle = \pm \int \frac{\mathrm{d}\omega}{2\pi} \omega n_B(\omega) \,. \tag{3.25}$$

The overall thermal current through a Luttinger liquid with sharp non-interacting leads is then given by

$$\left\langle j^{E} \right\rangle = \int \frac{\mathrm{d}\omega}{2\pi} \omega \mathcal{T}_E^{(\mathrm{tot})} \left[n_B^{+}(\omega) - n_B^{-}(\omega) \right] , \tag{3.26}$$

which resembles the structure of the well-known Landauer formula. Now, using $T_+ = T_- + \delta T$ and expanding in small δT leads to the thermal conductance

$$G_T = \mathcal{T}_E^{(\mathrm{tot})} \frac{\pi}{6} T \,. \tag{3.27}$$

The total transmission probability can be determined by summing up a geometric series similar to the above expressions. The result reads

$$\mathcal{T}_E^{(\mathrm{tot})} = t_E^2 \frac{1}{1 - r_E^2} = \frac{2K}{1 + K^2}, \tag{3.28}$$

which determines the thermal conductance of a Luttinger liquid to be

$$G_T = \frac{\pi}{3} \frac{K}{1 + K^2} T \,. \tag{3.29}$$

As mentioned before this result does depend on the interaction in contrast to the charge conductance which is given by $G = e^2/\pi$ (note that $h = 2\pi$) [Maslov and Stone (1995); Safi and Schulz (1995)]. In fact, the thermal conductance even vanishes in the strongly interacting case $K = 0$, while for $K = 1$ it indeed reduces to the Wiedemann-Franz law $G_T = GT\pi^2/3e^2$. Interestingly, this relatively simple derivation reproduces the result that was only recently obtained in a non-equilibrium functional bosonization study [Gutman *et al.* (2009)].

3.1.4 Spin

When considering spinful electrons, there are two different interaction parameters $K_{c/s}$. Since the charge is only carried by one of the modes, the argument for charge backscattering stays the same and one simply has to replace K by K_c. Energy however, can be transported by spin and charge modes. In the spin rotationally invariant case, $K_s = 1$ and a part of the excess energy from injecting a right-moving electron can be used to excite spin excitations that leave from the Luttinger liquid into the leads without backscattering. We therefore find

$$\varepsilon_{\pm}^{0} = \frac{\varepsilon_{c\pm}(1+K)^2 + \varepsilon_{c\mp}(1-K)^2}{2(1+K^2)} + \varepsilon_{s\pm}, \tag{3.30}$$

with $\varepsilon_{s-} = 0$. The energy current injected into the left lead is therefore independent of the spin excitations, when injecting right-moving electrons.

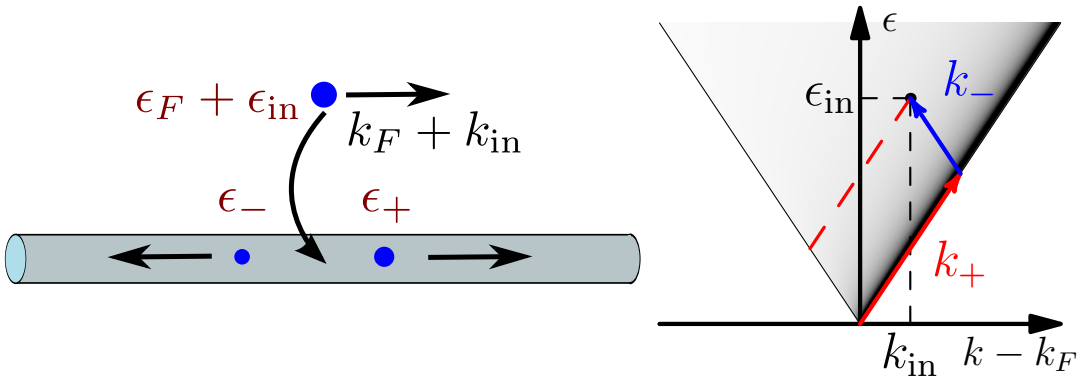

Figure 3.2: Schematic picture of energy partitioning, when injecting a momentum eigenstate. The right panel shows the projection of the injected state onto the right- and left-moving excitations. The shaded background represents the Luttinger liquid's spectral function.

3.2 General expressions for charge and energy partitioning

With the motivation that energy partitioning survives even including backscattering effects at Fermi liquid leads, it is now left to discuss the energy $\varepsilon_\pm$ of the initially induced right- and left-moving charge excitations. We start with discussing spinless electrons to avoid unnecessary complications.

It will turn out that energy partitioning depends crucially on the state of the injected electrons (*e.g.* local or momentum resolved). The main results can already be understood by a simple energy and momentum conservation argument if the electron tunnels into the Luttinger liquid as a momentum eigenstate.

3.2.1 An energy and momentum conservation argument

Consider inserting a right-moving electron with energy $\varepsilon_{\rm in}$ above the Fermi energy and momentum $mv_F + k_{\rm in}$ into the Luttinger liquid. The excess energy will be distributed by exciting right- and left-moving plasmons with overall momentum $k_\pm$ and energy $\varepsilon_\pm = c|k_\pm|$. From energy and momentum conservation we then find

$$\varepsilon_{\rm in} = c|k_+| + c|k_-| \tag{3.31}$$

$$mv_F + k_{\rm in} = Q_+ mc - Q_- mc + k_+ + k_- \,. \tag{3.32}$$

The terms involving the electron mass describes the zero energy part of the right- and left-moving holon momenta and is in line with the charge partitioning argument, which stays untouched. We can therefore solve the remaining part involving the excess energies and find

$$\varepsilon_\pm = \frac{1}{2}\left(\varepsilon_{\rm in} \pm c k_{\rm in}\right) \,, \tag{3.33}$$

which is illustrated in Fig. 3.2.

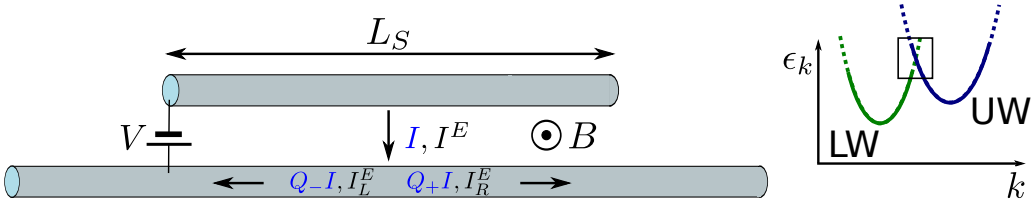

Figure 3.3: Schematic view of an extended source. The magnetic and electric fields can be used to shift the dispersions of the wires relative to each other. The right panel shows an example where the upper (source) wire only injects right-moving electrons into the lower wire.

Energy partitioning is therefore entirely independent of the fixed charge partitioning, and can be tuned to arbitrary values by varying the injected state, *i.e.* experimental parameters. In fact, when the momentum of the injected right-moving electron is smaller than the Fermi momentum ($k_{\text{in}} < 0$), and its energy close to $c|k_{\text{in}}|$, Eq. (3.33) implies that essentially all its excess energy is propagating to the left, while most of the charge moves to the right. A crucial ingredient in this result is the interaction-induced broadening of the Luttinger liquid spectral function which allows for injecting particles away from the mass shell. In a non-interacting system the spectral function would be a delta peak at the right-mover dispersion and no left-moving excitations would be excited.

The conservation law argument provides a simple picture of energy partitioning in terms of projections onto the right- and left-moving plasmon branches [*cf.* Fig. 3.2]. However, tunneling particles will in general not be momentum eigenstates and the associated superposition of different momentum states requires to calculate the energy current in a more formal approach. We will start with the instructive example of the particle current for tunneling into a Luttinger liquid.

3.2.2 Particle current

We consider the Hamiltonian

$$H = \frac{v_F}{4\pi} \int \mathrm{d}x \left\{ [\nabla\theta_+(x)]^2 + [\nabla\theta_-(x)]^2 \right\} + H_{TR}\,, \tag{3.34}$$

where H_{TR} describes tunneling of right-moving electrons between a source and the Luttinger liquid. In the following we will discuss the two extreme cases of an extended long source wire and local tunneling.

Extended source

We consider a long extended source of length L_S which can be realized in experimental setups of two parallel quantum wires [see Barak *et al.* (2010b) and Fig. 3.3]. Assuming that the dispersion of the source wire only couples to the right-moving electrons in the

Luttinger liquid [see Fig. 3.3], the tunneling Hamiltonian takes the form

$$H_{TR} = t \int_S \mathrm{d}x \left[\psi_R^\dagger(x)\psi_S(x) + \psi_S^\dagger(x)\psi_R(x) \right] , \tag{3.35}$$

where $\int_S$ denotes an integral over the length of the source and t is the tunneling amplitude. We will define the injected right- and left-moving particle currents $I_\pm$ as the change of the integrated chiral density $\int_S \mathrm{d}x \rho_\pm(x)$ due to the tunneling, which can be expressed as [see Eq. (2.40)]

$$I_\pm = \frac{\mathrm{d}}{\mathrm{d}t} \left[\int \mathrm{d}x \rho_\pm(x) \right] = \mathrm{i} \left[H_{TR}, \pm \frac{K}{2\pi} \int_S \mathrm{d}x \nabla\theta_\pm(x) \right] . \tag{3.36}$$

From Eqs. (2.14,2.15) we can find the useful relation

$$\nabla\theta_\pm(x) = \pm \frac{2\pi}{K} \left[Q_\pm :\rho_R(x): + Q_\mp :\rho_L(x): \right] . \tag{3.37}$$

Since H_{TR} contains only right-moving electrons the commutator involving $\rho_L(x) = \psi_L^\dagger(x)\psi_L(x)$ vanishes and the current takes the form

$$I_\pm = Q_\pm I . \tag{3.38}$$

Here, I can be evaluated with the fermion commutation relations[2] and yields

$$I = -\mathrm{i}t \left[\psi_R^\dagger(x)\psi_S(x) - \psi_S^\dagger(x)\psi_R(x) \right] . \tag{3.39}$$

The result in Eq. (3.38) implies that charge partitioning can already be described on the operator level and is thus independent of experimental details that are involved in the expectation value of I. For a comparison to the energy currents it is however helpful to evaluate $\langle I \rangle$ which can be done to leading order in the tunneling by

$$\begin{aligned} \langle I \rangle &= -\mathrm{i} \int_{-\infty}^0 \mathrm{d}t' \left\langle \left[I(0), H_{TR}(t') \right] \right\rangle & (3.40) \\ &= t^2 \int_{-\infty}^0 \mathrm{d}t' \int_S \mathrm{d}x \mathrm{d}x' 2\Re \Big\langle \psi_R(x',t')\psi_R^\dagger(x)\psi_S^\dagger(x',t')\psi_S(x) & (3.41) \\ &\quad -\psi_R^\dagger(x)\psi_R(x',t')\psi_S(x)\psi_S^\dagger(x',t') \Big\rangle \mathrm{e}^{\mathrm{i}eVt'} , \end{aligned}$$

where $\Re$ denotes the real part and we included the chemical potential into the time dependence. The latter can be accounted for by replacing $\psi(t) \to \psi(t)\mathrm{e}^{-\mathrm{i}\mu t}$ and using that the source chemical potential $\mu_S = \mu + eV$ is shifted by the applied bias V. The expectation values in the source and in the Luttinger liquid can then be evaluated separately in terms

[2] Note that the constant that is subtracted for the normal ordering commutes with H_{TR}.

of the Green's functions

$$\mathrm{i}G^{>}(x,t) = \left\langle \psi(x,t)\psi^{\dagger}(0,0)\right\rangle \tag{3.42}$$

$$-\mathrm{i}G^{<}(x,t) = \left\langle \psi^{\dagger}(0,0)\psi(x,t)\right\rangle \tag{3.43}$$

and one finds

$$\langle I\rangle = L_S t^2 2\Re\int_{-\infty}^{0}\mathrm{d}t'\int_S \mathrm{d}x\left[G_R^{>}\left(x,t'\right)G_S^{<}\left(-x,-t'\right)-G_R^{<}\left(x,t'\right)G_S^{>}\left(-x,-t'\right)\right]\mathrm{e}^{\mathrm{i}t'eV}. \tag{3.44}$$

The integral over time can be extended via $2\Re\int_{-\infty}^{0}\mathrm{d}t' \to \int_{-\infty}^{\infty}\mathrm{d}t'$ by noting that the Hermitian conjugation implied by $\Re$ transforms the Green's functions such that $\left(\mathrm{i}G^{>}(x,t)\right)^{\dagger} = \left\langle\psi(x,t)\psi^{\dagger}(0,0)\right\rangle^{\dagger} = \left\langle\psi(0,0)\psi^{\dagger}(x,t)\right\rangle = \mathrm{i}G^{>}(-x,-t)$ which is equivalent to shifting $t\to -t$. Finally we Fourier transform $G(x,t) = \int\frac{\mathrm{d}k}{2\pi}\frac{\mathrm{d}\omega}{2\pi}\mathrm{e}^{\mathrm{i}(kx-\omega t)}G(k,\omega)$ and represent our result with

$$\mathrm{i}G^{>}(k,\omega) = 2\pi A(k,\omega)\left(1-f(\omega)\right) \tag{3.45}$$

$$-\mathrm{i}G^{<}(k,\omega) = 2\pi A(k,\omega)f(\omega), \tag{3.46}$$

in terms of the spectral function $A(k,\omega)$ and Fermi function $f(\omega) = [\exp(\omega/T)+1]^{-1}$ as

$$\langle I\rangle = t^2 L_S\int \mathrm{d}k\mathrm{d}\omega A_R\left(k,\omega\right)A_S\left(k,\omega-eV\right)\left[f_S(\omega-eV)-f(\omega)\right]. \tag{3.47}$$

Here, f_S denotes the Fermi function at a source temperature T_S that can be different from T. Eq. (3.47) is a well-known and quite general result for the tunneling current and it allows for a simple interpretation. Eq. (3.47) describes both, tunneling into and out of the wire, depending on the sign of eV. For positive eV it is an average of states with energies such that the source is occupied and the wire is empty weighted by the overlap of the spectral functions of wire and source. In the case of a non-interacting source with dispersion $\varepsilon_k = \varepsilon_k^S - eV$ (ε_k^S is the energy of a particle in the source measured relative to μ) the spectral function takes the form $A_S(k,\omega) = \delta(\omega-\varepsilon_k)$. Then, the tunneling current probes the spectral function of the Luttinger liquid via

$$\left\langle I^{(0)}\right\rangle = t^2 L_S\int \mathrm{d}k A_R\left(k,\varepsilon_k^S\right)\left[f(\varepsilon_k^S-eV)-f(\varepsilon_k^S)\right]. \tag{3.48}$$

Experimentally one often measures $\mathrm{d}\langle I\rangle/\mathrm{d}V$ to obtain (for small temperatures) directly the spectral function as

$$\frac{\mathrm{d}\left\langle I^{(0)}\right\rangle}{\mathrm{d}(eV)} = 2\pi t^2\nu_S A_R\left(k_V,eV\right). \tag{3.49}$$

Here k_V is determined by $\varepsilon_{k_V}^S = eV$ and $\nu_S = L_S/(2\pi\partial_k\varepsilon_k^S)$ is the density of states of the source wire. Note that in the double wire geometry of Barak *et al.* (2010b), changing

the voltage V requires an additional adjustment of the magnetic field B such that the dispersion ε_k^S stays fixed and only the chemical potential of the source is altered.

Local source

Even for local tunneling it is possible that the source mainly couples to the right-moving electrons of the Luttinger liquid, as we will discuss later. For now we simply assume that the local source can be described by the tunneling Hamiltonian

$$H_{TR} = t_{\mathrm{loc}} \left[\psi_R^\dagger(x=0)\psi_S + \psi_S^\dagger \psi_R(x=0) \right] \tag{3.50}$$

(with t_{loc} having the units energy$\times\sqrt{\text{length}}$). In contrast to the extended case, the source's spectral function $A_S(\omega)$ is local and describes the tunneling density of states. A similar calculation as in the extended case leads to

$$\langle I \rangle = t_{\mathrm{loc}}^2 \int \mathrm{d}k \int \mathrm{d}\omega A_R(k,\omega)\, A_S(\omega - eV) \left[f(\omega - eV) - f(\omega) \right] . \tag{3.51}$$

In the case of tunneling from a single level at energy ε_0 measured relative to μ we set $A_S^{(0)}(\omega) = \delta(\omega - [\varepsilon_0 - eV])$ and

$$\left\langle I^{(0)} \right\rangle = 2\pi t_{\mathrm{loc}}^2 \nu_R(\varepsilon_0) \left[f(\varepsilon_0 - eV) - f(\varepsilon_0) \right] \tag{3.52}$$

directly measures the tunneling density of states $\nu_R(\varepsilon_0) = \int \frac{\mathrm{d}k}{2\pi} A_R(k, \varepsilon_0)$. This density of states vanishes in a Luttinger liquid with a power law $\nu_R(\omega) \propto \omega^{2\gamma}$ [*cf.* Eq. (2.58)] which is known as zero bias anomaly. There is a distinct difference between the finite $\nu_R(\omega)$ in the non-interacting case where $\gamma = 0$ and the zero bias anomaly for any finite $\gamma > 0$. This shows again that it is not possible to describe the low energy behavior in a perturbative expansion in the interaction strength, due to the strongly interacting nature of the Luttinger liquid.

3.2.3 Energy current

Using the Hamiltonian (3.34) we will now calculate the injected right- and left-moving energy currents by going through the same steps as in the case of the particle current.

Extended source

The injected energy current is defined as the change of the right- and left-moving energy due to the tunneling Hamiltonian

$$I_\pm^E = \frac{\mathrm{d}}{\mathrm{d}t} E_\pm = \mathrm{i} \int_S \mathrm{d}x \left[H_{TR}, \int \mathrm{d}x \frac{v_F}{4\pi} \left[\nabla \theta_\pm(x) \right]^2 \right] . \tag{3.53}$$

Evaluating the commutator we then find

$$I_{\pm}^{E} = \pm\frac{ct}{2\mathrm{i}}Q_{\pm}\int_{S}\mathrm{d}x\left(\left\{\psi_{R}^{\dagger}(x),\nabla\theta_{\pm}(x)\right\}\psi_{S}(x)-\psi_{S}^{\dagger}(x)\left\{\psi_{R}(x),\nabla\theta_{\pm}(x)\right\}\right). \tag{3.54}$$

where the curly brackets denote the anti commutator. This expression is strikingly different from the particle current [Eq. (3.38)] in the sense that I_{+}^{E} and I_{-}^{E} are described by different operators and not simply by a change of prefactor. It is therefore essential to discuss partitioning at the level of the expectation value

$$\left\langle I_{\pm}^{E}\right\rangle = -\mathrm{i}\int_{-\infty}^{0}\mathrm{d}t'\left\langle\left[I_{\pm}^{E},H_{TR}(t')\right]\right\rangle, \tag{3.55}$$

which makes energy partitioning dependent on details of the tunneling state and therefore experimentally tunable. In similar steps as for the particle current the expectation value can be written as

$$\begin{aligned}\left\langle I_{\pm}^{E}\right\rangle = {} & \mp ct^{2}Q_{\pm}L_{S}\int_{-\infty}^{0}\mathrm{d}t'\int_{S}\mathrm{d}x' \\ & \Re\Bigg(\left\langle\left\{\psi_{R}^{\dagger}(0,0),\nabla\theta_{\pm}(0,0)\right\}\psi_{R}(x',t')\right\rangle\left\langle\psi_{S}(0,0)\psi_{S}^{\dagger}(x',t')\right\rangle\mathrm{e}^{\mathrm{i}t'eV} \\ & -\left\langle\psi_{R}(x',t')\left\{\psi_{R}^{\dagger}(0,0),\nabla\theta_{\pm}(0,0)\right\}\right\rangle\left\langle\psi_{S}^{\dagger}(x',t')\psi_{S}(0,0)\right\rangle\mathrm{e}^{\mathrm{i}t'eV}\Bigg).\end{aligned} \tag{3.56}$$

The more complicated expectation values that contain the bosonic and fermionic fields can be efficiently computed by writing $\psi_{R}^{\dagger}\sim\mathrm{e}^{-\mathrm{i}(Q_{+}A_{+}\nabla\theta_{+}+Q_{-}A_{-}\nabla\theta_{-})}$, in terms of formal derivatives with respect to the auxiliary operators $A_{\pm}=\nabla^{-1}$. Then by tracing the modifications due to $A_{\pm}$ in the standard calculation of the Luttinger liquid Green function [see Appendix A.2] we find that the resulting energy current can be written as

$$\begin{aligned}\left\langle I_{\pm}^{E}\right\rangle = {} & t^{2}\frac{Q_{\pm}^{2}}{K}L_{S}\int_{0}^{\infty}\mathrm{d}\omega_{q}\int\mathrm{d}k\int\mathrm{d}\omega A_{S}\left(k,\omega-eV\right) \\ & \times\Bigg\{A_{R}\left(k\mp q,\omega-\omega_{q}\right)\Big[\left\{1-f\left(\omega-\omega_{q}\right)\right\}f_{S}(\omega-eV) \\ & +n_{B}(\omega_{q})\left\{f_{S}(\omega-eV)-f\left(\omega-\omega_{q}\right)\right\}\Big] \\ & +A_{R}\left(k\pm q,\omega+\omega_{q}\right)\Big[f\left(\omega+\omega_{q}\right)\left\{1-f_{S}(\omega-eV)\right\} \\ & +n_{B}(\omega_{q})\left\{f\left(\omega+\omega_{q}\right)-f_{S}(\omega-eV)\right\}\Big]\Bigg\},\end{aligned} \tag{3.57}$$

where $n_{B}(\omega)=\left(\mathrm{e}^{\omega/T}-1\right)^{-1}$ is the Bose distribution function and we used $\omega_{q}=cq$. Eq. (3.57) is the main result of this section. At zero temperature it describes energy transfer

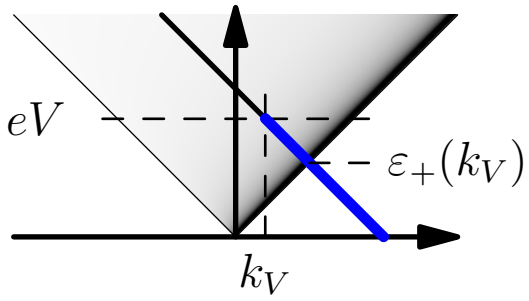

Figure 3.4: Overlap of the occupied states on the non-interacting source wire dispersion (blue) and the Luttinger liquid's spectral function (shaded background). The velocity of the source wire dispersion was chosen as $v_S = c$.

to the Luttinger liquid by spontaneous plasmon emission while tunneling into or out of the Luttinger liquid ($2^{\text{nd}}, 4^{\text{th}}$ line). At finite temperature the 3^{rd} and 5^{th} line capture stimulated plasmon emission as well as a possible cooling of the Luttinger liquid (negative energy current) via plasmon absorption. The structure of Eq. (3.57) is more involved than for the particle current because of an additional integral over the right- and left-moving plasmon modes that can be excited or annihilated during the tunneling process.

Non-interacting extended source

To elucidate the above result for the energy current we will now consider tunneling from a non-interacting source into the Luttinger liquid ($eV > 0$) at zero temperature. The spectral function of the source $A_S^{(0)}(k,\omega) = \delta\left(\omega - \varepsilon_k^S + eV\right)$ then simply replaces ω in Eq. (3.57) by the source's single particle dispersion ε_k^S measured relative to the Luttinger liquid's chemical potential μ. The corresponding differential energy current then takes the form

$$\frac{\mathrm{d}\left\langle I_\pm^{E(0)}\right\rangle}{\mathrm{d}(eV)} = t^2 \frac{Q_\pm^2}{K} L_S \int_0^{eV} \mathrm{d}\omega_q A_R\left(k_V \mp q, eV - \omega_q\right) , \tag{3.58}$$

which can be evaluated with the Luttinger liquid spectral function [see Eq. (2.55)] and indeed reproduces the result of the energy and momentum conservation argument (3.33)

$$\frac{\mathrm{d}\left\langle I_\pm^{E(0)}\right\rangle}{\mathrm{d}(eV)} = \frac{1}{2}\left(eV \pm ck_V\right)\frac{\mathrm{d}\left\langle I^{(0)}\right\rangle}{\mathrm{d}(eV)} . \tag{3.59}$$

The differential energy current $\mathrm{d}\left\langle I_\pm^{E(0)}\right\rangle/\mathrm{d}(eV)$ is therefore a direct probe for the energy partitioning of energy and momentum eigenstates. The overall energy current is then given by the average over all occupied states on the source wire's dispersion [see Fig. 3.4] weighted with their tunneling probability, which is controlled by the Luttinger liquid's spectral function. For voltages close to the threshold $eV = ck_V$ the left-moving energy current vanishes. Increasing the voltage then leads to more and more energy flowing to the left. Due to the fact that the spectral function only decays slowly with the distance

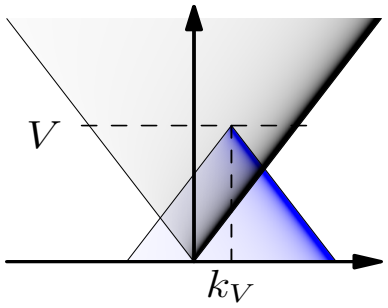

Figure 3.5: Overlap of the spectral functions of the source (blue) and drain (black) wire, focusing on the region where the source is occupied and drain is empty. The velocity of the source wire dispersion was chosen to $c_S = c$.

to the right-moving plasmon dispersion, it is even possible to reach the regime $I_-^E \gg I_+^E$. This can be illustrated by choosing a source dispersion $\varepsilon_k^S = 2\varepsilon_+(k_V) - ck$ which intersects the right-moving plasmon dispersion at energy $\varepsilon_+(k_V) = (V + ck_V)/2 = \varepsilon_+$ and is parallel to the left-moving plasmon dispersion [see Fig. 3.4]. The spectral function then becomes proportional to $(ck - \varepsilon_+)^{\gamma-1}\varepsilon_+^\gamma$ and the injected right-moving energy takes the k independent value $\varepsilon_+(k) = \varepsilon_+$ while $\varepsilon_-(k) = (ck - \varepsilon_+)$. Integrating over ck up to eV then yields

$$\frac{I_+^E}{I_-^E} = \frac{\varepsilon_+}{eV - \varepsilon_+}\frac{\gamma+1}{\gamma} = \frac{\varepsilon_+}{eV-\varepsilon_+}\frac{Q_+^2}{Q_-^2}\,. \tag{3.60}$$

The energy current ratio I_+^E/I_-^E can thus be tuned by the voltage to take in principle arbitrary values. Note that reaching the regime $I_+^E/I_-^E < 1$ requires higher and higher voltages if the interaction becomes weaker and $Q_- = 0$ indeed yields the non-interacting result of a vanishing left-moving energy current.

Interacting Luttinger liquid source

If the source wire is also an interacting Luttinger liquid, the energy current is controlled by the overlap of two Luttinger liquid spectral functions as depicted in Fig. 3.5. The finite broadening of the source's spectral functions leads to the fact that $\mathrm{d}\left\langle I_\pm^E\right\rangle/\mathrm{d}(eV)$ is not only probing the state at (k_V, eV) such that the differential energy current does not reproduce Eq. (3.59).

Making the source interacting does not introduce any qualitative changes in the behavior of the energy current. Specifically, the left-moving energy current is again enhanced by increasing V, while fixing the point where the mass shells of left- (source) and right-moving (drain) plasmons intersect. Setting the velocities and Luttinger parameters of source and drain wire equal, the energy currents read

$$\left\langle I_\pm^E\right\rangle = \frac{1}{2}\left(eV \pm ck_V\right)\frac{Q_\pm^2}{Q_+^2+Q_-^2}\left\langle I\right\rangle\,, \tag{3.61}$$

which shows that Eq. (3.60) also holds for an interacting source.

Local source

The energy currents in the case of a local injection of right-moving electrons can be directly read off from the nonlocal results of Eq. (3.57) by setting $t^2 L_S \to t_{\mathrm{loc}}^2$ and using the local form of the source's spectral function $A_S(k,\omega) \to A_S(\omega)$. The crucial difference to an extended source is that the integrals over the spectral functions then become independent of the direction of the transferred plasmon momenta q and the energy currents only differ by the prefactor $Q_\pm^2$, such that

$$\left\langle I_\pm^E \right\rangle = \frac{Q_\pm^2}{Q_+^2 + Q_-^2} \left\langle I^E \right\rangle . \tag{3.62}$$

Unlike for nonlocal injection, the local energy partitioning thus only depends on the interaction constant, but it is still distinctly different from the charge splitting. This difference can be traced to the fact that the charge density is linear in the Luttinger liquid fields, while the energy is quadratic. Note that also in contrast to charge partitioning, Eq. (3.62) only holds on the level of expectation values and is not an operator identity.

Local tunneling spectroscopies can be described by considering tunneling from a single energy level at ε_0. The total energy current then takes the simple form $\left\langle I^E \right\rangle = \varepsilon_0 \left\langle I^0 \right\rangle$, where $\left\langle I^0 \right\rangle$ is the local tunneling current given by Eq. (3.52).

3.3 Experimental consequences of energy partitioning

We now turn to experimental signatures of energy partitioning, emphasizing that unlike charge partitioning, it is not masked by the presence of Fermi liquid leads.

3.3.1 Local injection into quantum Hall edge states

The local injection of electrons with a definite chirality is in principle possible in quantum Hall systems as well as two dimensional topological insulators. In the latter, the edge states form a helical liquid [Wu *et al.* (2006)]. Helical liquids behave similarly to Luttinger liquids with the crucial difference that the right- and left-moving electrons have opposite spin. With a spin-polarized tunneling source, it is therefore possible to inject chiral electrons, which leads to partitioning effects as in a Luttinger liquid, due to the Coulomb interaction between the opposite spin directions [Das and Rao (2011)]. Energy partitioning can then be detected by measuring the different amounts of heat current that flow to the leads that are positioned right and left of the tunneling source.

The transferred heat to the leads may be addressed most conveniently in a quantum Hall geometry [see Fig. 3.6]. We consider two close-by quantum Hall edge states, which are coupled by the Coulomb interaction between them. Since tunneling depends exponentially on distance, it is possible to tunnel into only one of the edge modes, corresponding to only injecting only right-movers in the non-interacting case. Increasing the distance between the edges far from the tunneling source effectively switches off the interaction and leads to

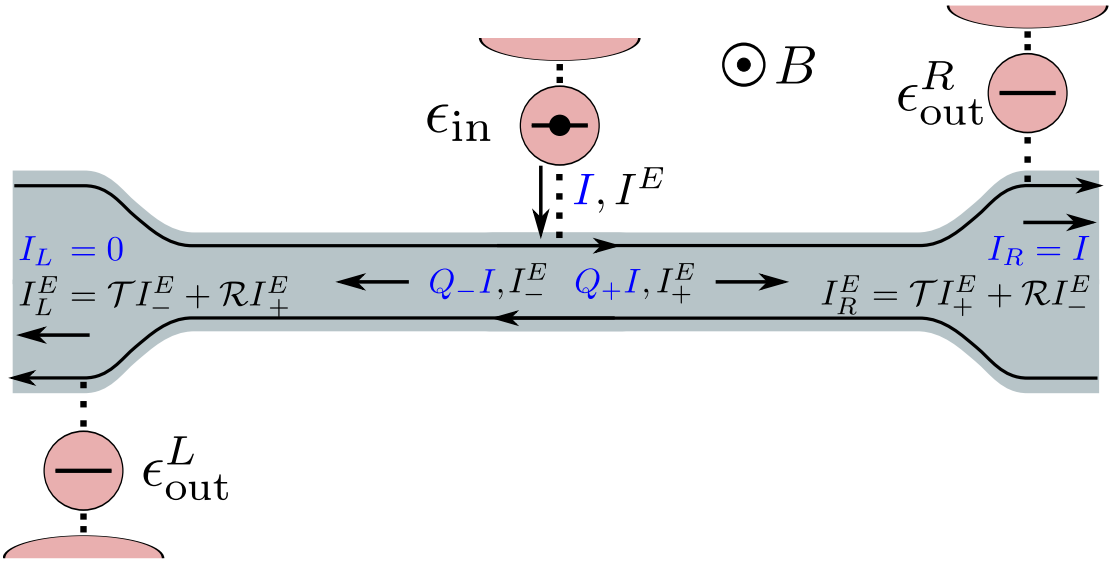

Figure 3.6: Local injection into one of two close-by quantum Hall edge channels. The figure indicates both the initial splitting of charge and energy at injection and the resulting splitting in the Fermi liquid leads.

backscattering of the charge currents [Berg *et al.* (2009)]. This is associated with the trivial charge partitioning as discussed in section 3.1.1.

On the other hand, the energy partitioning remains nontrivial after multiple reflections from the Luttinger-liquid-lead interfaces. These reflections only cause a quantitative change and the energy currents flowing into the right and left leads are $\mathcal{T} I^E_+ + \mathcal{R} I^E_-$ and $\mathcal{R} I^E_+ + \mathcal{T} I^E_-$, respectively. With the knowledge of the interface it is then possible to determine the original energy partitioning, even when measuring in the leads. For an interface which is smooth on the scale of the plasmon wavelength the reflections can be neglected completely because $\mathcal{T} = 1$ and $\mathcal{R} = 0$. Assuming the opposite limit, the injection energies are sufficiently small such that the Luttinger-liquid-lead interfaces can be treated as being abrupt, where we have $\mathcal{T} = 1/(1 + r_E)$ and $\mathcal{R} = r_E/(1 + r_E)$ [see Eq. (3.23)].

In the non-interacting region, it is possible to directly probe the electron distribution functions in the outgoing edge channels by tunneling spectroscopies [Altimiras *et al.* (2010a)] as indicated in Fig. 3.6. With the knowledge of the electron distribution function one can then deduce the different energy currents carried by the right- and left-moving modes.

3.3.2 Momentum conserved tunneling

Momentum conserved tunneling allows for an even more striking manifestation of the energy partitioning. For nonlocal injection, the right- and left-moving charge excitations have different maximal energies, given by $\varepsilon^R_{\text{max}} = (1/2)(eV + ck_V)$ and $\varepsilon^L_{\text{max}} = (1/2)(eV - ck_V)$ when injecting right-movers. Here, we assumed for definiteness that the source wire

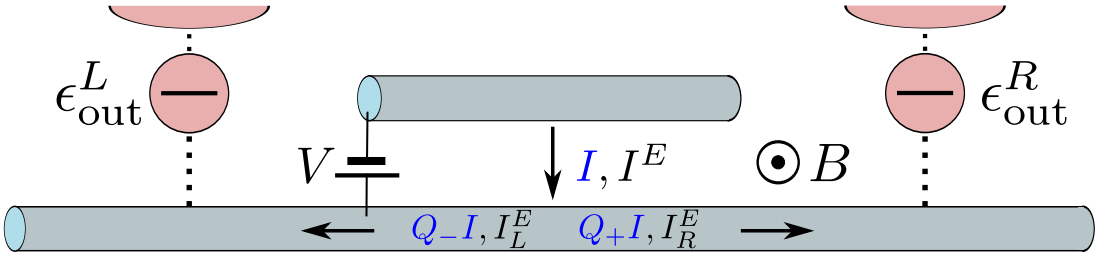

Figure 3.7: Nonlocal injection by momentum-conserving tunneling between parallel quantum wires. The quantum dots to the left and right of the injection region serve to probe the energy partitioning.

has a larger charge velocity than the lower wire. Note that these maximal energies remain valid even for an interacting source, *cf.* Fig. 3.5.

These results can be tested experimentally in some detail in the setup sketched in Fig. 3.7, in which the Luttinger liquid is probed by single-level quantum dots both to the left and to the right of the injection region. First, consider a long Luttinger liquid in the absence of Fermi liquid leads. In this case, the maximal energies of right- and left-moving excitations are directly observable as thresholds in the current flowing into the quantum dots. Indeed, current can flow into the quantum dots with gate-tunable dot level $\varepsilon^{R/L}_{\rm out}$ only as long as $\varepsilon^{R/L}_{\rm out} < \varepsilon^{R/L}_{\rm max}$.

In the vicinity of the threshold, the charge currents into the quantum dots will exhibit a power-law dependence on $\varepsilon^{R/L}_{\rm max} - \varepsilon^{R/L}_{\rm out}$. Extending the approach of Takei *et al.* (2010) to the nonlocal injection of electrons of definite chirality, we find for the injection of right-movers that [see section 3.4]

$$dI_R/dV \propto (\varepsilon^R_{\rm max} - \varepsilon^R_{\rm out})^{\gamma-1} \tag{3.63}$$

$$dI_L/dV \propto (\varepsilon^L_{\rm max} - \varepsilon^L_{\rm out})^{3\gamma-2\sqrt{\gamma(\gamma-1)}}, \tag{3.64}$$

where $I_{R/L}$ denote the charge currents into the right and left quantum dot. These results are valid for a noninteracting source. The presence of an interacting source modifies the form of the threshold exponents and we find in the case that the source and drain wires are identical ($K_S = K$, $c_S = c$) that

$$dI_R/dV \propto (\varepsilon^R_{\rm max} - \varepsilon^R_{\rm out})^{2\gamma-1} \tag{3.65}$$

$$dI_L/dV \propto (\varepsilon^L_{\rm max} - \varepsilon^L_{\rm out})^{4\gamma-2\sqrt{\gamma(\gamma-1)}+1}. \tag{3.66}$$

When taking the finite system size into account, the interfaces (of length d) will cause multiple reflections of energy currents for $\varepsilon^{R/L}_{\rm max} \ll c/d$. In this case, only the larger of the two thresholds can be directly probed experimentally. However, when the threshold energies are sufficiently large, $\varepsilon^{R/L}_{\rm max} \gg c/d$, energy reflection at the interfaces becomes negligible and both thresholds are directly accessible.

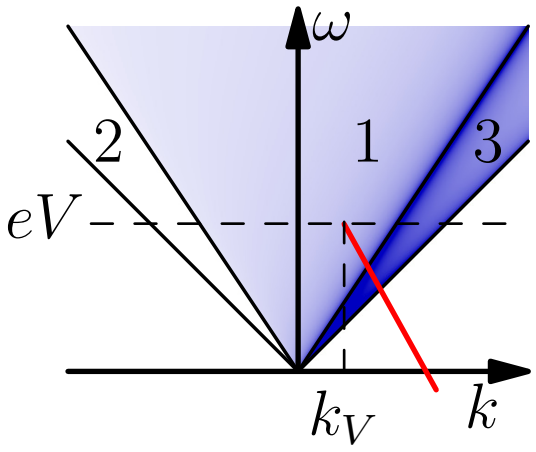

Figure 3.8: Overlap of the spectral function of a spin rotationally invariant Luttinger liquid (blue) with the occupied states of a non-interacting source wire (red). The main text discusses different energy thresholds depending on the position of (eV, k_V) with respect to the regions 1,2 and 3.

3.3.3 The spinful case

So far we have only considered the spin-polarized case. Spinful electrons introduce an additional degree of freedom such that the energy of tunneling particles can be used to excite charge and spin modes with velocities v_c and v_s. In a spin rotationally invariant system $v_s = v_F$ and it is not possible for a tunneling right-moving particle to excite a left-moving spin excitation [see Fig. 3.8]. With the three remaining modes, energy and momentum conservation [see Eq. (3.31)]

$$\varepsilon_{\text{in}} = v_c|k_{c+}| + v_c|k_{c-}| + v_F|k_{s+}| \tag{3.67}$$

$$k_{\text{in}} = k_{c+} + k_{c-} + k_{s+} \tag{3.68}$$

is not sufficient to fully determine the energy partitioning. It remains true that injecting close to the left-moving charge branch will create almost exclusively a left-moving energy current, and vice versa for injecting near the two right-moving branches. Thus, while the details of the injection process become more complicated the qualitative behavior remains the same as in the spinless case.

Also the presence of thresholds carries over to the case of a spin-degenerate system. We again assume for definiteness that the velocity of the source's dispersion is higher than v_c. Consider first the region with $eV > v_\rho|k_V|$ (region 1 in Fig. 3.8). Then, the right threshold ϵ^R_{max} remains the same as in the spinless case (with $c \to v_\rho$) while the left threshold becomes $\varepsilon^L_{\text{max}} = v_c(eV - v_s k_V)/(v_c + v_s)$ due to a process that excites a right-moving spin and a left-moving charge excitation. At lower voltages, $v_c|k_V| > eV > v_s|k_V|$, there is no tunneling for $k_V < 0$ (region 2), while we find $\varepsilon^R_{\text{max}} = \max\{v_c(eV - v_s k_V)/(v_c - v_s); v_s(eV + v_c k_V)/(v_c + v_s)\}$ and $\varepsilon^L_{\text{max}} = v_c(eV - v_s k_V)/(v_c + v_s)$ for $k_V > 0$ (region 3). The first term in $\varepsilon^R_{\text{max}}$ applies close to $eV = v_c k_V$ and is due to an excitation of a right-

moving charge and spin mode, while the second term leads to higher threshold energies close to $eV = v_s k_V$ and includes exciting a right-moving spin and left-moving charge mode. The latter process also determines the left-moving energy threshold $\varepsilon^L_{\max}$ for $k_V > 0$.

3.4 Quantum dot spectroscopy

In this section we calculate the tunneling current into a quantum dot (drain) that is located at a distance d to the right of the tunneling source. We will assume that $d \gg c/E_1$, where E_1 is the energy of the injected particle. In this regime there will be no tunneling process that couples source and drain directly. This limit was already considered by Takei *et al.* (2010) in the case of local tunneling of particles (without fixed chirality) within a Keldysh approach. We will first review the case of local tunneling but take [in contrast to Takei *et al.* (2010)] the limit $d \gg c/E_1$ already at the beginning which simplifies the calculation. The corresponding transport mechanism can then be imagined as an electron tunneling into the Luttinger liquid and splitting off into left- and right-moving eigenmodes. The latter then propagates ballistically to the right drain where it is extracted. Because transport is ballistic, the current is independent of d and we can set $d = 0$ in the course of the calculation. The important consequence of the large source drain distance is that we can assume that the left-moving excitations at the source and the right drain are decoupled.

3.4.1 Local injection

In the case of an occupied source and an empty drain (to the right of the source), the current is given by

$$I_{\alpha\beta}(t_1) = -|\eta_1|^2 |\eta_2|^2 \int \mathrm{d}t_2 \mathrm{d}t_3 \mathrm{d}t_4 \mathrm{e}^{\mathrm{i}E_2(t_1-t_2)} \mathrm{e}^{\mathrm{i}E_1(t_3-t_4)} \left\langle \psi_\beta(0,t_3)\psi^\dagger_\alpha(d,t_2)\psi_\alpha(d,t_1)\psi^\dagger_\beta(0,t_4)\right\rangle , \tag{3.69}$$

with $\alpha, \beta = R, L$ and η_1, η_2 are the tunnel couplings at the source and drain respectively. The times t_4 and t_3 belong to the source tunneling process, while t_1 and t_2 describe processes at the drain. The above formula can be deduced from [see Eq. (3.52)]

$$I_{\alpha\beta}(t_1) = |\eta_2|^2 \int \mathrm{d}t_2 \mathrm{e}^{\mathrm{i}E_2(t_1-t_2)} \left\langle \psi^\dagger_\alpha(d,t_2)\psi_\alpha(d,t_1)\right\rangle (1 - n_D(E_2)) , \tag{3.70}$$

which describes the tunneling current into a single energy level E_2 at the drain. The average is not taken with respect to the equilibrium ground state but in a state

$$\mathrm{e}^{-\mathrm{i}\int_0^{1/\eta_1} \mathrm{d}t \eta_1 \left(\psi^\dagger_\beta(0,t')\psi_S(t') + \mathrm{H.c.}\right)} |0\rangle \approx \left(1 - \mathrm{i}\eta_1 \int \mathrm{d}t' \psi^\dagger_\beta(0,t')\psi_S \mathrm{e}^{-\mathrm{i}E_1 t'}\right)|0\rangle \tag{3.71}$$

that is the result of an electron tunneling at the source. We then find Eq. (3.69) after setting $[1 - n_D(E_2)] = n_S(E_1) = 1$. To evaluate the four fermion correlator we use the holon operators [see Eq. (2.46); we omit the tilde in the notation of the holons for better

readability] that are the free quasi-particles of the Luttinger liquid

$$\psi_R^\dagger(x,t) = \left(\frac{1}{2\pi\lambda}\right)^{\frac{1}{2}} \mathrm{e}^{-\mathrm{i}k_F x} \left(\psi_+^\dagger(x,t)\right)^{\sqrt{\gamma+1}} \left(\psi_-^\dagger(x,t)\right)^{\sqrt{\gamma}} \tag{3.72}$$

$$\psi_L^\dagger(x,t) = \left(\frac{1}{2\pi\lambda}\right)^{\frac{1}{2}} \mathrm{e}^{\mathrm{i}k_F x} \left(\psi_+^\dagger(x,t)\right)^{\sqrt{\gamma}} \left(\psi_-^\dagger(x,t)\right)^{\sqrt{\gamma+1}}, \tag{3.73}$$

with $\sqrt{\gamma+1} = Q_+/\sqrt{K}$ and $\sqrt{\gamma} = Q_-/\sqrt{K}$. Now we will set $d = 0$ and drop the position dependence. In the following we treat the injection of right- and left-movers simultaneously by using α and β as $\sqrt{\gamma+1}$ for R and $\sqrt{\gamma}$ for L, when written as exponents while $\bar{\alpha}, \bar{\beta}$ denotes the opposite value (*i.e.* if $\alpha = \sqrt{\gamma+1}$ then $\bar{\alpha} = \sqrt{\gamma}$). Using the independence of the left-movers at the source and the right drain we then can write

$$\begin{aligned} &\left\langle \psi_\beta(t_3)\psi_\alpha^\dagger(t_2)\psi_\alpha(t_1)\psi_\beta^\dagger(t_4)\right\rangle \\ = &\left(\frac{\Lambda}{2\pi}\right)^2 \left\langle (\psi_+(t_3))^\beta \left(\psi_+^\dagger(t_2)\right)^\alpha (\psi_+(t_1))^\alpha \left(\psi_+^\dagger(t_4)\right)^\beta \right\rangle \\ &\times \left\langle (\psi_-(t_3))^{\bar{\beta}} \left(\psi_-^\dagger(t_4)\right)^{\bar{\beta}} \right\rangle \left\langle \left(\psi_-^\dagger(t_2)\right)^{\bar{\alpha}} (\psi_-(t_1))^{\bar{\alpha}} \right\rangle. \end{aligned} \tag{3.74}$$

The fields ψ are exponentials of free bosons, therefore we can use the independent boson theorem [see Eq. (2.50)] to find

$$\left\langle \psi_\pm^\alpha \psi_\pm^{\dagger\alpha} \right\rangle = \left\langle \psi_\pm \psi_\pm^\dagger \right\rangle^{\alpha^2}. \tag{3.75}$$

Then we can use the known Green's functions of the holons to find [see Eqs. (2.47,2.48)]

$$\left\langle (\psi_-(t_3))^{\bar{\beta}} \left(\psi_-^\dagger(t_4)\right)^{\bar{\beta}} \right\rangle \left\langle \left(\psi_-^\dagger(t_2)\right)^{\bar{\alpha}} (\psi_-(t_1))^{\bar{\alpha}} \right\rangle = G_{\bar{\beta}^2}^{>}(t_3-t_4) G_{\bar{\alpha}^2}^{<}(t_1-t_2), \tag{3.76}$$

where we defined $G_\alpha^{\gtrless}(t) = \left[G^{\gtrless}(0,t)\right]^\alpha$.

We now evaluate the four-right-mover correlator. For brevity we introduce the short form $\theta_i = \mathrm{i}\sqrt{K}\theta_+(0,t_i)$ for the exponent of the holon fields. Using the independent boson theorem we then find

$$\begin{aligned} &\left\langle (\psi_+(t_3))^\beta \left(\psi_+^\dagger(t_2)\right)^\alpha (\psi_+(t_1))^\alpha \left(\psi_+^\dagger(t_4)\right)^\beta \right\rangle \\ = &\left\langle \mathrm{e}^{\beta\theta_3} \mathrm{e}^{-\alpha\theta_2} \mathrm{e}^{\alpha\theta_1} e^{-\beta\theta_4} \right\rangle && (3.77) \\ = &\left\langle \mathrm{e}^{\beta\theta_3 - \alpha\theta_2 + \alpha\theta_1 - \beta\theta_4} \right\rangle \mathrm{e}^{\frac{\alpha\beta}{2}(-[\theta_3,\theta_2]-[\theta_1,\theta_4]+[\theta_3,\theta_1]+[\theta_2,\theta_4]) - \frac{\alpha^2}{2}[\theta_2,\theta_1] - \frac{\beta^2}{2}[\theta_3,\theta_4]} && (3.78) \\ = &\mathrm{e}^{\frac{1}{2}\left\langle(\beta\theta_3 - \alpha\theta_2 + \alpha\theta_1 - \beta\theta_4)^2\right\rangle} \mathrm{e}^{\frac{\alpha\beta}{2}(-[\theta_3,\theta_2]-[\theta_1,\theta_4]+[\theta_3,\theta_1]+[\theta_2,\theta_4]) - \frac{\alpha^2}{2}[\theta_2,\theta_1] - \frac{\beta^2}{2}[\theta_3,\theta_4]} && (3.79) \end{aligned}$$

Now we use

$$\begin{aligned}&(\beta\theta_3-\alpha\theta_2+\alpha\theta_1-\beta\theta_4)^2\\ =\;&\alpha\beta\left\{(\theta_3-\theta_2)^2+(\theta_1-\theta_4)^2-(\theta_3-\theta_1)^2-(\theta_2-\theta_4)^2\right\}+\alpha^2(\theta_2-\theta_1)^2+\beta^2(\theta_3-\theta_4)^2\end{aligned}\tag{3.80}$$

and

$$\mathrm{e}^{\frac{1}{2}\left\langle(\theta_3-\theta_2)^2\mp[\theta_3,\theta_2]\right\rangle}=\begin{cases}\left\langle\psi(t_3)\psi^\dagger(t_2)\right\rangle\\ \left\langle\psi^\dagger(t_2)\psi(t_3)\right\rangle\end{cases}\tag{3.81}$$

to obtain

$$\begin{aligned}&\left\langle(\psi_+(t_3))^\beta\left(\psi_+^\dagger(t_2)\right)^\alpha(\psi_+(t_1))^\alpha\left(\psi_+^\dagger(t_4)\right)^\beta\right\rangle\\ =\;&G^<_{\alpha^2}(t_1-t_2)G^>_{\beta^2}(t_3-t_4)\frac{G^<_{\alpha\beta}(t_2-t_3)G^>_{\alpha\beta}(t_1-t_4)}{G^<_{\alpha\beta}(t_1-t_3)G^>_{\alpha\beta}(t_2-t_4)}.\end{aligned}\tag{3.82}$$

We now define

$$\Pi^{<>}_{\alpha\beta}=\frac{G^<_{\alpha\beta}(t_2-t_3)G^>_{\alpha\beta}(t_1-t_4)}{G^<_{\alpha\beta}(t_1-t_3)G^>_{\alpha\beta}(t_2-t_4)}.\tag{3.83}$$

Finally using Eq. (3.69) and setting $t_1=0$ we find (note that $\alpha^2+\bar{\alpha}^2=2\gamma+1$)

$$\begin{aligned}I_{\alpha\beta}\;=\;&-|\eta_1|^2|\eta_2|^2\left(\frac{\Lambda}{2\pi}\right)^2\int \mathrm{d}t_2\mathrm{d}t_3\mathrm{d}t_4\mathrm{e}^{-\mathrm{i}E_2t_2}\mathrm{e}^{\mathrm{i}E_1(t_3-t_4)}\\ &\times\begin{cases}\Pi^{<>}_{\gamma+1} & (\alpha=R;\,\beta=R)\\ \Pi^{<>}_{\gamma'} & (\alpha=R;\,\beta=L)\ \text{or}\ (\alpha=L;\,\beta=R)\\ \Pi^{<>}_{\gamma} & (\alpha=L;\,\beta=L)\end{cases},\end{aligned}\tag{3.84}$$

which is indeed the leading order for the current calculated by Takei *et al.* (2010). The different cases in the above expression correspond to the choice of whether in injected particle at the source (α index) and the extracted particle at the right drain (β index) are right- or left-movers. The physical interpretation of the terms in Eq. (3.84) is that the Green's functions $G^{\lessgtr}$ give the tunneling density of states for injecting and extracting particles as the source and drain while Π describes the propagation along the wire.

For the case of injecting and extracting right-movers Eq. (3.84) takes the form

$$\begin{aligned}I_{RR}\;=\;&\int \mathrm{d}t\mathrm{d}\Delta t\mathrm{d}t_4\frac{\mathrm{e}^{-\mathrm{i}\left(E_1-\frac{\Delta E}{2}\right)\Delta t+\mathrm{i}\Delta Et}}{-4\pi^2/\Lambda^2}\left(\frac{\eta}{\eta+\mathrm{i}\left(t+\frac{\Delta t}{2}\right)}\right)^{2\gamma+1}\left(\frac{\eta}{\eta+\mathrm{i}\left(t-\frac{\Delta t}{2}\right)}\right)^{2\gamma+1}\\ &\times\left(\frac{\eta+\mathrm{i}\left(t+t_4-\frac{\Delta t}{2}\right)}{\eta+\mathrm{i}\left(t_4-\Delta t\right)}\right)^{\gamma+1}\left[\left(\frac{\eta+\mathrm{i}\left(t-t_4+\frac{\Delta t}{2}\right)}{\eta-\mathrm{i}t_4}\right)^{\gamma+1}-\left(\frac{\eta-\mathrm{i}\left(t-t_4+\frac{\Delta t}{2}\right)}{\eta+\mathrm{i}t_4}\right)^{\gamma+1}\right],\end{aligned}\tag{3.85}$$

where $\eta=1/\Lambda$ and $\Delta E=E_1-E_2$. The integral can be evaluated analytically in the limit $\Delta E\ll E_1$, which corresponds to tunneling close to the tunneling threshold. Note that as

mentioned above the threshold energy for tunneling out of the Luttinger liquid is the same as the total injected energy since we are dealing with local tunneling. Making repeated use of [3.382.7 in Gradshteyn and Ryzhik (2007)]

$$\int \mathrm{d}\Delta t \mathrm{e}^{-\mathrm{i}E_1\Delta t}\left(\frac{1}{\eta+\mathrm{i}\,(t_4-\Delta t)}\right)^{\gamma+1} = \frac{2\pi E_1^{\gamma}\mathrm{e}^{-\eta E_1-\mathrm{i}E_1 t_4}}{\Gamma\,(\gamma+1)}\,, \tag{3.86}$$

we then find

$$I_{RR} = -\frac{|\eta_1|^2\,|\eta_2|^2\,2\pi\,(\eta E_1)^{4\gamma}\left(\frac{\Delta E}{E_1}\right)^{2\gamma-1}}{c^2E_1\Gamma^2(\gamma+1)\Gamma\,(2\gamma)}\Theta(\Delta E)\,, \tag{3.87}$$

which indeed recovers the result by Takei *et al.* (2010) who considered local tunneling of particles without a fixed chirality. The reason why I_{RR} already describes the non-chiral local injection is that the other contributions

$$I_{RL} = I_{LR} = -\frac{|\eta_1|^2\,|\eta_2|^2\,2\pi\,(\eta E_1)^{4\gamma}\left(\frac{\Delta E}{E_1}\right)^{2(2\gamma-\gamma')+1}}{c^2E_1\Gamma^2(\gamma')\Gamma\,(4\gamma-2\gamma'+2)}\Theta(\Delta E) \tag{3.88}$$

$$I_{LL} = -\frac{|\eta_1|^2\,|\eta_2|^2\,2\pi\,(\eta E_1)^{4\gamma}\left(\frac{\Delta E}{E_1}\right)^{2\gamma+1}}{c^2E_1\Gamma^2(\gamma)\Gamma\,(2\gamma+2)}\Theta(\Delta E) \tag{3.89}$$

are subdominant close to $\Delta E = 0$. Here I_{RL} describes injection of right-movers and extraction of left-movers and we defined $\gamma' = \sqrt{\gamma(\gamma+1)}$. Having generalized the calculation of Takei *et al.* (2010) for a chiral local injection we now turn to non-local tunneling at the source.

3.4.2 Momentum resolved injection

We now consider the injection of a momentum eigenstate

$$\mathrm{e}^{-\mathrm{i}\int_0^{1/\eta_1}\mathrm{d}t\int_S\mathrm{d}x\eta_1\left(\psi_\beta^\dagger(x,t')\psi_S(x,t')+\mathrm{h.c.}\right)}|0\rangle \approx \left\{1-\mathrm{i}\int_0^{1/\eta_1}\mathrm{d}t\int_S\mathrm{d}x\eta_1\psi_\beta^\dagger(x,t')\psi_S(x,t')\right\}|0\rangle \tag{3.90}$$

with momentum k_1 at the source. This can be implemented by setting

$$\left\langle\psi_S^\dagger(x_3)\psi_S(x_4)\right\rangle = \frac{1}{L_S}\sum_k n_k\exp\left(-\mathrm{i}k_1(x_3-x_4)\right) \tag{3.91}$$

such that Eq. (3.69) is modified to

$$\begin{aligned} I_{\alpha\beta}(t_1) = &-|\eta_1|^2\,|\eta_2|^2\int\mathrm{d}t_2\mathrm{d}t_3\mathrm{d}t_4\int_S\mathrm{d}x_3\mathrm{e}^{\mathrm{i}E_2(t_1-t_2)}\mathrm{e}^{\mathrm{i}E_1(t_3-t_4)}\mathrm{e}^{-\mathrm{i}k_1x_3} \\ &\times\left\langle\psi_\beta(x_3,t_3)\psi_\alpha^\dagger(t_2)\psi_\alpha(t_1)\psi_\beta^\dagger(t_4)\right\rangle. \end{aligned} \tag{3.92}$$

The calculation then follows the same steps as for the local injection with the difference that we now need to distinguish the right and left-moving Greens functions

$$\mathrm{i}G(x,t)_{\beta}^{\pm>} = \frac{1}{2\pi\lambda}\left(\frac{\eta}{\eta+\mathrm{i}\left(t\mp\frac{x}{c}\right)}\right)^{\beta} \tag{3.93}$$

such that

$$\begin{aligned}\left\langle\psi_\beta(x_3,t_3)\psi_\alpha^\dagger(t_2)\psi_\alpha(t_1)\psi_\beta^\dagger(t_4)\right\rangle &= \mathrm{e}^{\pm\mathrm{i}k_F x}G_{\alpha^2}^{<}(t_1-t_2)G_{\beta^2}^{>}(t_3-t_x-t_4) \\ &\times\frac{G_{\alpha\beta}^{<}(t_2-t_3+t_x)\,G_{\alpha\beta}^{>}(t_1-t_4)}{G_{\alpha\beta}^{<}(t_1-t_3+t_x)\,G_{\alpha\beta}^{>}(t_2-t_4)}G_{\bar\beta^2}^{>}(t_3+t_x-t_4)\,G_{\bar\alpha^2}^{<}(t_1-t_2)\end{aligned} \tag{3.94}$$

where the $\pm$ sign in front of k_F corresponds to the extraction of right- and left-movers and we defined $t_x = x/c$. Measuring all momenta with respect to k_F, we can set $k_F = 0$. Shifting $t_3 \to t_3 + t_x$ we then find

$$\begin{aligned}I_{\alpha\beta} &= |\eta_1|^2\,|\eta_2|^2\int_S \mathrm{d}x\int \mathrm{d}t_2\mathrm{d}t_3\mathrm{d}t_4\frac{\mathrm{e}^{\mathrm{i}E_1(t_3-t_4)-\mathrm{i}E_2t_2}\mathrm{e}^{\mathrm{i}(E_1-ck_1)t_x}}{-4\pi^2/\Lambda^2}\left(\frac{\eta}{\eta+\mathrm{i}t_2}\right)^{2\gamma+1} \\ &\times\left(\frac{\eta}{\eta+\mathrm{i}\,(t_3-t_4)}\right)^{\beta^2}\left(\frac{\eta}{\eta+\mathrm{i}\,(t_3+2t_x-t_4)}\right)^{\bar\beta^2}\left(\frac{\eta+\mathrm{i}t_3}{\eta+\mathrm{i}\,(t_3-t_2)}\right)^{\alpha\beta}\left(\frac{\eta+\mathrm{i}\,(t_2-t_4)}{\eta-\mathrm{i}t_4}\right)^{\alpha\beta}.\end{aligned} \tag{3.95}$$

Now we introduce the right- and left-moving injected energies $\varepsilon_\pm = (E_1 \pm ck_1)/2$. Similar to the case of local injection the integrals can be performed close to the out-tunneling threshold given by ε_+ because we consider the drain to be to the right of the tunneling source. The result reads

$$I_{\alpha\beta} = -|\eta_1|^2\,|\eta_2|^2\,E_2^{2\alpha\beta-2}\varepsilon_-^{\bar\beta^2-1}\frac{2\pi^2\eta^{4\gamma}\,(\varepsilon_+-E_2)^{2\gamma+\beta^2-2\alpha\beta}\,\Theta\,(\varepsilon_+-E_2)}{c\Gamma\left(\bar\beta^2\right)\Gamma^2\left(\alpha\beta\right)\Gamma\left(2\gamma+1+\beta^2-2\alpha\beta\right)}. \tag{3.96}$$

Specifically, we find

$$I_{RR} = -|\eta_1|^2|\eta_2|^2E_2^{2\gamma}\varepsilon_-^{\gamma-1}\,(\varepsilon_+-E_2)^{\gamma-1}\frac{2\pi^2\eta^{4\gamma}\Theta\,(\varepsilon_+-E_2)}{c\Gamma^2\,(\gamma)\,\Gamma^2\,(\gamma+1)} \tag{3.97}$$

$$I_{RL} = -|\eta_1|^2|\eta_2|^2E_2^{2\gamma'-2}\varepsilon_-^{\gamma-1}\,(\varepsilon_+-E_2)^{3\gamma+1-2\gamma'}\frac{2\pi^2\eta^{4\gamma}\Theta\,(\varepsilon_+-E_2)}{c\Gamma\,(\gamma)\,\Gamma^2\,(\gamma')\,\Gamma\,(3\gamma+2-2\gamma')} \tag{3.98}$$

$$I_{LR} = -|\eta_1|^2|\eta_2|^2E_2^{2\gamma'-2}\varepsilon_-^{\gamma}\,(\varepsilon_+-E_2)^{3\gamma-2\gamma'}\frac{2\pi^2\eta^{4\gamma}\Theta\,(\varepsilon_+-E_2)}{c\Gamma\,(\gamma+1)\,\Gamma^2\,(\gamma')\,\Gamma\,(3\gamma+1-2\gamma')} \tag{3.99}$$

$$I_{LL} = -|\eta_1|^2|\eta_2|^2E_2^{2\gamma-2}\varepsilon_-^{\gamma}\,(\varepsilon_+-E_2)^{\gamma}\frac{2\pi^2\eta^{4\gamma}\Theta\,(\varepsilon_+-E_2)}{c\Gamma^2\,(\gamma)\,\Gamma^2\,(\gamma+1)}, \tag{3.100}$$

with $\gamma' = \sqrt{\gamma(\gamma+1)}$. This gives a formal derivation that the threshold is indeed given by the initial energy partitioning because the above expressions vanish for $E_2 > \varepsilon_+$. Note that although we only considered extraction to the right of the source we can apply the

results to extracting to the right and left of the source by the reflection symmetry of the problem. For example, the current for injecting a left-mover and extracting a right-mover at the right drain is the same as for injecting a right-mover and extracting a left-mover at the left drain. If we then take only the leading order contribution close to the threshold we obtain Eqs. (3.63,3.64) of the section above.

3.4.3 Interacting source

The above calculation can also be generalized to an interacting source. Is this case differential conductance measurements cannot address a single momentum eigenstate. We therefore have to integrate Eq. (3.96) over different possible k_1 and E_1 weighted by the source wire spectral function. If we assume $c_S = c$ we then find

$$I_{\alpha\beta} \propto \int_{E_2}^{\varepsilon_+^V} \mathrm{d}\omega_+ \int_0^{\varepsilon_-^V} \mathrm{d}\omega_- \left(\varepsilon_+^V - \omega_+\right)^{2\gamma-\beta^2} \left(\varepsilon_-^V - \omega_-\right)^{2\gamma-\bar{\beta}^2} E_2^{2\alpha\beta-2} \omega_-^{\bar{\beta}^2-1} (\omega_+ - E_2)^{2\gamma+\beta^2-2\alpha\beta} \quad (3.101)$$

$$\propto E_2^{2\alpha\beta-2} \left(\varepsilon_-^V\right)^{2\gamma} \left(\varepsilon_+^V - E_2\right)^{4\gamma-2\alpha\beta+1} , \quad (3.102)$$

with $\varepsilon_\pm^V = (eV \pm ck_V)/2$ and the spectral function in Eq. (2.55). [Note that $2\gamma - \beta^2$ is just a general way of writing $\gamma - 1$ or γ depending on the chirality of the injected particles.] The leading order result close to the tunneling threshold then yields Eqs. (3.65,3.66). Interestingly, the threshold exponents for the momentum resolved injection from a source with $c_S = c$ are the same as for a local injection from a noninteracting source. We already encountered this coincidence in Eq. (3.61), which states that the energy partitioning of such an interacting source is the same as for a local noninteracting source that injects right- and left-movers at different energies $\varepsilon_\pm^V = (eV \pm ck_V)/2$.

3.5 Conclusions

While energy and charge of an injected electron travel together in a noninteracting system, this is no longer the case in the presence of interactions. This decoupling is especially peculiar in one dimensional systems, where it is not possible to distinguish between collective plasmon and single quasi-particle excitations. The strong correlations in a Luttinger liquid lead to fractional excitations, which are deeply connected to the charge partitioning ratio when injecting particles with a well-defined chirality.

In this chapter we showed that energy partitioning is distinctly different from charge partitioning. Although it also relies on strong interactions it does not depend on the Luttinger parameter K alone. In fact it is crucially controlled by the state of the injected electron and one may even reach conditions such that charge and energy of an injected particle propagate in opposite directions.

While charge partitioning cannot be measured in dc setups due to backscattering effects at the weakly interacting Fermi liquid leads, we showed that this is possible for energy

partitioning. Importantly, this allows for direct experimental probes of energy partitioning and we presented several possible setups for this.

4 Curvature induced relaxation in quantum wires

A finite curvature of the electron dispersion leads to a breakdown of the integrability of the Luttinger model, which allows for true thermalization in clean one dimensional electron systems. A tremendous theoretical progress in the description of one dimensional systems beyond the Luttinger paradigm has increased our understanding of the effects of the curvature of the dispersion, as reviewed by Imambekov *et al.* (2011). It turns out that it is most promising to employ a description in terms of the fermionic picture to avoid the divergences that plague a perturbative treatment of the curvature in the bosonic language [Samokhin (1998)].

Fermionic theories of one dimensional systems can be categorized in two complementary approaches, one relying on a perturbative treatment in terms of the original electrons and the other based on a refermionization of the Luttinger Hamiltonian. Refermionization maps the non-interacting bosonic Luttinger model back to non-interacting Fermions. The resulting non-interacting fermionic quasi-particles (holons and spinons, see section 2.2.2) cannot be probed directly but represent a valuable theoretical tool. The finite curvature introduces an interaction between these quasi-particles, which can be modeled phenomenologically [Imambekov and Glazman (2009a,b); Schmidt *et al.* (2010a,b)]. Curvature thus leads to a decay of the quasi-particles, which sets an upper bound $\varepsilon < mv_F V_0$ for the holon energy beyond which the holon and spinon modes are no longer well-defined. Here V_0 is the $q = 0$ component of the (Fourier transformed) Coulomb interaction.

For higher energies it is possible to work perturbatively in the interaction between the original electrons. This can be understood by the following argument. Consider an electron injected into a quantum wire with an excitation energy ε above the Fermi energy ε_F. Due to the quadratic dispersion $\varepsilon_k = k^2/2m$, its velocity differs from that of the electrons in the Fermi sea by at least $\Delta v = \varepsilon/mv_F$. (Here, v_F is the Fermi velocity.) According to the standard condition for the validity of the Born approximation in quantum mechanics [Landau and Lifshitz (1977)] we therefore expect a perturbative approach to be appropriate when $\varepsilon \gg mv_F V_0$. Note that this exactly complements the limit of the refermionization approaches and from the point of view of Luttinger liquid theory, this condition ensures that the original electrons retain their integrity during the collision process. Indeed, at weak coupling the difference between the spin and charge velocities of the Luttinger liquid is $v_c - v_s \simeq V_0/\pi$ [see Eq. (2.27)], so that the condition can be recast as $v_c - v_s \ll \Delta v$. Hence, spin and charge do not separate appreciably during the collision

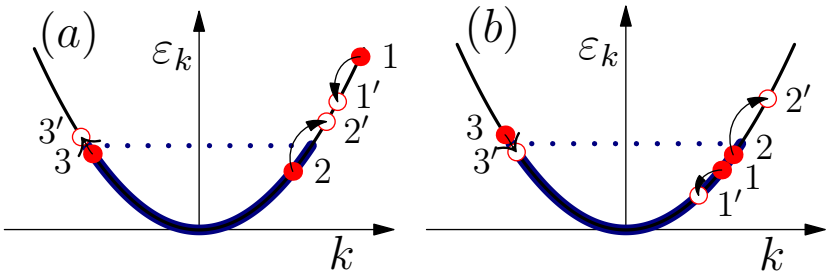

Figure 4.1: Three-body relaxation process for (a) particle and (b) hole excitations. Note that hole relaxation is not allowed at $T = 0$.

process.

This weak interaction approaches were previously applied to study curvature induced corrections to the conductance and thermopower [Lunde *et al.* (2007); Rech and Matveev (2008); Rech *et al.* (2009); Levchenko *et al.* (2011a,b)].

Here we focus on energy relaxation of hot electrons in quantum wires [based on Karzig *et al.* (2010)][1] aiming for an understanding of the experiment by Barak *et al.* (2010b) [see section 1.1.1] that observes a strong asymmetry in the relaxation behavior of particle and hole excitations. It will turn out that quantitative agreement between theory and experiment requires to take both the long range Coulomb interaction and the spin of the electrons into account, which has not been considered in previous approaches.

4.1 Basics of three-body scattering

The relaxation of hot particle and hole excitations in the weakly interacting limit is described by three-body processes [see Lunde *et al.* (2007) and section 1.1.2]. The asymmetry in energy relaxation between hot particles and holes can be readily understood from the basic three-body collisions as sketched in Fig. 4.1a. Suppose a hot particle 1 on, say, the right-moving branch transfers momentum $q_1 = k_{1'} - k_1$ to a right-mover in the Fermi sea. Due to the positive curvature of the dispersion relation, the energy loss $\Delta\varepsilon$ of the hot particle exceeds the energy of the created particle-hole pair. This mismatch can be fixed by simultaneously exciting a left-moving particle-hole pair. In line with the energy mismatch, the energy transfer to the left-moving particle-hole pair is of order $(\varepsilon/\varepsilon_F)\Delta\varepsilon$, while the typical energy loss $\Delta\varepsilon$ of the hot particle in a single three-body collision is of order ε.

Compare this with the relaxation of hot holes sketched in Fig. 4.1b, where for a given momentum transfer the energy gain due to filling the hole by a higher-energy electron is smaller than the energy cost of exciting a co-moving particle-hole pair. Fixing this energy mismatch is therefore possible only if a counter-propagating electron gives up energy. Clearly, the Pauli principle forbids such a process at zero temperature and the hole is unable to relax. Indeed, this conclusion remains true for arbitrary n-body processes [Barak

[1] See also related works by Levchenko *et al.* (2010); Micklitz and Levchenko (2011)

et al. (2010b)].

Hot holes do however relax at finite temperatures. Due to thermal smearing, the counter-propagating electron can give up an energy of order T. Thus, the hot hole can relax its energy, with a maximal energy loss of $\Delta\varepsilon \sim \varepsilon_F T/\varepsilon$. This implies that hot holes float towards the Fermi energy in many small steps as long as $\varepsilon \gg \varepsilon_T$. Here, $\varepsilon_T = \sqrt{\varepsilon_F T}$ is a new characteristic energy scale introduced by finite temperature. Conversely, for $\varepsilon \ll \varepsilon_T$, the energy loss of the hole per three-body collision would be comparable to its energy.

Although hot particles always relax in a small number of three-body collisions, the energy scale ε_T is also relevant in this case. Indeed, for $\varepsilon \ll \varepsilon_T$, the energy transfer to the counter-propagating particle-hole pair is small compared to temperature. This has two important consequences. First, the phase space of the left-moving particle-hole pair is no longer controlled by the typical energy transfer $\varepsilon^2/\varepsilon_F$ but by temperature T so that the energy relaxation rate of hot particles becomes temperature dependent. Second, it is no longer relevant whether the counter-propagating electron gains or loses energy so that for $\varepsilon \ll \varepsilon_T$, energy relaxation becomes equally fast for hot particles and holes.

Before entering the details of the derivation we summarize the results for the relaxation rate in the different energy regimes. The energy relaxation rate of hot particles is given by

$$\frac{1}{\tau_\mathrm{p}} = \frac{9\varepsilon_F}{32\pi^3}\left(\frac{e^2}{\epsilon v_F}\right)^4 \left[\ln\left|\frac{1}{2k_F a}\right| \ln\left|\frac{\varepsilon}{4\varepsilon_F}\right|\right]^2 \left(\frac{\varepsilon}{\varepsilon_F}\right)^2 \tag{4.1}$$

at high energies $\varepsilon \gg \varepsilon_T$. Here e and ϵ are the electron charge and the dielectric constant, respectively while a denotes the width of the wire and k_F the Fermi momentum with $k_F a \ll 1$. Note that the $(\varepsilon/\varepsilon_F)^2$ dependence is only accidentally similar to the Fermi liquid result. It stems from a cancellation of a factor $(\varepsilon/\varepsilon_F)^2$ by the energy denominator of the second order perturbation theory. This additional enhancement is absent in the spinless case which then yields an overall $(\varepsilon/\varepsilon_F)^4$ dependence.

As mentioned above the relaxation becomes temperature dependent in the low energy regime $\varepsilon \ll \varepsilon_T$ and takes the form

$$\frac{1}{\tau_\mathrm{p}} = \frac{1}{\tau_\mathrm{h}} = \frac{3\,(4\ln(2)-1)}{4\pi^3}\varepsilon_F \left(\frac{e^2}{\epsilon v_F}\right)^4 \left[\ln\left|\frac{1}{2k_F a}\right| \ln\left|\frac{\varepsilon}{4\varepsilon_F}\right|\right]^2 \left(\frac{T}{\varepsilon_F}\right), \tag{4.2}$$

which is identical for particles and holes in this regime. For $\varepsilon \gg \varepsilon_T$, the hole relaxation rate is further suppressed by a factor of $(\varepsilon_T/\varepsilon)^2$ such that

$$\frac{1}{\tau_\mathrm{h}} = \frac{2\varepsilon_F}{\pi}\left(\frac{e^2}{\epsilon v_F}\right)^4 \left[\ln\left|\frac{1}{2k_F a}\right| \ln\left|\frac{\varepsilon}{4\varepsilon_F}\right|\right]^2 \left(\frac{T}{\varepsilon}\right)^2. \tag{4.3}$$

In the high energy regime the hole relaxation is therefore (at a comparable excitation energy) by a factor $(\varepsilon_T/\varepsilon)^4$ smaller than $1/\tau_\mathrm{p}$. The relevant thermalization rate for the entire distribution function is thus always controlled by the slower hole relaxation processes. Note that this even holds for injecting hot particles, since the relaxation of high-energy

particles necessarily involves the excitation of deep holes.

4.2 Calculation of the relaxation rates

The above relaxation rates are calculated within the Boltzmann equation approach by considering an electron distribution function $n = n^0 + \delta n$, which is perturbed from its equilibrium form n^0 by the injection of a hot particle into the wire. The full Boltzmann equation for a homogeneous wire

$$\partial_t n(k_1, \sigma_1) = \partial_t n(k_1, \sigma_1)\Big|_{\text{coll}} \tag{4.4}$$

then describes the equilibration of the distribution due to collisions between the electrons. Since two-particle scattering is ineffective in changing the distribution function in the presence of energy and momentum conservation the collision integral is dominated by three-body processes

$$\begin{aligned} \partial_t n_1\Big|_{\text{coll}} \;=\; & -\sum_{\text{states}} W_{123,1'2'3'}\big[n_1 n_2 n_3 (1-n_{1'})(1-n_{2'})(1-n_{3'}) \\ & -n_{1'} n_{2'} n_{3'} (1-n_1)(1-n_2)(1-n_3)\big]\,. \end{aligned} \tag{4.5}$$

Here, the index i stands for (k_i, σ_i) and the sum goes over all initial states of particles 2 and 3, as well as over all possible final states $(1', 2', 3')$. The equilibrium distribution function n^0 is a stationary solution of the Boltzmann equation, which leads to a vanishing collision integral (detailed balance). Expanding to first order in the perturbation δn away from equilibrium one obtains

$$\begin{aligned} \partial_t(\delta n_1)\Big|_{\text{coll}} \;=\; & -\sum_{\text{states}} W_{123,1'2'3'} n_1^0 n_2^0 n_3^0 (1-n_{1'}^0)(1-n_{2'}^0)(1-n_{3'}^0)\left[\frac{\delta n_1}{n_1^0(1-n_1^0)}\right. \\ & \left. +\frac{\delta n_2}{n_2^0(1-n_2^0)}+\frac{\delta n_3}{n_3^0(1-n_3^0)}-\frac{\delta n_{1'}}{n_{1'}^0(1-n_{1'}^0)}-\frac{\delta n_{2'}}{n_{2'}^0(1-n_{2'}^0)}-\frac{\delta n_{3'}}{n_{3'}^0(1-n_{3'}^0)}\right]. \end{aligned} \tag{4.6}$$

Even in this linearized form, solving the Boltzmann equation is still a hard problem and exact solutions can only be obtained in some special cases [see *e.g.* Micklitz and Levchenko (2011) who consider spinless electrons]. The difficulty comes with the fact that Eq. (4.6) does not only describe the relaxation of the injected hot particle but also all the secondary particle and hole excitations that are created during the equilibration process. In the following we will restrict the attention on the initial out-scattering rate of the injected hot particle. This can be done by setting (k_1, σ_1) at the momentum and spin of the injected hot electron and considering the initial time $t = 0$, where δn vanishes for all $2, 3, 1', 2', 3' \neq 1$. In the relaxation time approximation $\partial_t(\delta n_1) = -\delta n_1 / \tau_{\text{p}}^{\text{out}}$ we define the out-scattering

rate as

$$\frac{1}{\tau_{\mathrm{p}}^{\mathrm{out}}} = \frac{1}{2} \sum_{k_2 k_3 q_1 q_2 q_3} \sum_{\sigma_2 \sigma_3 \sigma_{1'} \sigma_{2'} \sigma_{3'}} W_{123,1'2'3'} n_2^0 n_3^0 (1 - n_{1'}^0)(1 - n_{2'}^0)(1 - n_{3'}^0) \,. \tag{4.7}$$

Here, $q_i = k_{i'} - k_i$ and we replaced the abstract sum over states as sums over the quantum numbers $i = (k_i, \sigma_i)$ and used the convention that the particles at $1', 2, 2'$ lie on the right-moving branch while 3 and $3'$ are left-movers [see Fig. 4.1]. The factor of $1/2$ then accounts for double counting because exchanging $1'$ and $2'$ does lead to the same final state.

The three-body matrix element $W_{123,1'2'3'}$ describes the transition probability from a state $|123\rangle = c^\dagger_{k_1\sigma_1} c^\dagger_{k_2\sigma_2} c^\dagger_{k_3\sigma_3} |0\rangle$ to $|1'2'3'\rangle$ (where $c^\dagger_{k\sigma}$ creates a particle with momentum k and spin σ relative to the vacuum $|0\rangle$) and can be calculated from the generalized Fermi golden rule expression

$$W_{123,1'2'3'} = 2\pi |\langle 1'2'3'|VG_0(E_i)V|123\rangle_c|^2 \delta(E_i - E_f) \,. \tag{4.8}$$

The subscript c means connected in the sense that it excludes effectively two-particle processes which do not contribute to relaxation. G_0 and V are the free propagator and the interaction part of the Hamiltonian $V = H - H_0$, respectively. They take the form

$$G_0(E_i) = \frac{1}{E_i - H_0 + \mathrm{i}0^+} \,, \tag{4.9}$$

$$V = \frac{1}{2L} \sum_{k_1 k_2 q \sigma_1 \sigma_2} V_q c^\dagger_{k_1+q\sigma_1} c^\dagger_{k_2-q\sigma_2} c_{k_2\sigma_2} c_{k_1\sigma_1} \,. \tag{4.10}$$

Note that the corresponding hole relaxation rate is determined by the same matrix element $W_{123,1'2'3'}$. Hole relaxation takes place when a particle at state 1 scatters into the hole at $1'$ [see Fig. 4.1]. With the same notation as for the particles, the hole out-scattering rate is thus given by

$$\frac{1}{\tau_{\mathrm{h}}^{\mathrm{out}}} = \frac{1}{2} \sum_{k_2 k_3 q_1 q_2 q_3} \sum_{\sigma_2 \sigma_3 \sigma_{1'} \sigma_{2'} \sigma_{3'}} W_{123,1'2'3'} n_1^0 n_2^0 n_3^0 (1 - n_{2'}^0)(1 - n_{3'}^0) \,. \tag{4.11}$$

4.2.1 The Coulomb interaction in one dimension

We now discuss the form of the Coulomb matrix element V_q in one dimensional systems. In the long wavelength limit $qa \ll 1$ (where a is the width of the wire), V_q does not depend on details of the transverse wave function of the electrons. It is then possible to determine V_q by taking the Fourier transform of

$$V(r) = \frac{e^2}{\epsilon \sqrt{r^2 + a^2}} \,. \tag{4.12}$$

The additional a^2 term in the denominator introduces a small distance cutoff beyond which the one dimensional approximation breaks down. While internal screening in one

dimensional systems is weak, the Coulomb interaction will eventually be screened by external gates. Modeling the gates as metal plates, the presence of a charge e in the wire induces a mirror charge at distance $2d$, where d is the distance to the gate. Thus V_q takes the form

$$V_q = \frac{2e^2}{\epsilon}\int_0^\infty \mathrm{d}r \left[\frac{1}{\sqrt{r^2+a^2}} - \frac{1}{\sqrt{r^2+(2d)^2}}\right]\cos(qr) \tag{4.13}$$

$$= \frac{2e^2}{\epsilon}\left[K_0(|q|a) - K_0(2|q|d)\right], \tag{4.14}$$

where we used

$$\int_0^\infty \mathrm{d}x \frac{\cos(qx)}{\sqrt{x^2+a^2}} = K_0\left(|qa|\right), \tag{4.15}$$

in terms of the modified Bessel function K_0. We can then use the well-known asymptotic expansion

$$K_0(z) = \begin{cases} -\ln\left(\frac{z}{2}\right) - \gamma + \frac{z^2}{4}\left(-\ln\left(\frac{z}{2}\right) - \gamma + 1\right) & , z \ll 1 \\ \sqrt{\frac{\pi}{2z}}\mathrm{e}^{-z} & , z \gg 1 \end{cases} \tag{4.16}$$

[Abramowitz and Stegun (1964) (chapters 9.6 and 9.7), $\gamma \approx 0.577$ is the Euler-Mascheroni constant] to find an approximate description of V_q in different screening regimes. The result reads in leading logarithmic order

$$V_q = \frac{2e^2}{\epsilon}\begin{cases} \ln\left|\frac{1}{qa}\right| & , qd \gg 1 \\ \ln\left|\frac{2d}{a}\right|\left(1 - \left(\frac{q}{q_0}\right)^2\right) & , qd \ll 1 \end{cases} \tag{4.17}$$

$$q_0(q) = \frac{1}{d}\sqrt{\frac{\ln\left|\frac{2d}{a}\right|}{\ln\left|\frac{1}{qd}\right|}}. \tag{4.18}$$

In the unscreened case ($qd \gg 1$), the Fourier transform V_q diverges logarithmically for $q \to 0$ due to the long range nature of the Coulomb interaction. This divergence is cut off at a scale $q \sim 1/d$ and the screening dominated regime ($qd \ll 1$) yields a typical short range interaction (of the type $1 - q^2$).[2]

4.2.2 The three-body matrix element

The description of the three-body matrix element $W_{123,1'2'3'}$ is the central part of a calculation of the relaxation rate. A brute force calculation of $W_{123,1'2'3'}$ can quickly become laborious because it consists of $36^2 = 1296$ terms after taking the square of the amplitudes $\langle 1'2'3'|VG_0(E_i)V|123\rangle_c$ due to the various virtual processes contributing in second order perturbation theory as well as possible exchange terms. It is thus crucial combine as

[2] Note that the slow logarithmic dependence of $q_0(q)$ can usually be ignored by setting $q_0 = q_0(\bar{q})$, where $\bar{q}$ is a typical momentum transfer of the problem

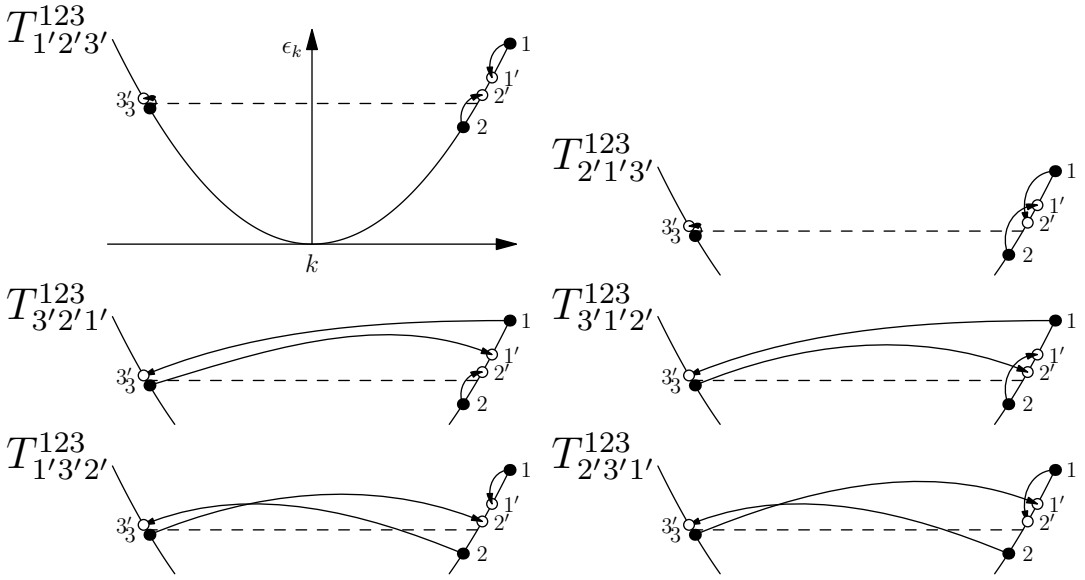

Figure 4.2: Schematic illustration of the six amplitudes $T^{123}_{\mathcal{P}(1'2'3')}$ that contribute to the three-body matrix element.

many terms as possible before finally taking the square. To this end Lunde *et al.* (2007) introduced the following decomposition

$$\langle 1'2'3'|VG_0V|123\rangle_c = \sum_{\mathcal{P}}(-1)^p \delta^{\sigma(123)}_{\sigma\mathcal{P}(1'2'3')} T^{123}_{\mathcal{P}(1'2'3')} \,. \tag{4.19}$$

Here p denotes the parity of the six possible permutations $\mathcal{P}$ of the final states $1'2'3'$ and $\delta^{\sigma(123)}_{\sigma\mathcal{P}(1'2'3')}$ results from permutations of $\delta^{\sigma(123)}_{\sigma(1'2'3')} = \delta_{\sigma_1,\sigma_{1'}}\delta_{\sigma_2,\sigma_{2'}}\delta_{\sigma_3,\sigma_{3'}}$. The amplitudes $T^{123}_{\mathcal{P}(1'2'3')}$ include the momentum conservation $\delta_{q_1+q_2+q_3,0}$ which can be used to eliminate q_2 from the momentum summation. Using additionally the energy conservation condition

$$2\,(k_1q_1 + k_2q_2 + k_3q_3) + q_1^2 + q_2^2 + q_3^2 = 0 \tag{4.20}$$

Lunde *et al.* (2007) showed that the direct three-body amplitude takes the form (see Appendix A.3)

$$T^{123}_{1'2'3'} = \frac{m(-q_2)}{L^2}\frac{q_1V_{q_2}V_{q_3} + q_2V_{q_1}V_{q_3} + q_3V_{q_1}V_{q_2}}{(k_{1'}-k_3)q_1q_3(k_1-k_{3'})} \,. \tag{4.21}$$

Although the matrix elements V_q tend to be suppressed for larger q, this suppression is only weak because of the slow logarithmic q dependence of the long range Coulomb interaction. In fact it is one of the main results of this chapter that this suppression is compensated by a much smaller energy denominator for large momentum transfer processes and that it is therefore necessary to consider all five exchange terms. The resulting amplitude for these terms can be directly read off from Eq. (4.21) by replacing the momenta $k_{1'}, k_{2'}, k_{3'}$ corresponding to the required exchanges.

Note that the three-body amplitude vanishes identically for point like interactions

($V_q = \text{const.}$) and it is thus beneficial to expand the nominator of Eq (4.21) to first non vanishing order. To keep this expansion general for all exchange terms we note that the six involved amplitudes [see Fig. 4.2] fall into two main categories. The direct term $T^{123}_{1'2'3'}$ as well as $T^{123}_{2'1'3}$ involve no large momentum transfer processes and have a clearly smallest momentum transfer q_3. The remaining four exchange processes do contain two large momentum transfers of the order of $2k_F$. The fact that in all six terms it is possible to choose one momentum transfer $\tilde{q}_3$ which is much smaller than the remaining two $(\tilde{q}_1, \tilde{q}_2)$ allows for a general expansion of the nominator of Eq. (4.21).

$$\tilde{q}_1 V_{\tilde{q}_2} V_{\tilde{q}_3} + \tilde{q}_2 V_{\tilde{q}_1} V_{\tilde{q}_3} + \tilde{q}_3 V_{\tilde{q}_1} V_{\tilde{q}_2} \approx \tilde{q}_3 \left(V'_{\tilde{q}_1} \tilde{q}_1 V_{\tilde{q}_3} + V_{\tilde{q}_1} \left[V_{\tilde{q}_1} - V_{\tilde{q}_3} \right] \right) . \tag{4.22}$$

Assuming an unscreened Coulomb potential, we only keep the leading logarithmic order and all six amplitudes take the compact form

$$T^{123}_{\mathcal{P}(1'2'3')} = \delta^{\sigma(123)}_{\sigma\mathcal{P}(1'2'3')} \frac{m}{L^2} \frac{V_{\tilde{q}_1} \left[V_{\tilde{q}_1} - V_{\tilde{q}_3} \right]}{(k_{\tilde{1}'} - k_{\tilde{3}})(k_{\tilde{1}} - k_{\tilde{3}'})} , \tag{4.23}$$

from which all amplitudes can be derived. The two small momentum transfer amplitudes [see Fig. 4.2] take the form

$$T^{123}_{1'2'3'} = \frac{V_{q_1}}{8\varepsilon_F L^2} \left(V_{q_1} - V_{q_3} \right) \tag{4.24}$$

$$T^{123}_{2'1'3'} = \frac{V_{q_1}}{8\varepsilon_F L^2} \left(V_{p_1} - V_{q_3} \right) , \tag{4.25}$$

where we introduced

$$p_1 = k_{2'} - k_1 . \tag{4.26}$$

Similarly, we find for the four $2k_F$-processes

$$T^{123}_{3'2'1'} = -T^{123}_{1'3'2'} = \frac{V_{2k_F}}{2v_F p_1 L^2} \left(V_{2k_F} - V_{q_1} \right) \tag{4.27}$$

$$T^{123}_{3'1'2'} = -T^{123}_{2'3'1'} = \frac{V_{2k_F}}{2v_F q_1 L^2} \left(V_{2k_F} - V_{p_1} \right) . \tag{4.28}$$

The $2k_F$ processes dominate the small q amplitudes because of $\varepsilon \ll \varepsilon_F$. Note however that the leading order of the $2k_F$ amplitudes comes in pairs with opposite signs. This becomes important when calculating the total three-body amplitude

$$\begin{aligned} \sum_{\text{spin}} \left| \langle 1'2'3' | V G_0 V | 123 \rangle_c \right|^2 = \sum_{\text{spin}} \Bigg| & \delta^{\sigma(123)}_{\sigma(1'2'3')} T^{123}_{1'2'3'} - \delta^{\sigma(123)}_{\sigma(2'1'3')} T^{123}_{2'1'3'} \\ & + \left(\delta^{\sigma(123)}_{\sigma(3'1'2')} - \delta^{\sigma(123)}_{\sigma(2'3'1')} \right) T^{123}_{3'1'2'} + \left(\delta^{\sigma(123)}_{\sigma(1'3'2')} - \delta^{\sigma(123)}_{\sigma(3'2'1')} \right) T^{123}_{3'2'1'} \Bigg|^2 . \end{aligned} \tag{4.29}$$

In the spinless case, all $\delta^{\sigma(123)}_{\sigma\mathcal{P}(1'2'3')} = 1$ and the leading order of the $2k_F$ processes vanishes.

In the next order, the contribution of the $2k_F$ amplitudes remains finite and the energy denominator is of the same order as for the small q processes. In this case one can then apply the argument of the logarithmic suppression of V_{2k_F} such that the leading order contribution is given by the small q processes, as assumed by Lunde *et al.* (2007).

Electrons in real quantum wires, however are not spinless, which increases the three-body matrix element by a factor of the order $(\varepsilon_F/\varepsilon)^2$. The importance of the electron spin can be understood in terms of the symmetry of the wavefunction. When the total spin of the three colliding particles is maximal, or when fermions are spinless, the orbital part of their wave function must be odd, which leads to a larger separation of the electrons and thus reduces the effect of the interaction. In contrast, no such suppression occurs when the total spin of the three colliding particles is $1/2$, since the interacting particles can be in the same orbital state.

Neglecting the small q processes in favor of the $2k_F$ exchange contributions, the resulting spin summation leads to

$$\sum_{\text{spin}} \left|\langle 1'2'3'|VG_0V|123\rangle_c\right|^2 = 6\left(\left[T^{123}_{3'1'2'}\right]^2 + \left[T^{123}_{3'2'1'}\right]^2\right). \tag{4.30}$$

Note that since the relaxation is controlled by $2k_F$ momentum transfer processes we can use the unscreened Coulomb interaction throughout the following calculations. The Fermi momentum in CEO quantum wires is typically of the order of the inverse wire width $1/a$ while distances to screening gates $d \gg a$ so that screening can be safely neglected for the $2k_F$ processes. The effect of screening on the scale of q_1, p_1 can be accounted for by replacing $q_1, p_1 \to 1/d$ in the Coulomb matrix elements in Eqs. (4.27,4.28) which results in replacing $\varepsilon \to v_F/d$ in the logarithms of the results (4.1,4.2,4.3).

4.2.3 The partial scattering rate

We now assembled all the required ingredients to calculate the out-scattering rates from Eqs. (4.7,4.11) by performing the remaining integrations over the Fermi functions. We note that the leading order of the three-body matrix element [see Eq. (4.30)] does not depend on the initial momentum and the small curvature induced momentum transfer of the left-moving particle. The sum over q_3 and k_3

$$\sum_{q_3k_3} n_3^0(1-n_{3'}^0)\delta(E_i - E_f) \tag{4.31}$$

can thus be carried out separately. The energy delta function

$$\delta(E_i - E_f) = m\delta\left(k_1q_1 + k_2q_2 + k_3q_3 + q_1^2/2 + q_2^2/2 + q_3^2/2\right) \tag{4.32}$$

ensures energy conservation. It is then possible to eliminate the sum over q_3, which yields to leading order

$$\sum_{q_3} \delta(E_i - E_f) = \frac{L}{2\pi} \frac{m}{2k_F}, \tag{4.33}$$

with the understanding that q_3 has to be replaced by

$$q_3 = -\frac{p_1 q_1}{2k_F} \tag{4.34}$$

in all remaining expressions. This result of energy and momentum conservation quantifies the qualitative argument of section 4.1 that $v_F q_3 \sim \varepsilon^2/\epsilon_F \ll v_F q_1, v_F q_2$. The remaining integral over k_3 results in the phase space

$$\sum_{k_3} n_3^0 (1 - n_{3'}^0) = \frac{L}{2\pi} \frac{q_3}{\mathrm{e}^{q_3/k_T} - 1}, \tag{4.35}$$

where we introduced the thermal momentum $k_T = T/v_F$. As mentioned above this phase space is controlled by q_3 for $|q_3| \gg k_T$ (note that q_3 is negative), which is equivalent to the condition $\varepsilon \gg \varepsilon_T = \sqrt{\varepsilon_F T}$. For lower excitation energies $\varepsilon \ll \varepsilon_T$ thermal broadening leads to a phase space $\sim k_T$.

The remaining integrals over q_1, k_2 or similarly over q_1, p_1 can be discussed most conveniently in terms of the partial scattering rate $P(q_1, p_1)\mathrm{d}q_1\mathrm{d}p_1$ that describes the transition rate from electrons at k_1, k_2 to final states in an interval $\mathrm{d}q_1$ and $\mathrm{d}p_1$ around $k_{1'} = k_1 + q_1$ and $k_{2'} = k_1 + p_1$. Using the out-scattering rate the partial scattering rate can then be defined as

$$\frac{1}{\tau_{\mathrm{p}}^{\mathrm{out}}} = \int \mathrm{d}q_1 \mathrm{d}p_1 P_{\mathrm{p}}(q_1, p_1) \tag{4.36}$$

with

$$P_{\mathrm{p}}(q_1, p_1) = \frac{3\varepsilon_F}{2\pi^3} \frac{L^4}{(2v_F)^4} \frac{q_1 p_1 / 2k_F^2}{\left(1 - \mathrm{e}^{-\frac{q_1 p_1}{2k_F k_T}}\right)} \frac{V_{2k_F}^2 \left[\frac{1}{q_1^2}\left(V_{2k_F} - V_{p_1}\right)^2 + \frac{1}{p_1^2}\left(V_{2k_F} - V_{q_1}\right)^2\right]}{\left(1 + \mathrm{e}^{\frac{k+p_1+q_1}{k_T}}\right)\left(1 + \mathrm{e}^{-\frac{k+q_1}{k_T}}\right)\left(1 + \mathrm{e}^{-\frac{k+p_1}{k_T}}\right)}. \tag{4.37}$$

Here we introduced the excess momentum of the hot particle as $k = k_1 - k_F = \varepsilon/v_F$.

It is also possible to read off the corresponding partial hole scattering rate from Eq. (4.37). Hole relaxation can be described by a particle at k_1 scattering into the unoccupied hole state at $k_{1'}$, which can be accounted for by replacing $(1 - n_{1'}^0) \to n_1^0$ [see Eq. (4.11)]. In Eq. (4.37), this corresponds to replacing $[1 + \exp(-(k + q_1)/k_T)]^{-1}$ by $[1 + \exp(k/k_T)]^{-1}$. To compare particle and hole relaxation it is reasonable to define the positive excess energies and momenta of a hole excitation as $\varepsilon_h = \varepsilon_F - \varepsilon_{k_{1'}}$ and $k_h = k_F - k_{1'} = -k - q_1$. Shifting the integration variable $p_1 \to p_{1h}$ with $p_{1h} = k_{1'} - k_2 \approx -p_1$ [Fig. 4.3 shows the different definitions for q_1 and p_1 for particle and hole relaxation] the partial hole scattering rate takes the form

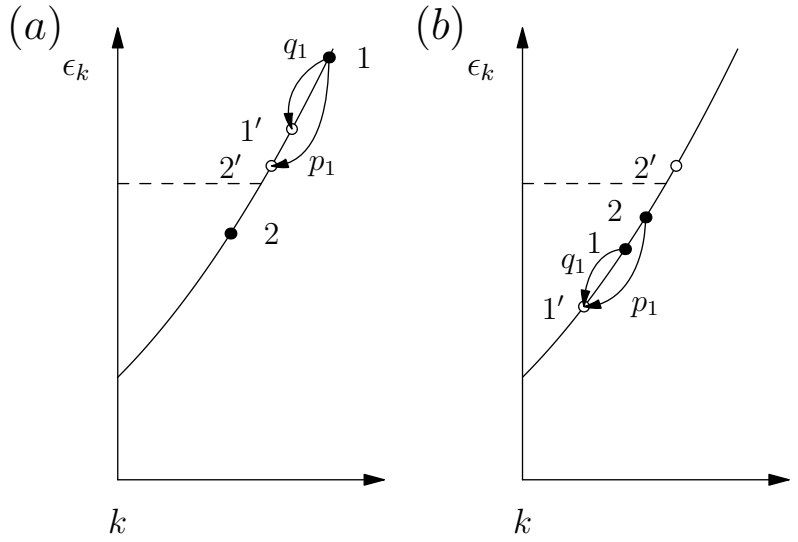

Figure 4.3: Visualization of the momentum transfers q_1 and p_1 in the case of (a) electron and (b) hole relaxation. The possibility to exchange the labels $1'$ and $2'$ (1 and 2) for electrons (holes) is reflected in the symmetry of q_1 and p_1 in Eqs. (4.37, 4.38).

$$P_{\mathrm{h}}(q_1,p_1)=\frac{3\varepsilon_F}{2\pi^3}\frac{L^4}{(2v_F)^4}\frac{q_1p_1/2k_F^2}{\left(\mathrm{e}^{\frac{q_1p_1}{2k_Fk_T}}-1\right)}\frac{V_{2k_F}^2\left[\frac{1}{q_1^2}\left(V_{2k_F}-V_{p_1}\right)^2+\frac{1}{p_1^2}\left(V_{2k_F}-V_{q_1}\right)^2\right]}{\left(1+\mathrm{e}^{\frac{k+p_1+q_1}{k_T}}\right)\left(1+\mathrm{e}^{-\frac{k+p_1}{k_T}}\right)\left(1+\mathrm{e}^{-\frac{k+q_1}{k_T}}\right)}\,. \quad (4.38)$$

Here we omitted again the index h, with the understanding that the definitions of ε and k are chosen appropriately in the case of hole relaxation. Comparing Eqs. (4.37) and (4.38), shows that the partial particle and hole scattering rates are equal up to a sign change of q_3. The change of the sign is crucial for $\varepsilon \gg \varepsilon_T$, and limits the small momentum transfer process to $|q_3| \lesssim k_T$ for holes while the particle relaxation does not show a similar restriction. For $\varepsilon \ll \varepsilon_T$, however, the partial scattering rates become independent of q_3 which leads to a particle-hole symmetric result.

4.2.4 Energy relaxation rates

We are interested in the relaxation of hot particle and hole excitations towards thermal equilibrium. The corresponding relaxation rate is not necessarily equivalent to the out-scattering rate. The latter only describes how fast the excitation leaves its initial state and does not take into account the number of relaxation steps required for the excitation to reach an energy of the order of temperature. The more relevant quantity for the relaxation process is thus given by the energy relaxation rate.

By thinking in terms of relaxation steps we essentially solve the Boltzmann equation (4.6), which describes the evolution of the initial excitation and will in general contain drift

and diffusion terms in momentum space. Unidirectional relaxation steps then assume that there is a strong asymmetry between relaxation and excitation of the hot particle (hole). As we will show in the following the typical energy relaxation steps $|\Delta\varepsilon| \gg T$, while a further excitation is only possible on the scale of $\Delta\varepsilon \sim T$. This asymmetry strongly favors relaxation which justifies the assumption of unidirectionality.

Particle relaxation at $\varepsilon \gg \varepsilon_T$

The particle relaxation is not limited by temperature and typical energy transfers are of the order $\Delta\varepsilon \sim \varepsilon$. Therefore, the out-scattering rate already captures energy relaxation. Since the relaxation rate does not rely on finite temperature we can set $T = 0$ for the $\varepsilon \gg \varepsilon_T$ limit and obtain

$$\frac{1}{\tau_\mathrm{p}} = \int \mathrm{d}q_1 \mathrm{d}p_1 \mathcal{P}_\mathrm{el}(q_1, p_1)|_{T=0} \tag{4.39}$$

$$= \int \mathrm{d}q_1 \mathrm{d}p_1 \frac{3\varepsilon_F}{4\pi^3} \frac{L^4 V_{2k_F}^2 \left(V_{2k_F} - V_k\right)^2}{(2v_F)^4 k_F^2} \left[\frac{p_1}{q_1} + \frac{q_1}{p_1}\right] \times \Theta(-k - p_1 - q_1)\Theta(k + p_1)\Theta(k + q_1)\,. \tag{4.40}$$

Due to the slow logarithmic dependence of V_q, the Coulomb matrix element can be approximated by a typical value of the integration variable which is of the order $q_1, p_1 \sim k$. The integral can then be done exactly and leads to the result of Eq. (4.1).

Comparison with the holon decay rate

Interestingly, there exists a connection between the particle relaxation [Eq. (4.1)] and the holon decay rate. Schmidt *et al.* (2010b) considered a spinful one dimensional system, where curvature effects of the dispersion lead to a decay of the fermionic quasi-particles of the Luttinger liquid (holons). As mentioned above the holon approach can be applied in the complementary limit of strong interaction such that $k \ll mV_0$.

For small k we can approximate V_k by the screened Coulomb matrix element V_0, which dominates V_{2k_F} for weak screening. Thus Eq. (4.1) takes the form

$$\frac{1}{\tau_\mathrm{p}} \sim \varepsilon_F \left(\frac{V_0 V_{2k_F}}{v_F^2}\right)^2 \left(\frac{k}{k_F}\right)^2. \tag{4.41}$$

The holon decay rate on the other hand is given by [Schmidt *et al.* (2010b)]

$$\Gamma \sim \varepsilon_F \frac{V_0}{v_F} \left(\frac{V_{2k_F}^2}{v_F^2}\right) \left(\frac{k}{k_F}\right)^3. \tag{4.42}$$

These expressions match at the limit of applicability of both approaches $k \sim mV_0$. This matching of the two complementary approaches is remarkable. It suggests that the fermionic quasi-particles of the Luttinger model transform into the original electrons for

higher excitation energies, where curvature effects destroy the holon integrity.

Particle and hole relaxation at $\varepsilon \ll \varepsilon_T$

In the limit $\varepsilon \ll \varepsilon_T$, the particle and hole relaxation rates become identical. Note that we still consider the injection of hot excitations such that we work in the intermediate regime $T \ll \varepsilon \ll \varepsilon_T = \sqrt{\varepsilon_F T}$. This still allows for approximating the Fermi functions that involve the right-moving particles as step functions such that the partial scattering rates are given by

$$\begin{aligned} P_{\mathrm{h}}(q_1, p_1) \;=\; P_p(q_1, p_1) = \frac{3\epsilon_F}{2\pi^3}\left(\frac{e^2}{\epsilon v_F}\right)^4 \frac{k_T}{k_F}\left[\left(\frac{1}{p_1}\right)^2 + \left(\frac{1}{q_1}\right)^2\right] \ln\left|\frac{1}{2k_F a}\right| \ln\left|\frac{\varepsilon}{4\varepsilon_F}\right| \\ \times\Theta(-k-p_1-q_1)\Theta(k+p_1)\Theta(k+q_1)\,. \end{aligned} \tag{4.43}$$

Here we again treat the logarithms as constants. Although temperature does not limit the typical energy transfer

$$\Delta\varepsilon = -v_{\mathrm{F}} \min\left(|q_1|, |p_1|\right)\,, \tag{4.44}$$

which can therefore still be of the order of ε it becomes problematic to approximate the energy relaxation rate with the out-scattering rate at finite temperature. The reason lies in a logarithmic divergence of the out-scattering rate due to processes with vanishing energy transfer $\Delta\varepsilon$. The processes that cause the divergence do therefore not contribute to the relaxation. This can be dealt with by considering the energy relaxation rate, which is still well-defined.

The change of the energy of the hot excitation is given by weighting the partial scattering rate with the corresponding energy transfer such that

$$\frac{\mathrm{d}\varepsilon}{\mathrm{d}t} = -\int \mathrm{d}q_1 \mathrm{d}p_1 v_F \min\left(|q_1|, |p_1|\right) P_p(q_1, p_1)\,. \tag{4.45}$$

The remaining integral is then indeed finite and can be performed exactly. The result reads

$$\frac{\mathrm{d}\varepsilon}{\mathrm{d}t} = -\frac{3\epsilon_F}{2\hbar\pi^3}\left(\frac{e^2}{\epsilon v_F}\right)^4 T\frac{\varepsilon}{\varepsilon_F}\left(2\ln(2) - \frac{1}{2}\right)\left(\ln\left|\frac{1}{2k_{\mathrm{F}}a}\right| \ln\left|\frac{k}{2k_{\mathrm{F}}}\right|\right)^2\,, \tag{4.46}$$

such that the energy relaxation rate can be extracted through

$$\frac{\varepsilon}{\tau_{\mathrm{p}}} \;=\; -\frac{\mathrm{d}\varepsilon}{\mathrm{d}t}, \tag{4.47}$$

which results in Eq. (4.2).

Hole relaxation at $\varepsilon \gg \varepsilon_T$

In contrast to the particle relaxation, the energy transfer in a single relaxation process of hot holes cannot reach ε. It is instead limited to $\Delta\varepsilon \lesssim \epsilon_F T/\varepsilon$ and it is therefore again

essential to consider the energy relaxation rate. Since $\Delta\varepsilon \ll \varepsilon$, one of the momentum transfers q_1 or p_1 is small while the corresponding exchange term becomes of the order of k. Due to the symmetry of the partial scattering rate with respect to q_1 and p_1 we can choose without loss of generality

$$|q_1| \ll |p_1| \approx k\,, \tag{4.48}$$

by adding a factor of 2 in Eq. (4.38). The leading order contribution of the partial scattering rate then takes the form

$$\begin{aligned} P_{\rm h}(q_1,p_1) &= \frac{3\epsilon_F}{2\hbar\pi^3}\left(\frac{e^2}{\epsilon v_F}\right)^4 \frac{1}{k_F^2}\frac{1}{\mathrm{e}^{\frac{q_1 k}{2k_F k_T}}-1}\left[\frac{p_1}{q_1}\right]\left(\ln\left|\frac{1}{2k_{\rm F}a}\right|\ln\left|\frac{k}{2k_{\rm F}}\right|\right)^2 \\ &\quad\times\Theta(-k-p_1-q_1)\Theta(k+p_1)\Theta(k+q_1)\,. \end{aligned} \tag{4.49}$$

With $\Delta\varepsilon = v_{\rm F}q_1$ we now use the same approach for the energy relaxation rate as above to find

$$\frac{\mathrm{d}\varepsilon}{\mathrm{d}t} = -\frac{1}{\pi}\left(\frac{e^2}{\epsilon v_F}\right)^4 \frac{\varepsilon_{\rm F}}{\varepsilon}T^2\left(\ln\left|\frac{1}{2k_{\rm F}a}\right|\ln\left|\frac{k}{2k_{\rm F}}\right|\right)^2. \tag{4.50}$$

The energy relaxation time of a hole is controlled by the time it spends in the high energy regime $\varepsilon \gg \varepsilon_T$. We can thus integrate the differential equation above, assuming that we do not leave the regime $\varepsilon \gg \varepsilon_T$ such that

$$\tau_{\rm h} = \int_{\varepsilon}^{\sqrt{4\varepsilon_{\rm F}T}} \mathrm{d}\varepsilon' \frac{\mathrm{d}t}{\mathrm{d}\varepsilon'} = \int_{\sqrt{4\varepsilon_{\rm F}T}}^{\varepsilon} \mathrm{d}\varepsilon' \frac{1}{\left|\frac{\mathrm{d}\varepsilon'}{\mathrm{d}t}\right|} \approx \frac{\varepsilon}{2}\frac{1}{\left|\frac{\mathrm{d}\varepsilon}{\mathrm{d}t}\right|}\,, \tag{4.51}$$

which gives the result of Eq. (4.3) as

$$\frac{1}{\tau_{\rm h}} = -\frac{2}{\varepsilon}\frac{\mathrm{d}\varepsilon}{\mathrm{d}t}\,. \tag{4.52}$$

4.3 Chiral relaxation process

The three-body processes discussed so far rely on the presence of right- and left-moving particles. Here we comment on a competing process shown in Fig. 4.4 that involves only co-moving electrons. In this process, two electrons near the Fermi energy are scattered in opposite directions in energy, allowing a high-energy particle to relax slightly by an energy $\Delta\varepsilon \sim T^2/\varepsilon$. Assuming that the interaction is screened for these small momentum transfers, the resulting particle-hole symmetric energy relaxation rate takes the form

$$\frac{1}{\tau_{\rm p}} = \frac{1}{\tau_{\rm h}} \sim \varepsilon_F\left(\frac{e^2}{\epsilon v_F}\right)^4 \frac{T}{\varepsilon_F}\frac{\varepsilon_T^6}{\varepsilon^2\varepsilon_d^4}\ln^4|d/a| \tag{4.53}$$

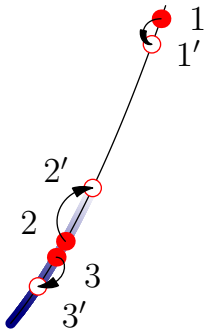

Figure 4.4: Chiral relaxation process. A hot particle can relax a small part of its energy by using curvature effects on the order of the temperature. Here the color gradient indicates the thermal smearing.

as we will show below. (Here, $\varepsilon_d = v_F/d$.) By comparing with Eqs. (4.1,4.2,4.3), one can conclude that these processes are sub-dominant when $\varepsilon \gg \varepsilon_T$ or $T \ll \varepsilon_F/(k_F d)^4$. Note however that these processes control the relaxation in chiral systems such as quantum Hall edge states as we will discuss in chapter 5.

4.3.1 Derivation of the energy relaxation rate

The approach for the calculation of the energy relaxation rate is the same as for the non-chiral processes discussed before (see section 4.2). Here we sketch the main differences and discuss the parametric dependence of the corresponding energy relaxation rate.

Considering again the relaxation of a hot particle $\varepsilon \gg T$, energy and momentum conservation results in

$$q_1 = q_3 \frac{k_2 - k_3 - q_3}{k}, \tag{4.54}$$

such that $q_1 \sim k_T^2/k$ is the smallest momentum in the problem. The energy delta function can then be eliminated by

$$\sum_{q_1} \delta(E_i - E_f) = \frac{L}{2\pi} \frac{m}{k}, \tag{4.55}$$

with the understanding that q_1 should be replaced by Eq. (4.54). We now discuss the three-body matrix element starting with the case of an unscreened Coulomb interaction.

Three-body matrix element

The general expression (4.23) of the three-body amplitudes is still a valid starting point and we find

$$T^{123}_{1'2'3'} = T^{123}_{1'3'2'} = \frac{mV_{q_3}\left(V_{q_3} - V_{q_1}\right)}{L^2k^2} \tag{4.56}$$

$$T^{123}_{2'1'3'} = -T^{123}_{3'2'1'} = \frac{mV_k\left(V_k - V_{q_3}\right)}{L^2(k_2 - k_3 - q_3)k} \tag{4.57}$$

$$T^{123}_{3'1'2'} = -T^{123}_{2'3'1'} = \frac{mV_k\left(V_k - V_{k_2-k_3-q_3}\right)}{L^2q_3k}\,. \tag{4.58}$$

These three-body amplitudes present another manifestation of the importance of the electron spin. In the spinful case the resulting three-body matrix element is finite and the leading order contribution is given by the exchange terms in Eqs. (4.57,4.58). For spinless electrons one would simply sum up the above terms and the overall matrix element vanishes, which would require to go to the next order in an expansion in k_T/k.

Summarizing the results for the chiral relaxation process obtained so far, the energy relaxation rate of spinful particles takes the form

$$\frac{1}{\tau_{\mathrm{P}}} \sim \frac{m^3}{kL^3}\sum_{q_3k_2k_3}\frac{-q_1}{k}n^0_2(1-n^0_{2'})n^0_3(1-n^0_{3'})\left(\left[\frac{1}{(k_2-k_3-q_3)k}\right]^2 + \left[\frac{1}{q_3k}\right]^2\right)V_k^2\left(V_k - V_{k_T}\right)^2\,, \tag{4.59}$$

where the additional factor $-q_1/k$ weights the out-scattering rate with the relative relaxed energy per scattering event.

Power counting

The leading order of the sum (4.59) cancels out completely because of q_1 momentum transfers that are compensated by corresponding $-q_1$ transitions. The next order in the T/ε expansion reveals that relaxation processes are more likely than additional excitations. This can already be understood from Fig. 4.4 and is a consequence of the small difference in the momentum transfers of the processes close to the Fermi energy. Relaxation ($q_1 < 0$) leads to a reduction of the momentum transfer for the scattering process that works against the Fermi function (in Fig. 4.4: $3 \to 3'$), while a positive q_1 has the opposite effect. Balancing relaxation and excitation effects is thus expected to add a factor of the order $|q_1|/k_T$.

More formally, the rate for exciting the hot particle can be estimated by the transforma-

tion $1,2,3 \leftrightarrow 1',2',3'$. Thus the effective energy relaxation rate is controlled by

$$\begin{aligned} & \frac{1}{2}\left[n_2^0(1-n_{2'}^0)n_3^0(1-n_{3'}^0) - n_{2'}^0(1-n_2^0)n_{3'}^0(1-n_3^0)\right] \\ = & \frac{1}{2\left(1+\mathrm{e}^{\frac{k_2}{k_T}}\right)}\frac{1}{\left(1+\mathrm{e}^{-\frac{k_2-q_1-q_3}{k_T}}\right)}\frac{1}{\left(1+\mathrm{e}^{\frac{k_3}{k_T}}\right)}\frac{1}{\left(1+\mathrm{e}^{-\frac{k_3+q_3}{k_T}}\right)} \\ & -\frac{1}{2\left(1+\mathrm{e}^{\frac{k_2-q_1-q_3}{k_T}}\right)}\frac{1}{\left(1+\mathrm{e}^{-\frac{k_2}{k_T}}\right)}\frac{1}{\left(1+\mathrm{e}^{\frac{k_3+q_3}{k_T}}\right)}\frac{1}{\left(1+\mathrm{e}^{-\frac{k_3}{k_T}}\right)} \end{aligned} \tag{4.60}$$

$$\approx n_2^0(1-n_{2'}^0)n_3^0(1-n_{3'}^0)n_{2'}^0\frac{-q_1}{k_T}\,, \tag{4.61}$$

where all momenta in the second and third line are measured relative to k_F. The Fermi functions set typical momentum transfers close to the Fermi energy to the order of k_T and therefore $q_1 \sim k_T^2/k$. The energy relaxation rate can then be estimated from Eqs. (4.59,4.61) by power counting and leads to

$$\frac{1}{\tau_p} \sim \frac{m^3}{kL^3}\left(Lk_T\right)^3\left(\frac{k_T}{k}\right)^2\frac{V_k^2\left(V_k-V_{k_T}\right)^2}{k^2k_T^2}\frac{k_T}{k}\,. \tag{4.62}$$

$$\frac{1}{\tau_p} \sim \frac{k_T^2}{m}\left(\frac{V_k\left(V_k-V_{k_T}\right)}{(\Delta v)^2}\right)^2\left(\frac{k_T}{k}\right)^2\,, \tag{4.63}$$

where we introduced the difference in velocity $\Delta v = k/m$ between the hot particle and the Fermi velocity. For an unscreened Coulomb interaction $V_k\left(V_k - V_{k_T}\right)$ can be replaced by (e^2/ϵ) up to logarithms while in the screened case [$kd \ll 1$, see Eq. (4.17)] it is given by $V_k\left(V_k - V_{k_T}\right) \sim (e^2/\epsilon)(kd)^2$ which results in Eq. (4.53).

4.4 Inter branch equilibration

So far we only discussed the energy relaxation within the branch of the injected hot particles. Since the relaxation of a, say, right-moving particle creates right- and left-moving particle-hole pairs there will also be an energy redistribution between the right- and left-moving branches. The parametric difference between the energies of the excited co- ($\sim \varepsilon$) and counter-propagating ($\sim \varepsilon^2/\varepsilon_F$) particle-hole pairs led to the conclusion [Karzig *et al.* (2010)] that the energy equilibration rate between right- and left-moving branches is much slower than the intra branch equilibration. The physical picture of the entire equilibration process was that the relaxation of the hot right-moving particle leads to a temperature difference between the right- and left-moving branches, which finally relaxes with a much slower rate

$$\frac{1}{\tau_{\text{inter}}} \sim \varepsilon_F\left(\frac{e^2}{\epsilon v_F}\right)^4\left(\frac{T}{\varepsilon_F}\right)^3\,. \tag{4.64}$$

Here we will argue that this picture was partially wrong. The main conclusion that there is almost no equilibration between right- and left-movers on experimentally relevant

time scales still holds, but for a different reason. In fact, the time scale of equilibration of the entire distribution function is the same as for the relaxation within the right-moving branch [$\sim T$, see Eq. (4.2)]. Momentum conservation, however, leads to an equilibrium distribution function with different temperatures for right- and left-movers such that the energy transfer to the left-moving branch remains small even after arbitrarily long times. In this sense the statement of Karzig *et al.* (2010) is even stronger than originally assumed.

Note that the result of $\tau_{\text{inter}} = \tau_{\text{h}}$ is consistent with Micklitz and Levchenko (2011) who calculated the relaxation rate for the entire distribution function in the case of *spinless* particles at small excitation energies $\varepsilon \sim T$. Their result $\tau_{\text{inter}}^{-1} \sim (T/\epsilon_F)^3$ agrees with with the expected $(\varepsilon/\varepsilon_F)^2$ suppression of Eq. (4.2) in the case of spinless particles.

Distribution functions

Karzig *et al.* (2010) overlooked that an initial distribution function

$$n(k) = \frac{\Theta(k)}{\mathrm{e}^{\frac{\varepsilon_k-\mu}{T+\Delta T/2}}+1} + \frac{\Theta(-k)}{\mathrm{e}^{\frac{\varepsilon_k-\mu}{T-\Delta T/2}}+1} \tag{4.65}$$

does not relax to an equilibrium distribution function of the form

$$n_{\text{eq}}^0(k) = \frac{1}{\mathrm{e}^{\frac{\varepsilon_k-\mu}{T}}+1} \tag{4.66}$$

and thus interpreted the initial change of the temperature difference as $\partial_t \Delta T(t)|_{t=0} = \Delta T(0)/\tau_{\text{inter}}$. The actual time dependence, however, is given by

$$\Delta T(t) = \Delta T(0)\left[1 - \left(\frac{T}{\varepsilon_F}\right)^2\left(1-\mathrm{e}^{-\frac{t}{\tau_{\text{h}}}}\right)\right], \tag{4.67}$$

which has the same initial time derivative $\partial_t \Delta T(t)|_{t=0} = \Delta T(0)/\tau_{\text{h}}(T/\varepsilon_F)^2$ because $1/\tau_{\text{h}} \sim T$ [see Eq. (4.2)]. The reason for the partial decay of ΔT lies in the form of the correct equilibrium distribution function [see *e.g.* Micklitz *et al.* (2010)]

$$n_{\text{eq}}(k) = \frac{\Theta(k)}{\mathrm{e}^{\frac{\varepsilon_k-uk-\mu_R}{T}}+1} + \frac{\Theta(-k)}{\mathrm{e}^{\frac{\varepsilon_k-uk-\mu_L}{T}}+1}. \tag{4.68}$$

The different chemical potentials reflect the fact that there is still no appreciable particle transfer between the right- and left-moving branches since the corresponding rate is exponentially small in T/μ. The uk term describes the boost of the distribution function reflecting the momentum conservation and is given by [Micklitz and Levchenko (2010)]

$$u = v_F \frac{\Delta T}{2T}\left(1 - \frac{3\pi^2}{8}\frac{T^2}{\mu^2}\right). \tag{4.69}$$

Note that the T^2/μ^2 corrections are due to the curvature of the dispersion. Interestingly,

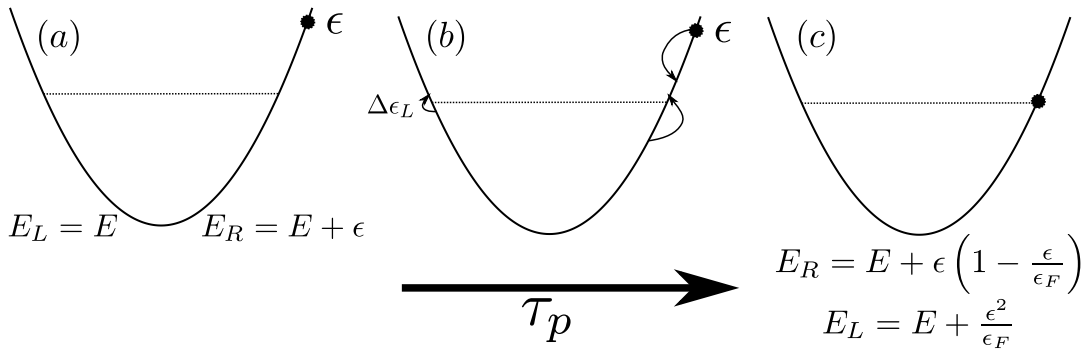

Figure 4.5: Illustration of the energy balance during the relaxation process (neglecting the hole relaxation).

the initial distribution function [Eq. (4.65)] with a small temperature difference for right- and left-movers is already a boosted equilibrium distribution function n_{eq} for a linear electron dispersion $\varepsilon_k = \Theta(k) v_F k$. This immediately follows from

$$\frac{\pm v_F k}{\left(T \pm \frac{\Delta T}{2}\right)} = \frac{\pm v_F k - v_F k \frac{\Delta T}{2T}}{T} \tag{4.70}$$

and signals again the absence of relaxation for a linear dispersion. The small T^2/μ^2 correction due to the curvature effects can then be interpreted as a small equilibration of the temperature difference on the order of $\Delta T (T/\mu)^2$ in line with Eq. (4.67).

Energy transfer to the left-moving branch

The most striking argument why there cannot be relaxation on a timescale longer than τ_{h} is that the energy transfer to the left-movers is due to three-body collisions [see Fig. 4.5b] and these collisions stop after the time τ_{h}, when the injected particle has relaxed.

We will now deduce the overall energy transfer to the left-moving branch during the relaxation of a hot particle with energy ε. Consider first the particle relaxation [see Fig. 4.5]. We assume that the energies of left- and right-movers before the relaxation are given by $E_L = E$ and $E_R = E + \varepsilon$, respectively. The energy transfer to the left-moving branch per three-body collision is given by the curvature effect as $\Delta\varepsilon_L = \varepsilon^2/\varepsilon_F$.

On the other hand, relaxation of the additionally excited hole transfers energy back from the left- to the right-moving branch [see Fig. 4.6]. The curvature induced small asymmetry between particle and hole processes leads to the fact that particle and hole processes do not cancel the energy transfer completely. A simple way to think about this is to consider the case where particles relax much faster than holes. After τ_{p} the particles relaxed all their energy $\varepsilon - \Delta\epsilon_L$ to hole excitations. The subsequent hole relaxation then transfers the energy $-\Delta\varepsilon_L\,(1 - \varepsilon/\varepsilon_F)$ back from the left-moving branch such that the total energy transfer after τ_{h} takes the form

$$\Delta\varepsilon_L^{\text{tot}} = \varepsilon \left(\frac{\varepsilon}{\varepsilon_F}\right)^2. \tag{4.71}$$

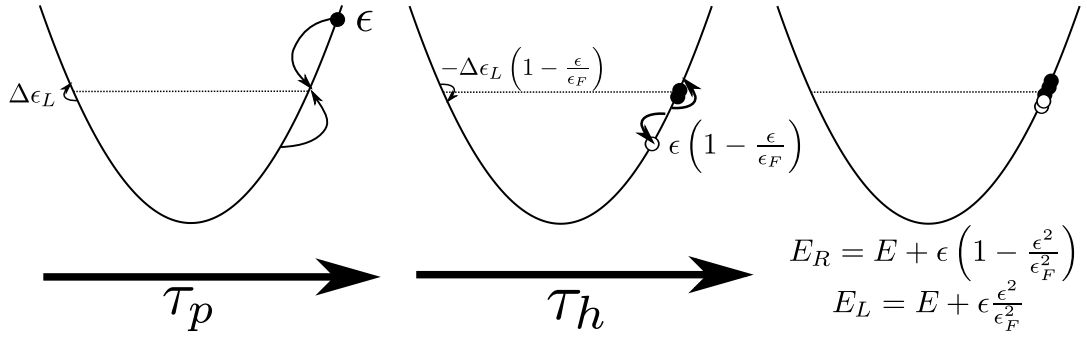

Figure 4.6: Illustration of the energy balance during the relaxation process (taking into account the hole relaxation).

Note that this is consistent with the $\Delta T(T/\mu)^2$ equilibration for the temperature difference. A higher right-mover temperature $T_R = T + \Delta T$ can be viewed as if a fraction $\Delta T/T$ of the particles is excited to energies $\varepsilon = T_R \approx T$. During the equilibration the temperature transfer is therefore $\Delta T/T \times T^3/\varepsilon_F^2$.

4.5 Comparison with experiment

The experiment of Barak *et al.* (2010b) addresses relaxation in one dimensional systems beyond the Luttinger liquid limit. The main idea is to insert hot particles and holes with fixed energy and momentum into a quantum wire and then probe for consequences of the possible relaxation processes (see section 1.1.1). If the hot excitation relaxes, it creates additional excited particle-hole pairs. Another tunneling contact at a distance of $2\,\mu$m from the source was then tuned in such a way that it is only possible for excited particles to flow into the drain, implying that relaxation was accompanied by an increase in current.

Barak *et al.* (2010b) did not measure the dependence of the energy relaxation rate on ε, but did provide bounds. Specifically, they observed particle relaxation and the absence of hole relaxation at excitation energies ε of order $\varepsilon_F/3$. With the corresponding time it takes the excitations to reach the drain (typical Fermi velocity $\sim 2\cdot 10^5$m/s) this leads to the following bounds for the energy relaxation rates

$$\frac{1}{\tau_{\mathrm{p}}^{\mathrm{exp}}} \gtrsim 10^{11}\,\mathrm{s}^{-1} \tag{4.72}$$

$$\frac{1}{\tau_{\mathrm{h}}^{\mathrm{exp}}} \ll 10^{11}\,\mathrm{s}^{-1}. \tag{4.73}$$

For numerical estimates based on our theoretical results we used $v_F \sim 2\cdot 10^5\,\mathrm{m/s}$, $m = 0.067\,\mathrm{m_e}$, $k_F \sim 1\cdot 10^8\,\mathrm{m}^{-1}$, $a \approx 20\,\mathrm{nm}$, $\epsilon = 12.4\,\epsilon_0$, $\epsilon_F = v_F k_F/2 \approx 6.6\,\mathrm{meV}$, which are

realistic parameters for the geometry of Barak *et al.* (2010b). The resulting estimates

$$\frac{1}{\tau_{\mathrm{p}}} \approx 10^{11}\mathrm{s}^{-1} \tag{4.74}$$

$$\frac{1}{\tau_{\mathrm{h}}} \approx 5\cdot 10^{9}\mathrm{s}^{-1} \tag{4.75}$$

are quantitatively consistent with the experimental bounds. Note that the temperature $T = 0.25\,\mathrm{K}$ of the experiment results in $\varepsilon_T = 0.38\,\mathrm{meV}$ such that with $\varepsilon = 2.2\,\mathrm{meV}$, the experiment was conducted in the high energy regime $\varepsilon > \varepsilon_T$.

Note that the experiment also does not observe signs of relaxation between right and left-movers which is consistent with the discussion in section 4.4.

4.5.1 Estimate for the Coulomb matrix element

Note that the numerical results (4.74,4.75) require a more accurate estimate of the Coulomb matrix element V_q that can be applied to the regime $k_F a \sim 1$. The latter can be determined as a matrix element of the operator $e^2/(\varepsilon r)\exp(-r/d)$ in the two-electron state which is controlled by the corresponding transverse wave functions. The result can be expressed as [Giuliani and Vignale (2005), Appendix 1]

$$V_q^{\phi} = \int \frac{\mathrm{d}\mathbf{q}_\perp}{(2\pi)^2}\frac{4\pi e^2/\epsilon}{\mathbf{q}_\perp^2 + q^2 + 1/d^2}\,|F(\mathbf{q}_\perp)|^2 \tag{4.76}$$

with the form factor

$$F(\mathbf{q}_\perp) = \int \mathrm{d}\mathbf{r}_\perp\,|\phi(\mathbf{r}_\perp)|^2\,\mathrm{e}^{-\mathrm{i}\mathbf{q}_\perp\mathbf{r}_\perp}\,, \tag{4.77}$$

where $\phi(\mathbf{r}_\perp)$ is the transverse wave function which we assumed to be described by the ground state of a particle in a box of size a

$$\phi(x,y) = \frac{2}{a}\cos\left(\frac{\pi x}{a}\right)\cos\left(\frac{\pi x}{b}\right). \tag{4.78}$$

Note that the interaction term $V_{2k_F}\,(V_{2k_F} - V_k)$, which controls the relaxation rates originates from Eq. (4.22). The numerical estimates (4.74,4.75) therefore rely on replacing

$$V_{2k_F}\,(V_{2k_F} - V_k) \to \frac{1}{\tilde{q}_3}\left(\tilde{q}_1 V_{\tilde{q}_1+\tilde{q}_3}V_{\tilde{q}_3} - (\tilde{q}_1+\tilde{q}_3)V_{\tilde{q}_1}V_{\tilde{q}_3} + \tilde{q}_3 V_{\tilde{q}_1}V_{\tilde{q}_1+\tilde{q}_3}\right)\,, \tag{4.79}$$

with $\tilde{q}_1 = 2k_F$ and $\tilde{q}_3 = k/2$ as is typical for the large momentum transfer processes.

4.6 Conclusions

The Luttinger liquid serves as a paradigm in one dimensional systems, comparable with the Fermi liquid theory for higher dimensional systems. Yet, the Luttinger model does not describe relaxation and thermalization and one is therefore forced to go beyond the

Luttinger model to address these issues.

The finite curvature of the electron dispersion breaks the Luttinger model's integrability and provides an intrinsic source of thermalization in translationally invariant one dimensional systems. This chapter discussed the corresponding equilibration and thermalization processes of hot carriers in quantum wires. The relaxation mechanism can be described in terms of a well-defined perturbative approach that relies on three-body processes. As a manifestation of the finite curvature of the electron dispersion three-body processes show a strong asymmetry in the energy relaxation rates of particle and hole excitations. In fact, hole relaxation is only possible at finite temperatures while there is no similar restriction for particles.

A crucial insight of this chapter is the importance of spin and the long range Coulomb interaction, which dramatically increases the energy relaxation rates of particle and hole excitations via $2k_F$ momentum transfer processes. This enhanced relaxation rate provides a quantitative interpretation of a recent experiment of Barak *et al.* (2010b) in terms of three-body processes. Also in line with this experiment, we argue that three-body processes do not transfer a substantial amount of energy between the right- and left-moving branches.

Finally, we also discussed a possible three-body process that involves only particles of the same chirality. While its effect is sub-dominant in typical quantum wire geometries it allows for three-body relaxation processes in quantum Hall edge states, which will be discussed in chapter 5.

5 Relaxation and edge reconstruction in integer quantum Hall systems

The interplay between the confinement potential and electron-electron interactions controls reconstructions of quantum Hall edge states. This chapter studies [based on Karzig *et al.* (2012)] the influence of reconstruction effects on the relaxation and equilibration of edge excitations of quantum Hall systems. Specifically, we consider energy relaxation of a hot particle injected into a translational invariant quantum Hall edge at Landau level filling factors $\nu = 1, 2$. With the assumption that the velocity v_1 of the injected particle differs sufficiently from the Fermi velocity v_F, the Coulomb interaction is treated perturbatively. In this limit, relaxation processes are dominated by three-body processes (see chapter 4) which depend sensitively on the electron dispersion and hence on edge reconstruction effects.

Edge reconstruction can be discussed in various limits and ranges from the absence of reconstruction in infinitely sharp edges [Halperin (1982)] to the development of compressible and incompressible stripes [Chklovskii *et al.* (1992)] for very smooth confinement potentials, which can be described by electrostatics. Here we focus on an intermediate regime, where the filling still only takes integer values but interaction effects can lead to a spin symmetry breaking [Dempsey *et al.* (1993)] or to additional edge states [de C. Chamon and Wen (1994)].

This chapter consists of three major parts. We begin by explaining the basic differences of the three-body processes in quantum Hall edge states compared to those in quantum wires within the setting of an unreconstructed edge. We then discuss two simple models of reconstructed quantum Hall edges. First, we address relaxation processes for a spin-reconstructed edge at filling factor $\nu = 2$ and then turn to a minimal model of charge reconstruction of a $\nu = 1$ edge which provides the simplest realization of counter-propagating edge modes.

5.1 Unreconstructed edge

A confinement potential $V_c(x)$ that is sharp on the scale of the Coulomb interaction (*i.e.*, $V_c' \gg e^2/\epsilon l_B^2$, where ϵ is the dielectric constant and $l_B = (eB)^{-1/2}$ denotes the magnetic length) remains stable against interaction-induced reconstructions and the electron dispersion $\varepsilon(k)$ can be obtained approximately from the noninteracting Schrödinger equation

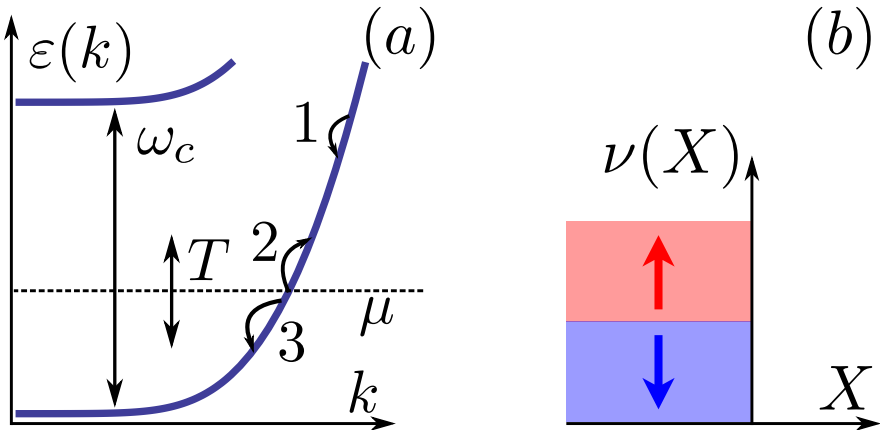

Figure 5.1: Edge without reconstruction effects. (a) Single particle dispersions and typical relaxation processes in the lowest Landau level for a spin degenerate system. Vertical arrows label temperature T and cyclotron energy ω_c. (b) The corresponding sharp ($T = 0$) occupation number as function of the guiding center position X.

$$H = \frac{1}{2m}\left[p_x^2 + (p_y - eBx)^2\right] + V_c(x)\,, \tag{5.1}$$

where we used the Landau gauge $\mathbf{A} = (0, Bx, 0)$ for the vector potential and x and y denote the directions perpendicular and along the edge, respectively. For a constant confinement potential the ground state solution of Eq. (5.1) is the lowest Landau level wave function

$$\psi_X(x,y) = (Ll_B\sqrt{\pi})^{-1/2} e^{-\mathrm{i}k_y y} e^{-(x-X)^2/2l_B^2}, \tag{5.2}$$

where $k_y = X/l_B^2$ is given in terms of the guiding center coordinate X. The characteristic energy scale of Eq. (5.1) is given by the cyclotron frequency $\omega_c = eB/m$, which also controls the gap to the next Landau level. In the limit of high magnetic fields ($V_c^{'} \ll \omega_c/l_B$), the electron states near the edge can still be approximated by the lowest Landau level wave functions and their energy simply follows the confinement potential $V_c(X)$. A generic electronic dispersion of an unreconstructed edge is sketched in Fig. 5.1a, exhibiting a confinement-induced bending of the Landau levels near the edge of the sample. The defining feature of the unreconstructed edge is the sharp zero-temperature occupation function $\nu_\sigma(X) = \Theta(-X)$ of Landau level states with guiding center X when the Zeeman splitting ε_Z is negligible [see Fig. 5.1b].

The single particle dispersion near the Fermi energy (corresponding to momentum k_F) is controlled by the confinement potential and can be approximated as

$$\varepsilon(k) = v_F(k - k_F) + (k - k_F)^2/2m_c\,. \tag{5.3}$$

The dispersion is parametrized through the edge velocity $v_F = V_c^{'} l_B^2$ at the Fermi energy and the curvature $1/m_c = V_c^{''} l_B^4$. Note that these parameters become maximal for an

infinitely sharp edge for which $v_F \sim \omega_c l_B$ and $1/m_c \sim 1/m$ [Halperin (1982)]. Note however, that a description in terms of the wave functions in Eq. (5.2) is no longer valid in this extreme limit.

The finite curvature of the dispersion implies that at least three particles are required for an energy and momentum conserving relaxation process. Relaxation of a high-energy electron (labeled by $i = 1$ in Fig. 5.1a) is possible by scattering two electrons (labeled $i = 2, 3$ in Fig. 5.1a) near the Fermi energy. Indeed, due to the curvature of the dispersion near the Fermi energy, exciting electron $i = 2$ from the Fermi energy requires more energy than scattering electron $i = 3$ deeper into the Fermi sea. Clearly, this relaxation process relies on finite temperature and typical energy transfers for electrons $i = 2, 3$ at the Fermi energy are of the order of T. Quantitatively, this process can relax the hot particle with excess energy $\varepsilon \approx v_F(k_1 - k_F) = v_F k$ by

$$q_1 = \frac{q_3(k_{2'} - k_3)}{k}\,, \tag{5.4}$$

which follows from energy and momentum conservation and $q_i = k_{i'} - k_i$ is the momentum transfered to particle i in the collision. Note that $q_1 \ll q_3$ so that relaxation occurs in many small steps $v_F q_1 \sim T^2/\varepsilon$.

For Landau-level filling factor $\nu = 2$, these considerations apply when the Zeeman splitting is small compared to temperature. In the opposite limit $\varepsilon_Z \gg T$, the curvature of the dispersion implies that the Fermi momenta and hence the Fermi velocities differ for the two spin directions. In this case, relaxation is dominated by processes in which the electrons $i = 1$ and $i = 2$ have opposite spins, and thus different Fermi momenta k_{Fj} and Fermi velocities v_j with $j = 1, 2$. To include a finite Zeeman splitting at Landau level filling factor $\nu = 2$ as well as for later convenience, it is thus beneficial to consider a modified dispersion

$$\varepsilon(k) = \begin{cases} v_j(k - k_{Fj}), & k \approx k_{Fj} \\ v_1(k - k_1) + \varepsilon, & k \approx k_1 \end{cases} \tag{5.5}$$

which is linearized in the vicinity of each of the three particles, including the hot particle with velocity v_1 and momentum k_1. This captures the behavior in the regime of strong Zeeman splitting $\varepsilon_Z \gg T$ on which we will focus in the following. Nevertheless, we can also recover the results for the quadratic dispersion and weak Zeeman splitting $\varepsilon_Z \ll T$ by identifying $v_2 - v_3$ with the typical velocity difference $T/(v_F m_c)$ due to the curvature of the dispersion. Using the dispersion in Eq. (5.5), energy and momentum conservation leads to

$$q_1 = \frac{v_2 - v_3}{v_1 - v_2} q_3\,. \tag{5.6}$$

The velocity difference $v_2 - v_3 \sim \varepsilon_Z/(v_2 m_c)$ is controlled by the Zeeman splitting which we assume to be small compared to the excitation energy ε such that $(v_2 - v_3) \ll (v_1 - v_2)$.

5.1.1 Three-body scattering formalism

Energy relaxation by processes of the kind shown in Fig. 5.1a was already discussed in section 4.3. While the calculation here follows the same outline, there are characteristic differences related to the nature of the interaction matrix elements. The energy relaxation rate via three-body collisions is again given by

$$\frac{1}{\tau_E} = \sum_{231'2'3'} \frac{-v_1 q_1}{\varepsilon} W^{123}_{1'2'3'} n_2 n_3 (1-n_{1'})(1-n_{2'})(1-n_{3'})\,. \tag{5.7}$$

where n_i is the Fermi-Dirac distribution function at k_i. The factor involving q_1 weights the out-scattering rate with the relative relaxed energy, accounting for the fact that the hot particle relaxes only a fraction of its energy in a single collision. The three-body matrix element can be evaluated by the generalized golden rule

$$W^{123}_{1'2'3'} = \frac{2\pi}{\hbar} |\langle 1'2'3'|VG_0V|123\rangle_c|^2 \delta(E-E'). \tag{5.8}$$

Here, G_0 is the free Green's function, $V = (1/2L)\sum_{k_1k_2q\sigma_1\sigma_2} V_q(k_1-k_2) a^\dagger_{k_1+q\sigma_1} a^\dagger_{k_2-q\sigma_2} a_{k_2\sigma_2} a_{k_1\sigma_1}$ is the generic two-body interaction potential, and the subscript c emphasizes that only connected processes contribute which involve all three particles.

The calculation for quantum Hall edges differs from that for quantum wires in the form of the Coulomb matrix element $V_q(k_1-k_2)$ which now have to be evaluated using the Landau level wave functions in Eq. (5.2). The main difference is that while the edge states are one dimensional in the sense that they only depend on a single quantum number k_y, changing k_y also affects their transverse position X, which is not the case for quantum wires.

Coulomb matrix element

We start from the interaction matrix element in real space

$$V_{\delta X}(X,X') = \left\langle \psi^{(1)}_{X+\delta X}, \psi^{(2)}_{X'-\delta X} \left| \frac{e^2/\epsilon}{|\mathbf{r}^{(1)}-\mathbf{r}^{(2)}|} \right| \psi^{(1)}_{X}, \psi^{(2)}_{X'} \right\rangle. \tag{5.9}$$

In the following we will measure all lengths scales in units of the magnetic length l_B. In these units the guiding center coordinate directly translates into momenta. With the lowest Landau level wave functions of Eq. (5.2) we then find

$$\begin{aligned} V_{\delta X}(X,X') \;=\; & \frac{e^2}{\pi\epsilon L^2} \int \mathrm{d}x\mathrm{d}y\mathrm{d}\Delta x\mathrm{d}\Delta y \frac{e^{-\sqrt{\Delta x^2+\Delta y^2}/d}}{\sqrt{\Delta x^2+\Delta y^2}} \\ & \times e^{-i\Delta y\delta X} e^{-\frac{1}{2}(x-X)^2} e^{-\frac{1}{2}(x-X-\delta X)^2} e^{-\frac{1}{2}(x+\Delta x-X')^2} e^{-\frac{1}{2}(x+\Delta x-X'+\delta X)^2}, \end{aligned} \tag{5.10}$$

where we used the screened Coulomb potential which carries an extra factor $e^{-\sqrt{\Delta x^2+\Delta y^2}/d}$ with d being the distance to a screening gate. The integration over Δy gives $2K_0(|\Delta x \delta X|)$ in

the case when $\delta X \gg 1/d$, where K_0 is a modified Bessel function. If, however, $\delta X \ll 1/d$ the integral is cut off and the result changes to $2K_0(|\Delta x/d|)$. We will derive results for the case $\delta X \gg 1/d$ and keep in mind the appropriate changes for the other limit. After the y integration, giving a factor of L, we obtain the intermediate result

$$V_{\delta X}(X, X') = \frac{2e^2}{\pi\epsilon L} e^{-\frac{1}{2}\delta X^2} \int \mathrm{d}x \mathrm{d}\Delta x K_0(|\Delta x \delta X|) e^{-\frac{1}{2}(2x-X-X'+\Delta x)^2} e^{-\frac{1}{2}(X-X'+\delta X+\Delta x)^2}. \quad (5.11)$$

Performing the Gaussian integral over x gives a factor of $\sqrt{\pi/2}$. Reinserting l_B and using the Landau gauge one arrives at

$$V_q(k_y) = \sqrt{\frac{\pi}{2}} \frac{e^2}{\epsilon} e^{-\frac{1}{2}q^2 l_B^2} \int \mathrm{d}\kappa l_B e^{-\frac{1}{2}(k_y+q+\kappa)^2 l_B^2} K_0(|\kappa q l_B^2|)\,. \quad (5.12)$$

Note that $V_q(k_y) = V_q(-k_y - 2q)$ and is therefore not symmetric in the argument, which plays an important role in the derivation of the three-body matrix element. In the limiting case of Eq. (5.12) when $k_y l_B \gg 1$ one can approximate the exponential under the integral by the delta-function $\sqrt{2\pi}\delta(k_y + q + \kappa)$, and thus obtains

$$V_q(k_y) = \frac{2e^2}{\epsilon} e^{-\frac{1}{2}q^2 l_B^2} K_0(|q(k_y+q) l_B^2|). \quad (5.13)$$

In the other limiting case when $k_y l_B \ll 1$ one can approximate the exponential under the integral of Eq. (5.12) by $\exp(-\kappa^2 l_B^2/2)$ and then complete the integration exactly with the result

$$V_q(k_y) = \frac{e^2}{\epsilon} e^{-\frac{1}{2}q^2 l_B^2} K_0(q^2 l_B^2/4). \quad (5.14)$$

The important conclusion is that for quantum Hall systems, the Coulomb matrix element is exponentially suppressed by a factor of $\exp(-q^2 l_B^2/2)$ for large momentum transfers. This is especially relevant because large momentum transfers yield the leading contribution to relaxation in quantum wires (see chapter 4.2). Moreover, $V_q(k_1 - k_2)$ does not only depend on the momentum transfer but also on the initial momentum difference which controls the distance of the guiding centers of the interacting electrons. Focusing on the remaining low momentum transfer processes ($q \ll 1/l_B$) and using the asymptotic expansion of the Bessel function [see Eq. (4.16)] one obtains

$$V_q(k_1 - k_2) \simeq \begin{cases} -\frac{2e^2}{\epsilon} \ln|q l_B|, & k_1 - k_2 \ll l_B^{-1} \\ -\frac{2e^2}{\epsilon} \ln|q(k_1 - k_2 + q) l_B^2|, & k_1 - k_2 \gg l_B^{-1} \end{cases}, \quad (5.15)$$

with the understanding that at small q, the matrix elements will be eventually cut off by a large length scale $d \gg l_B$ which is given by the distance to a screening gate. For $k_1 - k_2 \ll 1/l_B$ the Coulomb matrix element is that of a quantum wire of width l_B [see Eq. 4.17]. For $k_1 - k_2 \gg 1/l_B$, the interaction is that of electrons in two quantum wires separated by a distance of $(k_1 - k_2 + q) l_B^2$ which corresponds to the average of the

momentum differences of the electrons before and after the collision.

Three-body matrix element

With the absence of large momentum transfer processes the three-body scattering is dominated by the direct matrix element. The importance of the (k_1-k_2) dependence of the Coulomb matrix element can be seen from the fact that the linearized dispersion of Eq. (5.5) leads to a vanishing direct matrix element for a quantum-wire-like Coulomb interaction $V_q(0)$. Reiterating the derivation from Lunde *et al.* (2007) for the direct matrix element (see Appendix A.3), now using the dispersion relation of Eq. (5.5) yields

$$\begin{aligned} T^{123}_{1'2'3'} \approx \frac{1}{L^2}\Bigg[& \frac{V_{q_3}(k_3-k_2)V_{q_1}(k_1-k_2+q_3)-V_{q_1}(k_1-k_2)V_{q_3}(k_3-k_2+q_1)}{q_3(v_2-v_3)} \\ & + \frac{V_{q_2}(k_2-k_3)V_{q_1}(k_1-k_3+q_2)-V_{q_1}(k_1-k_3)V_{q_2}(k_2-k_3+q_1)}{q_2(v_3-v_2)} \\ & + \frac{V_{q_1}(k_3-k_1)V_{q_2}(k_2-k_1+q_3)-V_{q_2}(k_2-k_1)V_{q_3}(k_3-k_1+q_2)}{q_3(v_1-v_3)}\Bigg], \end{aligned} \tag{5.16}$$

where we omitted the trivial spin structure that contributes $\propto \delta_{\sigma_1,\sigma_{1'}}\delta_{\sigma_2,\sigma_{2'}}\delta_{\sigma_3,\sigma_{3'}}$ and used the property $V_q(k_y) = V_q(-k_y-2q)$. Note that this expression indeed vanishes for $V_q(k_y) = V_q$. To proceed further we make use of the assumptions that the injected particle is of high energy, such that $v_1 \gg v_{2,3}$ and $k_1 \gg k_{2,3}$. In this case we expand $V_{q_i}(k_y+q_i)$ in q_i and obtain

$$\begin{aligned} T^{123}_{1'2'3'} \approx \frac{2e^2}{\epsilon L^2}\Bigg[& -\frac{V_{q_3}(k_3-k_2)}{(v_2-v_3)(k_1-k_2)} - \frac{V_{q_1}(k_1-k_2)}{(v_1-v_2)(k_2-k_3)} + \frac{V_{q_2}(k_2-k_3)}{(v_2-v_3)(k_1-k_3)} \\ & + \frac{V_{q_1}(k_1-k_3)}{(v_1-v_3)(k_2-k_3)} + \frac{V_{q_3}(k_3-k_1)}{(v_1-v_3)(k_1-k_2)} + \frac{V_{q_2}(k_2-k_1)}{(v_1-v_2)(k_1-k_3)}\Bigg], \end{aligned} \tag{5.17}$$

where it was now possible to approximate $V_q(k_y) = -2e^2/\epsilon \ln(|k_y q| l_B^2)$ [*cf.* Eq. (5.15)]. Note that if we are in the regime when $k_2 - k_3 \ll l_B^{-1}$ we have to use the interaction potential $V_q(k_y) = -2e^2/\epsilon \ln(|q| l_B)$, which has a vanishing derivative with respect to k. This can be accounted for by removing the two terms with $V_{q_1}(\ldots)$ in the above formula for $T^{123}_{1'2'3'}$. Finally, to the leading logarithmic order we can set $V_{q_1}(k_1-k_2) = V_{q_1}(k_1-k_3)$ as well as $V_{q_2}(k_2-k_1) = V_{q_3}(k_3-k_1) = V_{q_3}(k_1-k_2)$ and $V_{q_3}(k_3-k_2) = V_{q_2}(k_2-k_3)$ to obtain the more compact result

$$T^{123}_{1'2'3'} = -\frac{2e^2}{L^2\epsilon}\left(\frac{k_2-k_3}{v_2-v_3}\frac{V_{q_3}(k_2-k_3)}{k^2} - \frac{2V_{q_3}(k)}{(\Delta v)\,k} + \frac{v_2-v_3}{k_2-k_3}\frac{V_{q_1}(k)}{(\Delta v)^2}\right). \tag{5.18}$$

Here, $v_1 - v_2 = \Delta v$ and $k_1 - k_2 = k$. Note that this expression applies with the assumption that all initial momentum differences are large compared to $1/l_B$ to also suit the reconstruction effects that will be discussed later. For the unreconstructed edge, it is however more reasonable to assume $k_2 - k_3 \ll 1/l_B$ (which holds for typical $\varepsilon_Z, T \ll e^2/\epsilon l_B$) in

which case the last term of Eq. (5.18), involving V_{q_1}, does not show up.

5.1.2 Results for the unreconstructed edge

For the unreconstructed edge, the momentum and velocity differences are linked by the curvature of the confinement potential via $v_2 - v_3 = (k_2 - k_3)/m_c$ and $\Delta v = k/m_1$. Here, we included the possibility that the confinement potential grows faster than quadratic which defines an effective $m_1^{-1} > m_c^{-1}$ that captures this effect. For brevity of the presentation, we assume $m_c \gg m_1$ so that the direct matrix element takes the form

$$T^{123}_{1'2'3'} = -\frac{2e^2 m_c}{L^2 \epsilon k^2} V_{q_3}(k_2 - k_3)\,. \tag{5.19}$$

Since for large Zeeman energy the particles at k_2 and k_3 have opposite spins, there is no exchange contribution (remember that exchange is appreciable for small momentum transfers only) and Eq. (5.19) fully determines the three-body matrix element. The corresponding energy relaxation rate can then be obtained by power counting which yields

$$\frac{1}{\tau_E} \sim \frac{L}{\Delta v}(Lk_T)^3 \frac{(v_2 - v_3)k_T}{(\Delta v)k} \left(\frac{e^4 m_c}{\epsilon^2 L^2 k^2}\right)^2 \frac{v_2 - v_3}{\Delta v} \tag{5.20}$$

$$= \frac{(k_2 - k_3)^2}{m_1} \left(\frac{e^2}{\epsilon \Delta v}\right)^4 \left(\frac{k_T}{k}\right)^4 . \tag{5.21}$$

In obtaining this result, a factor of $L/\Delta v$ emerges from eliminating the δ-function in Eq. (5.8), each summation over the remaining k_2, k_3, q_3 contributes a phase space factor of $\sim k_T = T/v_2$, and the last factor in the first line of Eq. (5.21) accounts for the competition between excitation ($q_1 > 0$) and relaxation ($q_1 < 0$) of the hot particle. The latter is slightly favored because the momentum transfer working against the Fermi distribution is reduced by a fraction $q_1/k_T \sim (v_2 - v_3)/\Delta v$ (see section 4.3).

Eq. (5.21) implies that the relaxation rate it strongly temperature dependent and can be enhanced [$(k_2 - k_3) \approx \varepsilon_Z/v_2$] by increasing the magnetic field.

The relaxation rate in Eq. (5.21) was obtained for large Zeeman energy $\varepsilon_Z \gg T$. As mentioned above, the relaxation rate in the opposite limit of weak Zeeman splitting $\varepsilon_Z \ll T$ can be obtained up to prefactors by replacing $(k_2 - k_3) \sim T/v_2 = k_T$. Note that this regime allows for a low momentum transfer exchange term $T^{123}_{1'3'2'}$ because the particles 2 and 3 are no longer necessarily of opposite spin. $T^{123}_{1'3'2'}$ can then be obtained from Eq. (5.19) by replacing $q_3 \to k_{2'} - k_3$, which does not change the power counting argument. For a spin polarized edge, however, Eq. (5.21) only applies if the Coulomb interaction is not screened for momenta of the order of k_T. For a screened short range interaction ($k_T \ll 1/d$), the Pauli principle leads to a suppression of the energy relaxation rate by an additional factor of $(k_T d)^4 \ll 1$ (see section 4.3).

Note that the fact that Eq. (5.21) reproduces the result of the corresponding relaxation rate in a quantum wire [Eq. (4.63)] only up to a factor of the order $(k_T/k)^2$ has its origin in

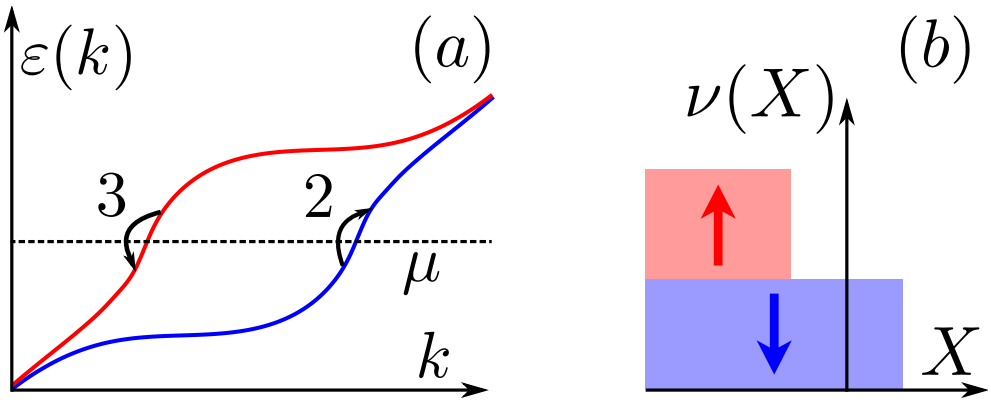

Figure 5.2: Spin reconstructed edge for $\varepsilon_Z = 0$. (a) depicts the Hartree-Fock single particle dispersion in the reconstructed region. The relaxing hot particle $i = 1$ lies outside this region and is not shown. Note that the curvature of the confinement potential was set to zero such that the velocity difference $v_2 - v_3 > 0$ is not obvious from the figure. (b) shows the $T = 0$ occupation numbers of the different spin species as function of the guiding center coordinate X.

the suppression of the large momentum transfer processes such that the energy relaxation in a quantum Hall edge without reconstruction effects is comparatively slow.

5.2 Spin reconstruction

Edge reconstruction in quantum Hall systems results from the competition between the Coulomb interaction and the confinement potential. Spin reconstruction at $\nu = 2$ takes place when the confinement potential V_c varies sufficiently slowly so that $V_c' < e^2/\epsilon l_B^2$ and can be understood at the level of the Hartree-Fock approximation [Dempsey *et al.* (1993)]. Once the slope of the confinement potential becomes weaker than that of the repulsive Hartree potential V_H, it is favorable to deposit charges outside the edge. This can be done without paying extra exchange energy by a relative shift of the Fermi momenta of spin up and spin down particles, as depicted in Fig. 5.2. In the absence of a Zeeman splitting, $\varepsilon_Z = 0$, this is a second order phase transition with spontaneous breaking of the spin symmetry. Then, the distance of the two Fermi momenta varies as $k_{F2} - k_{F3} \propto [V_c' - V_H']^{1/2}$, eventually saturating at $1/l_B$ [Dempsey *et al.* (1993)]. For finite Zeeman splitting ε_Z, the spin symmetry is lifted by the Zeeman field and the transition is smeared on the scale of $k_{F2} - k_{F3} \sim \varepsilon_Z/v_2$.

Spin reconstruction leads to characteristic changes in the single particle dispersion that develops an "eye structure" [see Fig. 5.2a]. Important for the relaxation dynamics is the increase of $v_2 - v_3 = (k_{F2} - k_{F3})/m_c$, which enhances the typical relaxed energy per relaxation step [*cf.* Eq. (5.6)].

For truly long range interactions, the particle velocity would exhibit a logarithmic singularity $\sim e^2/\epsilon \ln(|k - k_F|l_B)$ at the Fermi energy, which is however cut off in the presence of screening, say by a nearby gate electrode, at a scale $1/d$. The Fermi velocity is

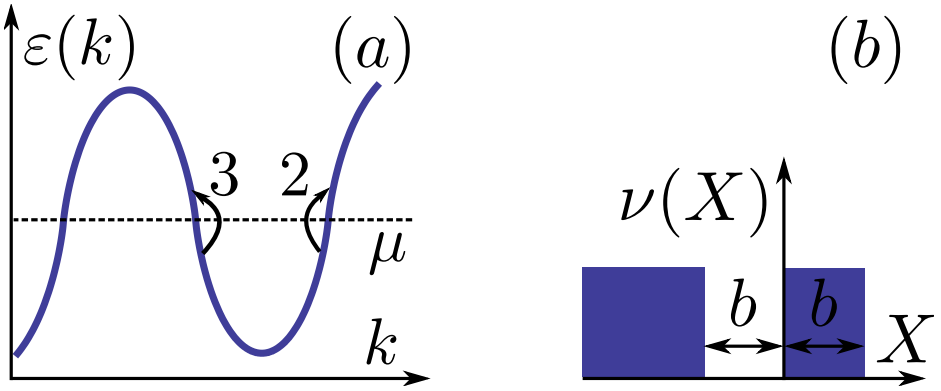

Figure 5.3: Charge reconstructed edge. (a) depicts the Hartree-Fock single particle dispersion in the reconstructed region of a spin polarized sample at $\nu = 1$. The relaxing hot particle $i = 1$ lies outside this region and is not shown. (b) shows the occupation number as function of guiding center coordinate X near the edge of the sample.

thus still of the order of $v_2, v_3 \sim e^2/\epsilon$ for typical choices of the screening length d.

Even with spin reconstruction, the relaxation of hot particles can still be described within the model dispersion of Eq. (5.5). We consider the case where the hot particle [not shown in Fig. 5.2] is injected well outside the reconstructed region of size $e^2/(\epsilon l_B)$. This is compatible with the condition for the validity of a perturbative expansion, which reduced to $v_1 \gg v_2$ for the case that the Fermi velocity is determined by the interaction.

The energy relaxation rate $1/\tau_E^{(s)}$ can now be derived in the same way as for the unreconstructed edge and consequently, Eq. (5.21) also applies to spin reconstructed edges. The crucial difference is that the momentum difference is now strongly enhanced by the spin reconstruction, taking values up to $k_2 - k_3 \sim 1/l_B$. Comparing the rates before ($k_2 - k_3 \sim \max\{\varepsilon_Z, T\}/v_2$) and well after spin reconstruction, one finds an enhancement of the relaxation rates given by

$$\frac{1}{\tau_E^{(s)}} = \left(\frac{e^2/(\epsilon l_B)}{\max\{\varepsilon_Z, T\}}\right)^2 \frac{1}{\tau_E}. \tag{5.22}$$

5.3 Charge reconstruction

For confinement potentials that vary even more smoothly, changing by $e^2/\epsilon l_B$ over a region $w > l_B$, spin reconstruction can be accompanied by an additional charge reconstruction such that part of the electrons at the edge are pushed away from the bulk by a length of the order of l_B [de C. Chamon and Wen (1994); Barlas *et al.* (2011)]. This corresponds to a non-monotonic behavior of the dispersion with momentum and the creation of two additional counter-propagating edge modes, as depicted in Fig. 5.3.

A minimal model for charge reconstruction considers filling factor $\nu = 1$ within the Hartree-Fock approximation [de C. Chamon and Wen (1994)]. Consider first a confinement

potential defined by a positive background charge which occupies lowest Landau level wave functions ψ_X with the occupation number $\nu_c(X) = \Theta(-X)$. Such a confinement potential exactly cancels the Hartree potential of the electrons for an unreconstructed edge. In this case, the electron occupation of the unreconstructed edge is stabilized by the (attractive) exchange potential.

The reconstruction transition can then be modeled by changing the abrupt drop of $\nu_c(X)$ into a linear decrease over a length w. For the unreconstructed electron occupations, this leads to negative (at $X < 0$) and positive (at $X > 0$) excess charges, causing a dipole field that favors separating electrons from the bulk. Once this dipole field overcomes the exchange potential, the charge reconstruction transition takes place. Within the Hartree-Fock approximation, this happens for $w \sim 8l_B$. Due to the particle-hole symmetric choice of the confinement potential around $X = 0$, the width and the distance of the additional stripe from the bulk electron droplet both take the same value b [see Fig. 5.3b]. Moreover, the transition is of first order in the sense that b changes abruptly at the transition from zero to a value of the order of l_B.

Note that the same mechanism induces new (weaker) effective dipole fields at each of the three Fermi points as the edge becomes yet smoother. Thus, increasing w even further causes additional stripes to appear, eventually approaching the limit of a compressible stripe which is expected for $w \gg l_B$ [Chklovskii *et al.* (1992)]. In the following we will focus on $w \gtrsim l_B$, remaining well outside the compressible limit.

Energy relaxation in the charge reconstructed case can also be captured by the dispersion (5.5) when setting $v_3 < 0$. The three Fermi velocities of the charge reconstructed edge are essentially determined by the variation of the exchange potential, which is short ranged such that $b \gtrsim l_B$ already approximates the bulk edge ($b \to \infty$) behavior. Consequently, the magnitude of the Fermi velocities is equal to that of the unreconstructed edge and $\sim e^2/\epsilon$. In line with the discussions above, we consider the relaxation of a hot particle injected well outside the reconstructed region with $v_1 \gg e^2/\epsilon$.

The nonmonotonic behavior of the dispersion introduces a new relaxation process which relaxes the hot particle by exciting two counter-propagating particle-hole pairs [see Fig. 5.3]. This eliminates the restriction that the energy transfers at the Fermi energy cannot exceed the temperature and makes a process similar to that for non-chiral quantum wires possible [see section 4.1]. Unlike for the discussion of the quantum wires, however, by considering the regime $v_1 \gg v_2, v_3$ the momentum transfers at the Fermi energy of the co- and counter-propagating branch are of the same order.

The three-body matrix element of Eq. (5.18) still applies in the presence of charge reconstruction because its derivation did not require a specific sign of v_3, again resulting in Eq. (5.19). The crucial difference for the energy relaxation rates arises from the large allowed $q_3 \sim 1/l_B$, which is limited only by the size of the reconstructed region for which the linearized dispersion applies. This increases both the momentum phase space to $(L/l_B)^3$ and the typical relaxed momentum to $(v_2 - v_3)/(\Delta v l_B)$. Moreover, excitation and

relaxation processes no longer need to be balanced when $e^2/\epsilon l_B \gg T$, and we find

$$\frac{1}{\tau_E^{(c)}} \sim \frac{m_c}{m_1^2}(k_2 - k_3)\Delta k \left(\frac{e^2}{\epsilon \Delta v}\right)^4 \left(\frac{1/l_B}{k}\right)^4 , \tag{5.23}$$

which allows for relaxation even at $T = 0$ and implies a dramatic increase of the relaxation rate.

5.4 Conclusions

We studied three-body processes as an intrinsic mechanism for relaxation of hot electrons in clean integer quantum Hall edges at Landau level filling factors $\nu = 1$ and $\nu = 2$. These processes rely crucially on the form of the electron dispersion and are thus susceptible to edge reconstruction effects. For an unreconstructed edge, energy relaxation requires a finite temperature which determines the phase space for the relaxation processes. The energy given up by the hot electron in a single three-body collision is controlled by curvature effects on the scale of temperature or Zeeman energy so that the relaxation rate can in principle be tuned by a magnetic field once $\varepsilon_Z \gg T$.

While unreconstructed edges are expected for steep confinement potentials, smoother confinement potentials with $V_c^{'} \lesssim e^2/(\epsilon l_B^2)$ may lead to an interaction-induced spin reconstruction, which causes a relative shift of the Fermi momenta of the two spin species by $\sim 1/l_B$. The three-body processes are then controlled by curvature effects on the scale of the interaction energy $e^2/(\epsilon l_B)$ which causes a strong increase of the relaxation rate.

Even softer confinement may cause charge reconstruction which introduces additional co- and counter-propagating edge modes. The presence of counter-propagating modes allows for relaxation even at $T = 0$. Consequently, the phase space for three-body collisions is no longer controlled by temperature but by the size of the reconstructed region $\sim e^2/(\epsilon l_B)$ which ensues an additional dramatic enhancement of the relaxation rate.

6 Scattering theory of current induced forces in nanoelectromechanical systems[1]

In this chapter we develop a scattering theory of the non-equilibrium forces that electrons exert on slowly varying mechanical degrees of freedoms in nanoelectromechanical systems. The separation of electronic and mechanical times scales allows one to treat the mechanical degrees of freedom as classical variables that are described by a Langevin equation

$$M_\alpha \ddot{X}_\alpha + \frac{\partial U}{\partial X_\alpha} = F_\alpha^{(0)} - \sum_\beta \gamma_{\alpha\beta}\dot{X}_\beta + \xi_\alpha \,. \tag{6.1}$$

Here M_α and U are the generalized mass and potential of the N mechanical degrees of freedom $\mathbf{X} = (X_1, .., X_N)$. The coupling to the electrons is then described by the mean and fluctuating force $F_\alpha^{(0)}$ and ξ_α as well as the damping matrix $\gamma_{\alpha\beta}$ which results from the first order of the adiabatic expansion. In out of equilibrium situations, it is no longer possible to relate $\gamma_{\alpha\beta}$ and ξ_α by the fluctuation dissipation theorem and the fully adiabatic scattering matrix will not be sufficient to describe the velocity dependent current induced forces [Bode *et al.* (2011, 2012)]. It is therefore important to account for a slow time dependence in scattering theory.

While the static scattering theory is a well-known standard tool for treating coherent transport in mesoscopic systems [see *e.g.* Blanter (2010) for a pedagogical discussion], its time dependent counterpart is far less elaborated. Scattering matrix expressions for slowly time dependent phenomena were mainly obtained in the context of adiabatic pumping [Brouwer (1998); Avron *et al.* (2001)] and further refined in the context of Floquet scattering theory [Moskalets (2011)] for systems with periodic time dependence.

In this chapter we will use an arbitrarily (but slowly) time dependent scattering theory. First, we will however start with a short review of the static scattering scattering theory which provides the reference point for an adiabatic expansion of the time dependent problem.

[1] This chapter is based on joint work with M. Thomas, S. Viola Kusminskiy, G. Zaránd and F. von Oppen.

6.1 Static scattering theory

Time independent scattering theory considers the Hamiltonian

$$H = H_0 + V, \tag{6.2}$$

where H_0 is a free Hamiltonian with plane wave eigenstates

$$H_0|\phi_m(E)\rangle = E|\phi_m(E)\rangle \tag{6.3}$$

and V describes the scattering potential. The latter is assumed to have a finite range such that the asymptotics of the system far from the scatterer are described by H_0. In mesoscopic systems H_0 is typically the Hamiltonian in the leads which are modeled as ideal waveguides. Consequently m is a combined index labeling channels and leads.

One of the central objects of scattering theory are the advanced $(-)$ and retarded $(+)$ scattering states which are eigenstates of the full Hamiltonian

$$H|\psi_m^{\pm}(E)\rangle = E|\psi_m^{\pm}(E)\rangle\,. \tag{6.4}$$

Both, the advanced and the retarded solutions span the full Hilbert space and correspond to different boundary conditions. The retarded solutions evolve from a plane wave state at $t \to -\infty$ when adiabatically switching on the scattering potential $V \to V\exp(-\eta|t|)$ (*i.e.* we consider the limit $\eta \to 0$). The advanced scattering states on the other hand are evolved backwards in time from a free state at $t \to +\infty$. In terms of the time evolution operator $U(t,t')$ the scattering states can therefore be written as

$$|\psi_m^{+}(E)\rangle = U(0,-\infty)|\phi_m(E)\rangle \tag{6.5}$$

$$|\psi_m^{-}(E)\rangle = U(0,\infty)|\phi_m(E)\rangle\,. \tag{6.6}$$

The solution of Eqs. (6.5,6.6) are given by the Lippman-Schwinger equation

$$|\psi_m^{\pm}(E)\rangle = |\phi_m(E)\rangle + G^{R/A}(E)V|\phi_m(E)\rangle\,, \tag{6.7}$$

in terms of the full Green's functions

$$G^{R/A}(E) = \frac{1}{E - H \pm \mathrm{i}\eta}\,. \tag{6.8}$$

The scattering matrix (S-matrix) is then defined as the unitary basis transformation from the retarded to the advanced states

$$S_{mn}(E',E) = \langle\psi_m^{-}(E')|\psi_n^{+}(E)\rangle \tag{6.9}$$

$$= \langle\phi_m(E')|U(\infty,-\infty)|\phi_n(E)\rangle \tag{6.10}$$

and is purely elastic $S(E', E) = S(E)\delta(E - E')$ due to the time independence of the problem. The physical interpretation of the S-matrix is that it gives the amplitude for an incoming wave packet ($t \to -\infty$) at energy E and quantum number n to scatter into an outgoing wave packet at E', m for ($t \to \infty$).[2]

6.2 Slowly time dependent scattering theory

In this section we depart from the purely static scattering theory and consider a Hamiltonian

$$H(t) = H_0 + V(t)\,, \tag{6.11}$$

where $V(t)$ varies slowly on the time scale of the electron interaction with the localized potential $V(t)$. In the setting of nanoelectromechanical systems the scattering potential depends only parametrically on time and takes the form

$$V(t) = V(\mathbf{X}(t)) \tag{6.12}$$

where $\mathbf{X}(t)$ denotes the slowly varying mechanical degrees of freedom. We now define the time dependent retarded (+) and advanced (−) scattering states as full solutions of the *time dependent* Schrödinger equation

$$\mathrm{i}\partial_t |\Psi_m^{\pm}(E,t)\rangle = H(t)\,|\Psi_m^{\pm}(E,t)\rangle, \tag{6.13}$$

where the index m labels quantum numbers within the degenerate subspace of eigenstates of H_0 with energy E. The difference between advanced and retarded scattering states lies again in their boundary conditions. Since the time an electron spends in the scattering region is finite its evolution will be determined only by the free Hamiltonian H_0 for $t \to \pm\infty$. This can be implemented similarly to the time independent problem by switching off the potential $V(t) \to V(t)\exp(-\eta|t|)$ at large times. The scattering states are now defined with the boundary conditions

$$|\Psi_m^{\pm}(E,t)\rangle = \mathrm{e}^{-\mathrm{i}Et}|\phi_m(E)\rangle \begin{cases} t \to -\infty \\ t \to +\infty \end{cases} \tag{6.14}$$

such that they evolve forward (+) and backward (−) in time from an eigenstate of the free Hamiltonian. In the following it will be convenient to write the time dependent scattering states as

$$|\Psi_m^{\pm}(E,t)\rangle = \mathrm{e}^{-\mathrm{i}Et}|\psi_m^{\pm}(E,t)\rangle\,, \tag{6.15}$$

[2] A detailed discussion that the overlap of the scattering states indeed gives the reflection and transmission amplitudes of scattering can be found in the formal, but nicely written scattering theory introduction in the book of Mello *et al.* (2004).

which extracts the fast dynamic time dependence. The Schrödinger equation then takes the form

$$\mathrm{i}\partial_t|\psi_n^{\pm}(E,t)\rangle = [H(t)-E]\,|\psi_n^{\pm}(E,t)\rangle\,. \tag{6.16}$$

The solution of the Schrödinger equation (6.16) can be obtained iteratively within an adiabatic expansion in the slow time dependence [Entin-Wohlman *et al.* (2002)]. To zeroth order one can ignore the time dependence of $|\psi_n^{\pm}(E,t)\rangle$. Eq. (6.16) is then solved by the frozen scattering states $|\psi_n^{t\pm}(E)\rangle$ that are a solution of a static scattering problem with fixed Hamiltonian $H(\mathbf{X}(t))$ and therefore depend only parametrically on t.

The first order in the adiabatic expansion can be obtained by noting that in this order $\partial_t|\psi_n^{\pm}(E,t)\rangle = \partial_t|\psi_n^{t\pm}(E)\rangle$ and one obtains

$$|\psi_m^{\pm}(E,t)\rangle = |\psi_m^{t\pm}(E)\rangle - \mathrm{i}G^{R/A}(E)\,|\partial_t\psi_m^{t\pm}(E)\rangle\,, \tag{6.17}$$

which is fully determined by the frozen scattering states. Here, $G^{R/A}(E) = 1/(E-H(t)\pm i\eta)$ denotes the (frozen) retarded and advanced Green's functions and $|\partial_t\psi_m^{t\pm}(E)\rangle = \partial_t\left(|\psi_m^{t\pm}(E)\rangle\right)$. By taking the derivative of the Lippman-Schwinger equation [see Eq. (6.7)] for the frozen scattering states one can then rewrite the time derivative of the scattering state as

$$|\partial_t\psi_n^{t\pm}(E)\rangle = G^{R/A}(E)\,[\partial_t V]\;|\psi_n^{t\pm}(E)\rangle\,. \tag{6.18}$$

Here we used

$$\partial_t G^{R/A}(E) = G^{R/A}(E)\,[\partial_t V]\,G^{R/A}(E), \tag{6.19}$$

which can be obtained by expanding G in powers of $V(t)$ and the time independent free Green's functions G_0.

6.2.1 Adiabatic expansion of the S-matrix

Starting from the time independent definition of the S-matrix it is natural to define the following generalization of a fully time dependent S-matrix

$$\begin{aligned}\mathcal{S}_{mn}(E',E,t_0) &= \langle\phi_m(E')|U(\infty,t_0)U(t_0,-\infty)|\phi_n(E)\rangle. &(6.20)\\ &= \langle\Psi_m^{-}(E',t_0)|\Psi_n^{+}(E,t_0)\rangle. &(6.21)\end{aligned}$$

Note that this S-matrix becomes time independent for a static Hamiltonian. For a slow time dependence of the Hamiltonian $\mathcal{S}_{mn}(E',E,t_0)$ will also only change slowly and t_0 has to be evaluated at an appropriate "average time". This can be implemented by the Wigner transform, which helps decoupling the slow central time t from the fast relative time oscillations that are due to the electronic energies. Usually the Wigner transform is defined as a mapping $f(t+\tau/2,t-\tau/2)\to f(E,t)$. Here we encounter the equivalent problem of a Wigner transform in energies, which decouples the central energy that leads to the fast time changes and the small energy difference that is due to the slowly varying

degrees of freedom. The two energy Wigner transform takes the form

$$\mathcal{S}_{mn}(E,t) = \int \mathrm{d}\varepsilon \mathrm{e}^{-\mathrm{i}\varepsilon t} \mathcal{S}_{mn}\left(E+\frac{\varepsilon}{2}, E-\frac{\varepsilon}{2}, t_0\right). \tag{6.22}$$

By setting t_0 equal to the Wigner central time t we then obtain up to first order in the adiabatic expansion

$$\begin{aligned}\mathcal{S}_{mn}(E,t) &= \int \mathrm{d}\varepsilon \Big(\Big\langle \psi_m^{t-}\left(E+\frac{\varepsilon}{2}\right) \Big| \psi_n^{t+}\left(E-\frac{\varepsilon}{2}\right) \Big\rangle + \frac{\mathrm{i}}{\varepsilon - \mathrm{i}\eta} \Big\langle \psi_k^{t-}\left(E+\frac{\varepsilon}{2}\right) \Big| \partial_t \psi_n^{t+}\left(E-\frac{\varepsilon}{2}\right) \Big\rangle \\ &\quad + \frac{\mathrm{i}}{\varepsilon + \mathrm{i}\eta} \Big\langle \partial_t \psi_m^{t-}\left(E+\frac{\varepsilon}{2}\right) \Big| \psi_n^{t+}\left(E-\frac{\varepsilon}{2}\right) \Big\rangle \Big) \qquad (6.23) \\ &= S_{mn}(E) + \pi \left(\langle \partial_t \psi_m^{t-}(E) | \psi_n^{t+}(E) \rangle - \langle \psi_k^{t-}(E) | \partial_t \psi_n^{t+}(E) \rangle \right) \\ &\quad + \mathcal{P} \int \mathrm{d}\varepsilon \frac{1}{\varepsilon} \mathrm{i}\delta(\varepsilon) \left\langle \psi_m^{t-}(E) \middle| \partial_t V \middle| \psi_n^{t+}(E) \right\rangle, \qquad (6.24)\end{aligned}$$

where

$$S_{mn}(E)\delta(E-E') = \left\langle \psi_m^{t-}(E') \middle| \psi_n^{t+}(E) \right\rangle \tag{6.25}$$

is the frozen S-matrix and we used the Dirac identity $(x+\mathrm{i}\eta)^{-1} = -\mathrm{i}\pi\delta(x) + \mathcal{P}(1/x)$, which is valid under the integral of x, where $\mathcal{P}$ denotes the principal value integral. Note that the principal value integral above vanishes such that we obtain

$$\mathcal{S}_{mn}(E,t) = S_{mn}(E) + A_{mn}(E) \tag{6.26}$$

with

$$A_{mn}(E) = \pi \left(\langle \partial_t \psi_m^{t-}(E) | \psi_n^{t+}(E) \rangle - \langle \psi_m^{t-}(E) | \partial_t \psi_n^{t+}(E) \rangle \right). \tag{6.27}$$

Eq. (6.26) is well-known in the context of time dependent scattering theory [Moskalets and Büttiker (2004, 2005a); Bode *et al.* (2011, 2012)]. The crucial advantage of the above derivation is that it gives an expression [Eq. (6.27)] for the form of first adiabatic correction to the full S-matrix in terms of the adiabatic scattering states. In previous works[3] A (A-matrix) was only given by Green's function expressions [Bode *et al.* (2011, 2012)] or had to be obtained from solving the entire time dependent problem [Moskalets and Büttiker (2004, 2005b)]. It is thus worth studying the properties of the A-matrix in this representation in more detail.

6.2.2 Properties of the A-matrix

An alternative definition of the A-matrix

$$A_{mn}(E) = \pi \langle \partial_E \psi_m^{t-}(E) | \partial_t V | \psi_n^{t+}(E) \rangle - \pi \langle \psi_m^{t-}(E) | \partial_t V | \partial_E \psi_n^{t+}(E) \rangle \tag{6.28}$$

[3] Note that the matrix A is closely related to the matrix U in the paper of Entin-Wohlman *et al.* (2002) who however did not point out the connection to the full S-matrix.

can be obtained by applying Eq. (6.18) to Eq. (6.27). Here we used

$$G^R(E)|\psi_n^{t+}(E)\rangle = -\partial_E|\psi_n^{t+}(E)\rangle\,, \tag{6.29}$$

which can be obtained by differentiating the Schrödinger equation $(E-H)\,|\psi_n^{t+}(E)\rangle = 0$ with respect to energy. Eq. (6.28) can be of practical use for a calculation of the A-matrix. The advantage is that when calculating the overlap of the scattering states in real space it restricts the integral to the finite scattering region unlike in Eq. (6.27) where the integral runs over all of space. Note also that for the same reason Eq. (6.28) nicely demonstrates that the A-matrix is always well-defined as long as the scattering potential is of finite range.

It will be useful in the following to express the time derivative of the frozen S-matrix in terms of the scattering states. This can be achieved by taking the derivative of the well-known relation

$$S_{mn}(E) = \delta_{mn} - 2\pi\mathrm{i}\langle\psi_m^{t-}(E)|V|\phi_n(E)\rangle\,, \tag{6.30}$$

which follows directly from Eq. (6.25). From Eqs. (6.7) and (6.19) we then obtain

$$\partial_t S_{mn}(E) = -2\pi\mathrm{i}\,\langle\psi_m^{t-}(E)|\,\partial_t V\,|\psi_n^{t+}(E)\rangle\,. \tag{6.31}$$

Note that this allows one to obtain the useful relation

$$\begin{aligned}
\langle\partial_t\psi_m^{t-}(E)|\psi_n^{t+}(E)\rangle &= \langle\psi_m^{t-}(E)|\,[\partial_t V]\,G^R(E)|\psi_n^{t+}(E)\rangle && (6.32)\\
&= -\langle\psi_m^{t-}(E)|\,[\partial_t V]\,|\partial_E\psi_n^{t+}(E)\rangle && (6.33)\\
&= -\langle\psi_m^{t-}(E)|\partial_t\psi_n^{t+}(E)\rangle - \frac{\mathrm{i}}{2\pi}\partial_E\partial_t S_{mn}\,. && (6.34)
\end{aligned}$$

With these relations we can now check whether Eq. (6.27) indeed fulfills the relation

$$S^\dagger A + A^\dagger S = \frac{\mathrm{i}}{2}\left(\partial_t S^\dagger\partial_E S - \partial_E S^\dagger\partial_t S\right) \tag{6.35}$$

which follows from the unitarity of the full S-matrix [Moskalets and Büttiker (2004, 2005a); Bode *et al.* (2011, 2012)]. Using Eqs. (6.29,6.34) as well as the unitarity of the frozen S-matrix we show that (omitting the quantum numbers for better readability)

$$
\begin{aligned}
& S^\dagger A + A^\dagger S \\
= \;& \pi S^\dagger \left(\langle \partial_t \psi_E^- | \psi_E^+ \rangle - \langle \psi_E^- | \partial_t \psi_E^+ \rangle \right) + \pi \left(\langle \psi_E^+ | \partial_t \psi_E^- \rangle - \langle \partial_t \psi_E^+ | \psi_E^- \rangle \right) S && (6.36) \\
= \;& 2\pi S^\dagger \left\langle \psi_E^- \right| \left[\partial_t V \right] G^R \left| \psi_E^+ \right\rangle + 2\pi \left\langle \psi_E^+ \right| G^A \left[\partial_t V \right] \left| \psi_E^- \right\rangle S + \frac{\mathrm{i}}{2} \left(S^\dagger \partial_E \partial_t S - \partial_E \partial_t S^\dagger S \right) && (6.37) \\
= \;& -2\pi \partial_E \left[\langle \psi_E^+ | \partial_t V | \psi_E^+ \rangle \right] + \frac{\mathrm{i}}{2} \left(S^\dagger \partial_E \partial_t S - \partial_E \partial_t S^\dagger S \right) && (6.38) \\
= \;& -\frac{\mathrm{i}}{2} \partial_E \left[S^\dagger \partial_t S - \partial_t S^\dagger S \right] + \frac{\mathrm{i}}{2} \left(S^\dagger \partial_E \partial_t S - \partial_E \partial_t S^\dagger S \right) && (6.39) \\
= \;& \frac{\mathrm{i}}{2} \left(\partial_t S^\dagger \partial_E S - \partial_E S^\dagger \partial_t S \right) , && (6.40)
\end{aligned}
$$

which confirms that the A-matrix defined in Eq. (6.27) does indeed fulfill the unitarity condition.

6.3 Reaction forces

The force that the (quantum coherent) electrons exert on the (classical) vibrational degrees of freedom $\mathbf{X}(t)$ is given by [Berry and Robbins (1993)]

$$\mathbf{F} = -\mathrm{Tr}\{\tilde{\rho}(t) \nabla \mathcal{H}\} , \tag{6.41}$$

where the gradient is taken with respect to $\mathbf{X}$, $\mathcal{H}$ is the many body Hamiltonian, and $\tilde{\rho}(t)$ the corresponding many body density matrix. In the scattering formalism one is interested in single particle operators. We thus use the general relation

$$\langle \mathcal{O} \rangle = \sum_{mk} o_{mk} \left\langle a_m^\dagger a_k \right\rangle , \tag{6.42}$$

where o_{mk} is a single particle matrix element (m, k are abstract quantum numbers) and we choose that $a_m^\dagger$ creates a retarded scattering states such that $\left\langle a_m^\dagger a_k \right\rangle = f_k \delta_{km}$. It is thus possible to calculate

$$\mathbf{F} = -\mathrm{Tr}\{\rho(t) \nabla H\} , \tag{6.43}$$

where H is the single particle Hamiltonian and we defined

$$\rho(t) = \int \mathrm{d}E \sum_n f_n(E) \left| \psi_n^+(E,t) \right\rangle \left\langle \psi_n^+(E,t) \right| . \tag{6.44}$$

Here, $f_n(E)$ describes the energy probability distribution for each quantum number n of the states $|\psi_n^+(E,t)\rangle$ [Eq. (6.13)] and is determined by the reservoirs in a scattering setting.

Similar to Berry and Robbins (1993) we now perform an adiabatic expansion of $\rho(t)$ which can be done by using the expansion of the scattering states [Eq. (6.17)]. The zeroth

order expansion is given by the frozen scattering states as

$$\rho_0(\mathbf{X}) = \int \mathrm{d}E \sum_n f_n(E)\, |\psi_n^{t+}(E)\rangle\langle\psi_n^{t+}(E)|\,, \tag{6.45}$$

while the first order takes the form

$$\begin{aligned} \rho_1(\mathbf{X}) &= -\mathrm{i}\int \mathrm{d}E \sum_n f_n(E)\, G^R(E)\, |\partial_t \psi_n^{t+}(E)\rangle\langle\psi_n^{t+}(E)| &(6.46)\\ &\quad +\mathrm{i}\int \mathrm{d}E \sum_n f_n(E)\, |\psi_n^{t+}(E)\rangle\langle\partial_t\psi_n^{t+}(E)|\, G^A(E)\,. &(6.47)\end{aligned}$$

The zeroth order term of Eq. (6.43) describes the mean force $\mathbf{F}^{(0)}(\mathbf{X})$ that the quantum mechanical electrons exert on the classical mechanical degrees of freedom. The first order term involves derivatives of the form $\partial_t = \dot{\mathbf{X}}\cdot\nabla$ and leads to velocity dependent forces. These forces can lead to rich behavior such as cyclic motions through Lorentz-like forces or negative and positive damping. In the following we will discuss the different forces step by step.

6.3.1 Mean force

The mean force can be expressed as

$$F_\alpha^{(0)} = -\int \mathrm{d}E \sum_n f_n(E)\, \langle\psi_n^{t+}(E)|\partial_\alpha H|\psi_n^{t+}(E)\rangle\,, \tag{6.48}$$

where ∂_α indicates the partial derivative with respect to X_α. To turn Eq. (6.48) into an expression involving the S-matrix, we insert the resolution of the identity

$$\mathbf{1} = \int \mathrm{d}E \sum_k |\psi_k^{t-}(E)\rangle\langle\psi_k^{t-}(E)|, \tag{6.49}$$

and obtain

$$F_\alpha^{(0)} = -\int \mathrm{d}E \int \mathrm{d}E' \sum_{nm} f_n(E)\, \langle\psi_n^{t+}(E)|\psi_m^{t-}(E')\rangle\langle\psi_m^{t-}(E')|\partial_\alpha H|\psi_n^{t+}(E)\rangle\,. \tag{6.50}$$

We note that Eq. (6.31) can also be applied to spatial derivatives such that

$$\partial_\alpha S_{mn}(E) = -2\pi\mathrm{i}\,\langle\psi_m^{t-}(E)|\partial_\alpha V|\psi_n^{t+}(E)\rangle\,, \tag{6.51}$$

from which we immediately obtain

$$F_\alpha^{(0)} = -\int \mathrm{d}E \sum_{nm} f_n(E)(S)^\dagger_{mn}(E)\left[-\frac{1}{2\pi\mathrm{i}}\partial_\alpha S_{mn}(E)\right]. \tag{6.52}$$

In a more compact notation, this can be written to give the mean force

$$F_\alpha^{(0)} = \int \frac{\mathrm{d}E}{2\pi\mathrm{i}} \sum_n f_n(E) \mathrm{tr}\left\{\Pi_n S^\dagger(E)\partial_\alpha S(E)\right\}, \tag{6.53}$$

where $\mathrm{tr}\{\ldots\}$ denotes a trace (over the channel/lead index) excluding the energy integral, so that $\mathrm{Tr}\{\ldots\} = \int \mathrm{d}E\, \mathrm{tr}\{\ldots\}$, and Π_n is a projector onto the generalized channel/lead index n. In the case that the distribution functions $f_n(E)$ depend only on the lead and not on the channels, the projector can be replaced by Π_ν which projects on lead ν. Eq. (6.53) then indeed coincides with the corresponding expression of Bode *et al.* (2011, 2012).

6.3.2 Friction and Lorentz-like force

The first order correction to the mean force is given by

$$F_\alpha^{(1)} = -\int \mathrm{d}E \sum_m \langle \psi_m^{t-}(E)|\rho_1 \partial_\alpha H|\psi_m^{t-}(E)\rangle, \tag{6.54}$$

where we chose the advanced scattering states as a complete basis for evaluating the trace, which will be convenient for expressing the force in terms of the S-matrix. Note that $\partial_\alpha H = \partial_\alpha V$ such that we can use Eq. (6.18) to rewrite

$$\begin{aligned}
\partial_\alpha H|\psi_m^{t-}(E)\rangle &= \left(G^A(E)\right)^{-1} G^A(E)\partial_\alpha H|\psi_m^{t-}(E)\rangle & (6.55)\\
\partial_\alpha H|\psi_m^{t-}(E)\rangle &= \left(G^A(E)\right)^{-1} |\partial_\alpha \psi_m^{t-}(E)\rangle & (6.56)\\
\langle\psi_m^{t-}(E)|\partial_\alpha H &= \langle\partial_\alpha\psi_m^{t-}(E)|\left(G^R(E)\right)^{-1}. & (6.57)
\end{aligned}$$

Using the cyclic property of the trace the Green's functions in the expression (6.46) of ρ_1 cancel out and we find

$$\begin{aligned}
F_\alpha^{(1)} = \mathrm{i}\int \mathrm{d}E\mathrm{d}E' \sum_{mn} f_n(E') \Big[&\langle\partial_\alpha\psi_m^{t-}(E)|\partial_t\psi_n^{t+}(E')\rangle\langle\psi_n^{t+}(E')|\psi_m^{t-}(E)\rangle \\
&-\langle\psi_m^{t-}(E')|\psi_n^{t+}(E)\rangle\langle\partial_t\psi_n^{t+}(E)|\partial_\alpha\psi_m^{t-}(E')\rangle\Big].
\end{aligned} \tag{6.58}$$

With $\partial_t = \sum_\beta \dot{X}_\beta \partial_\beta$ one realizes that F_1 is indeed a velocity dependent force. It is thus convenient to define the a generalized "damping matrix" γ through

$$F_\alpha^{(1)} = -\sum_\beta \gamma_{\alpha\beta}\dot{X}_\beta. \tag{6.59}$$

It is generalized in the sense that it describes all velocity dependent forces. Only the symmetric part of $\gamma^s_{\alpha\beta} = (\gamma_{\alpha\beta} + \gamma_{\beta\alpha})/2$ corresponds to physical damping, while the anti-symmetric part $\gamma^a_{\alpha\beta} = (\gamma_{\alpha\beta} - \gamma_{\beta\alpha})/2$ describes Lorentz-like forces. For an interpretation

of the different forces it will thus be useful to decompose

$$\begin{aligned}\gamma_{\alpha\beta} &= -\mathrm{i}\int \mathrm{d}E \sum_{mn} f_n(E)\Big[S^\dagger_{nm}(E)\langle\partial_\alpha\psi^{t\,-}_m(E)|\partial_\beta\psi^{t\,+}_n(E)\rangle \\ &\quad -\langle\partial_\beta\psi^{t\,+}_n(E)|\partial_\alpha\psi^{t\,-}_m(E)\rangle S_{mn}(E)\Big]\,. \end{aligned} \tag{6.60}$$

into its symmetric and antisymmetric parts, which we denote by $\{...\}_{s/a}$.

Symmetric part

We consider the term in the first line of Eq. (6.60) and omit the energy dependence which is the same for all quantities and the sum over m is implicitly taken. We can then rewrite

$$\begin{aligned} & S^\dagger_{nm}\langle\partial_\alpha\psi^{t\,-}_m|\partial_\beta\psi^{t\,+}_n\rangle \\ =\ & S^\dagger_{nm}\left(\partial_\alpha\langle\psi^{t\,-}_m|\partial_\beta\psi^{t\,+}_n\rangle - \langle\psi^{t\,-}_m|\partial_\alpha\partial_\beta\psi^{t\,+}_n\rangle\right) && (6.61)\\ =\ & \partial_\alpha\left(S^\dagger_{nm}\langle\psi^{t\,-}_m|\partial_\beta\psi^{t\,+}_n\rangle\right) - \partial_\alpha S^\dagger_{nm}\langle\psi^{t\,-}_m|\partial_\beta\psi^{t\,+}_n\rangle - S^\dagger_{nk}\langle\psi^{t\,-}_m|\partial_\alpha\partial_\beta\psi^{t\,+}_n\rangle && (6.62)\\ =\ & -\partial_\alpha S^\dagger_{nm}\langle\psi^{t\,-}_m|\partial_\beta\psi^{t\,+}_n\rangle + \langle\partial_\alpha\psi^{t\,+}_n|\partial_\beta\psi^{t\,+}_n\rangle\,. && (6.63)\end{aligned}$$

In the same sense one obtains

$$\langle\partial_\beta\psi^{t\,+}_n|\partial_\alpha\psi^{t\,-}_m\rangle S_{mn} = \langle\psi^{t\,+}_n|\partial_\beta\psi^{t\,-}_m\rangle\partial_\alpha S_{mn} - \langle\partial_\beta\psi^{t\,+}_n|\partial_\alpha\psi^{t\,+}_n\rangle\,. \tag{6.64}$$

In the symmetric part the last term cancels and one obtains

$$\gamma^s_{\alpha\beta} = \mathrm{i}\int \mathrm{d}E \sum_{mn} f_n(E)\left\{\partial_\alpha S^\dagger_{nm}(E)\langle\psi^{t-}_m(E)|\partial_\beta\psi^{t+}_n(E)\rangle - \langle\partial_\beta\psi^{t+}_n(E)|\psi^{t-}_m(E)\rangle\partial_\alpha S_{mn}(E)\right\}_s\,. \tag{6.65}$$

Now we define A_α as $A = \sum_\alpha A_\alpha \dot{X}_\alpha$ and use

$$(A_\alpha)_{mn} = -2\pi\,\langle\psi^{t\,-}_m|\partial_\alpha\psi^{t\,+}_n\rangle - \frac{\mathrm{i}}{2}\partial_E\partial_\alpha S_{mn}\,, \tag{6.66}$$

which follows directly from Eqs. (6.27) and (6.34). Finally we obtain

$$\begin{aligned}\gamma^s_{\alpha\beta} &= \int\frac{\mathrm{d}E}{4\pi}\sum_n[-\partial_E f_n(E)]\,\mathrm{tr}\left\{\Pi_n\partial_\alpha S^\dagger(E)\partial_\beta S(E)\right\}_s \\ &\quad +\int\frac{\mathrm{d}E}{2\pi\mathrm{i}}\sum_n f_n(E)\mathrm{tr}\left\{\Pi_n\left[\partial_\alpha S^\dagger(E)A_\beta(E) - A^\dagger_\alpha(E)\partial_\beta S(E)\right]\right\}_s\,. \end{aligned} \tag{6.67}$$

Eq. (6.67) recovers the result of Bode *et al.* (2011, 2012). The second part involving the A-matrix vanishes in equilibrium [Bode *et al.* (2011, 2012)]. Since the expression only involving S is positive definite, γ^s describes a usual friction and damping force in equilibrium. Interestingly, the out of equilibrium contribution involving A can change the sign of γ^s and leads to negative damping.

Note that it is not trivial to obtain a friction force that is mediated by a quantum system.

Indeed, assuming a closed finite size system, Berry and Robbins (1993) obtained $\gamma^s = 0$. The crucial difference with our approach is that Berry and Robbins (1993) considered a finite gaped system.

Antisymmetric part

The antisymmetric part of the damping matrix has the role of an effective orbital magnetic field acting on the multidimensional space of $\mathbf{X}$. From Eq. (6.60) and using that terms symmetric in the indices α, β (such as $\partial_\alpha \partial_\beta$) will cancel, we can write

$$\begin{aligned} \gamma^a_{\alpha\beta} &= -\mathrm{i}\int \mathrm{d}E \sum_{mn} f_n(E)\Big\{ S^\dagger_{nm}(E)\partial_\alpha \left[\langle \psi^{t-}_m(E)|\partial_\beta \psi^{t+}_n(E)\rangle\right] \\ &\quad -\partial_\alpha \left[\langle \partial_\beta \psi^{t+}_n(E)|\psi^{t-}_m(E)\rangle\right]\, S_{mn}(E)\Big\}_a . \end{aligned} \tag{6.68}$$

Comparing this expression with Eq. (6.66) directly yields

$$\gamma^a_{\alpha\beta} = \int \frac{\mathrm{d}E}{2\pi\mathrm{i}} \sum_n f_n(E)\mathrm{tr}\left\{\Pi_n \left(\partial_\alpha A^\dagger_\beta(E) S(E) - S^\dagger(E)\partial_\alpha A_\beta(E)\right)\right\}_a . \tag{6.69}$$

This antisymmetric part vanishes for time reversal invariant systems in equilibrium [Bode *et al.* (2011, 2012)]. In a general non-equilibrium situation γ^a will however be finite and can lead to cyclic motions of the slow mechanical variables. Note that within the scattering formalism all the above relations are well-defined and we do not encounter any divergences in contrast to Lü *et al.* (2010). The reason for this is that the finite time the electrons stays in the scattering region effectively broadens the electron Green's functions.

6.3.3 Stochastic force

For a full determination of the equation of motion of the slow mechanical degrees of freedom we still need to determine the stochastic force

$$\xi_\alpha(t) = \partial_\alpha \mathcal{H}(t) - \langle \partial_\alpha \mathcal{H}(t)\rangle \tag{6.70}$$

[see Eq. (6.1)]. The leading order of the fluctuating force will be given only in terms of the frozen S-matrix. Note that in equilibrium the fluctuation-dissipation theorem relates the fluctuating force to the dissipative part γ^s and the latter can therefore also be expressed only in terms of the frozen S-matrix [see Eq. (6.67)].

Since the electronic degrees of freedom are fast compared to the mechanical motion the correlator

$$D_{\alpha\beta}(t,t') = \{\langle \xi_\alpha(t)\xi_\beta(t')\rangle\}_s = D_{\alpha\beta}(t)\delta(t-t') \tag{6.71}$$

will be local on the relevant time scales of the Langevin equation (6.1). In order to determine $D_{\alpha\beta}(t)$ we average $D_{\alpha\beta}(t,t')$ over the fast electronic degrees of freedom such

that

$$D_{\alpha\beta}(t_0) = D_{\alpha\beta}\left(\mathbf{X}(t_0)\right) = \int \mathrm{d}\tau D_{\alpha\beta}\left(t_0 + \frac{\tau}{2}, t_0 - \frac{\tau}{2}\right) \tag{6.72}$$

and work in the frozen scattering state basis $|\psi^{t_0}\rangle$. Since the correlatior is a two-body operator we first have to rewrite it in terms of single-body expectation values to find an S-matrix expression.

In second quantization language, we find in zeroth order of the adiabatic expansion

$$\begin{aligned} \partial_\alpha \mathcal{H}^{t_0}(t) &= \int \mathrm{d}E \int \mathrm{d}E' \sum_{mk} a_m^{t_0\dagger}(E,t)\, \left(\partial_\alpha H^{t_0}\right)_{mk}\, a_k^{t_0}(E',t) && (6.73)\\ &= \int \mathrm{d}E \int \mathrm{d}E' \sum_{mk} a_m^{t_0\dagger}(E)\, \left(\partial_\alpha H^{t_0}\right)_{mk}\, a_k^{t_0}(E') \mathrm{e}^{\mathrm{i}(E-E')t}\,, && (6.74) \end{aligned}$$

where $a_m^{t_0\dagger}(E)$ creates a frozen (retarded) scattering state with quantum number m and energy E which is an eigenstate of the Hamiltonian H^{t_0}. The time evolution therefore takes the simple form $a_k^{t_0}(E,t) = \exp(-\mathrm{i}Et) a_k^{t_0}(E)$. The correlator can now be obtained by using the well-known expression [Büttiker (1992)]

$$\begin{aligned} &\langle a_m^\dagger(E)\, a_n(E')\, a_k^\dagger(E'')\, a_l(E''')\rangle - \langle a_m^\dagger(E)\, a_n(E')\rangle\, \langle a_k^\dagger(E'')\, a_l(E''')\rangle \\ &\quad = f_m(E)\left(1 \mp f_k(E')\right) \delta_{ml}\, \delta_{nk}\, \delta(E - E''')\, \delta(E' - E'')\,. \end{aligned} \tag{6.75}$$

where the minus sign refers to fermions and the plus sign indicates bosons. The distribution function is given by $f_k(E) = \langle a_k^\dagger(E)\, a_k(E)\rangle$. Applying Eq. (6.75) to Eq. (6.72) we find

$$\begin{aligned} D_{\alpha\beta}(t_0) &= \int \mathrm{d}\tau \int \mathrm{d}E \mathrm{d}E' \sum_{mk} f_m(E)\left(1 \mp f_k(E')\right) \Big\{ \langle \psi_m^{t_0+}(E)|\, \partial_\alpha H(t)\, |\psi_k^{t_0+}(E')\rangle \mathrm{e}^{\mathrm{i}(E'-E)\frac{\tau}{2}} \\ &\quad \times \langle \psi_k^{t_0+}(E')|\, \partial_\beta H(t)\, |\psi_m^{t_0+}(E)\rangle \mathrm{e}^{-\mathrm{i}(E-E')\frac{\tau}{2}} \Big\}_s \end{aligned} \tag{6.76}$$

The time integral yields $\int_{-\infty}^{\infty} \mathrm{d}\tau e^{-\mathrm{i}(E'-E)\,\tau} = 2\pi\, \delta(E' - E)$. Inserting two resolutions of the identity in terms of advanced scattering states, *i.e.* $\mathbf{1} = \int \mathrm{d}E \sum_k |\psi_k^{t\,-}(E)\rangle\langle\psi_k^{t\,-}(E)|$, then allows for identifying the S-matrix with $\langle \psi_n^{t\,-}(E)|\psi_k^{t\,+}(E')\rangle = S_{nk}^t(E)\, \delta(E - E')$ as well as its derivatives given by Eq. (6.31). We then find

$$D_{\alpha\beta}(t_0) = \frac{1}{2\pi} \int \mathrm{d}E \sum_{nmkl} f_n(E)\left(1 \mp f_m(E)\right) \left\{ \partial_\alpha S_{nk}^\dagger(E)\, S_{km}(E)\, S_{ml}^\dagger(E)\, \partial_\beta S_{ln}(E) \right\}_s, \tag{6.77}$$

which can be rewritten in matrix notation as

$$D_{\alpha\beta}(t_0) = \sum_{nm} \int \frac{\mathrm{d}E}{2\pi} f_n(E)\, \left[1 \mp f_m(E)\right] \mathrm{tr} \left\{ \Pi_n\, \left[S^\dagger(E)\, \partial_\alpha S(E)\right]^\dagger\, \Pi_m\, S^\dagger(E)\, \partial_\beta S(E) \right\}_s . \tag{6.78}$$

Also Eq. (6.78) agrees with Bode *et al.* (2011, 2012). Note however that this derivation is completely model independent and even applies when dealing with bosons instead of

fermions.

6.4 Application: current induced forces in a mesoscopic quantum dot

As mentioned above, the S-matrix expressions for the current induced forces forces were already obtained from a model of a mesoscopic quantum dot [Bode *et al.* (2011, 2012)]. It is instructive to study the connection between our general definition of A in terms of the scattering states and the Green's functions expression for a mesoscopic quantum dot.

Bode *et al.* (2011, 2012) considered the Hamiltonian

$$H(\mathbf{X}) = H_X + H_L + H_D + H_T\,, \tag{6.79}$$

which models a mesoscopic quantum dot (D) connected (T) to leads (L). The slow classical degrees of freedom $\mathbf{X}(t) = (X_1(t), X_2(t) \ldots X_N(t))$ are in this case the mechanical vibrational modes of the (*e.g.* suspended) dot, which couple to the electrons in the dot. Specifically, the Hamiltonian takes the form

$$H_L = \sum_{\eta} \left(E_\eta - \mu_\eta\right) c_\eta^\dagger c_\eta \tag{6.80}$$

$$H_X = \sum_{\nu} \left[\frac{P_\nu^2}{2M_\nu} + U(\mathbf{X})\right] \tag{6.81}$$

$$H_D = \sum_{mm'} d_m^\dagger \left[h_0(\mathbf{X})\right]_{mm'} d_{m'} \tag{6.82}$$

$$H_T = \sum_{\eta m} \left(c_\eta^\dagger W_{\eta m} d_m + h.c.\right)\,. \tag{6.83}$$

H_L models the leads, where $c_\eta^\dagger$ (c_η) creates (annihilates) an electron in channel η with chemical potential μ_η [η combines channel and lead index, the chemical potential depends only on the lead index]. H_X represents the free evolution of the mechanical degrees of freedom of the dot. H_D is the Hamiltonian of the dot, containing the electronic levels plus the coupling of the electrons in the dot to $\mathbf{X}$ via a general function $h_0(\mathbf{X})$. The operators $d_m^\dagger$ (d_m) create (annihilate) an electron with quantum number m. Finally, H_T indicates the tunneling process between the dot and the leads with tunneling amplitudes $W_{\eta m}$.

The Hamiltonian in Eq. (6.79) implies that the scattering states can be decomposed as

$$|\Psi_\eta^+(E,t)\rangle = \Pi_L|\Psi_\eta^+(E,t)\rangle + \Pi_D\,|\Psi_\eta^+(E,t)\rangle \tag{6.84}$$

where Π_L and Π_D denote projection operators onto the leads and dot, respectively. Note that $\Pi_L \cdot \Pi_D = \Pi_D \cdot \Pi_L = 0$. We can write the Lippman-Schwinger equation as

$$|\psi_\eta^{t\,+}(E)\rangle = \Pi_L\,|\phi_\eta(E)\rangle + G^R(E) V\,\Pi_L\,|\phi_\eta(E)\rangle\,, \tag{6.85}$$

where $\Pi_L |\phi_\eta(E)\rangle \equiv c_\eta^\dagger(E)|0\rangle$ is an eigenvector of H_L and, therefore a state of a free electron in the lead η, $G^R(E) = (E - H + i\eta)^{-1}$ is the full Green's function of the dot and the lead and $V = \Pi_D W^\dagger \Pi_L + \Pi_L W \Pi_D + \Pi_D h_0 \Pi_D$. Hence we can project the Lippman-Schwinger Eq. (6.85) onto the dot space

$$\Pi_D |\psi_\eta^{t+}(E)\rangle = \Pi_D G^R(E) \Pi_D W^\dagger \Pi_L |\phi_\eta(E)\rangle \tag{6.86}$$

$$= G_D^R(E) W^\dagger |\phi_\eta(E)\rangle , \tag{6.87}$$

where $G_D^R(E) = \Pi_D G^R(E) \Pi_D$ is the dot's Green function.

We are interested in an explicit expression for the A-matrix. Since only the dot Hamiltonian is time dependent we can use $\partial_t V = \Pi_D \partial_t h_0 \Pi_D$ and obtain from Eq. (6.28)

$$A_{\eta\mu}(E) = \pi \left[\langle \partial_E \psi_\eta^{t-}(E)| \Pi_D (\partial_t h_0) \Pi_D |\psi_\mu^{t+}(E)\rangle - \langle \psi_\eta^{t-}(E)| \Pi_D (\partial_t h_0) \Pi_D |\partial_E \psi_\mu^{t+}(E)\rangle \right] \tag{6.88}$$

In matrix form $A_{\eta\mu}(E) = \langle \psi_\eta^t(E)|A|\psi_\mu^t(E)\rangle$ is equivalent to

$$A_{\eta\mu}(E) = \pi \left[\partial_E \left(W G_D^R \right) (\partial_t h_0) G_D^R W^\dagger - W G_D^R (\partial_t h_0) \partial_E \left(G_D^R W^\dagger \right) \right] . \tag{6.89}$$

This indeed gives the result of Bode *et al.* (2011, 2012) which was obtained by an adiabatic expansion of the time dependent dot-Green's function $\mathcal{G}_D$ and using the Wigner transform of the full time dependent S-matrix

$$\mathcal{S}(E,t) = 1 - 2\pi \mathrm{i} \left[W \mathcal{G}_D^R W^\dagger \right] (E,t) . \tag{6.90}$$

6.5 Conclusion

We provided a full scattering theory derivation of the forces that are exerted onto the mechanical degrees of freedom in a nanoelectromechanical system. We could indeed confirm the expressions found by Bode *et al.* (2011, 2012) and show that these results hold on a general, model independent level. Indeed with small modifications for the fluctuating force Eqs. (6.53,6.67,6.69,6.78) remain valid for the forces that bosons exert onto mechanical degrees of freedom such that the presented scattering theory may also have interesting applications to optomechanical systems.

Finally, we also want to draw attention to the explicit expressions for the A-matrix [see Eqs. (6.27,6.28)] that provide a straight forward recipe for the calculation of the first order adiabatic correction to the S-matrix in terms of the frozen scattering states. This will be useful for applying the approach to concrete examples.

7 Conclusions and outlook

Low dimensional electron systems can behave strikingly different form their higher dimensional counterparts. This is especially pronounced in one dimensional systems whose low energy physics is controlled by strong correlations. Recent experimental advances in one dimensional systems draw more and more attention to their rich non-equilibrium behavior. Motivated by these developments the main part of this thesis addressed two important elementary non-equilibrium processes. In chapter 3 we discussed the main characteristics of the out of equilibrium state that is introduced when a low energy particle tunnels into a Luttinger liquid. Chapters 4 and 5 then went beyond the Luttinger liquid paradigm and studied relaxation and thermalization of an introduced non-equilibrium state due to the finite curvature of the electron dispersion.

Tunneling of an electron into a Luttinger liquid leads to partitioning of its charge into right- and left-moving currents. The charge partitioning ratio is closely related to the fractional excitations of the Luttinger liquid and only determined by the Luttinger parameter K. In chapter 3 we studied the corresponding energy partitioning and found that it is distinctly different from that of the charge. Although it also relies on the strong correlations it does not depend on the Luttinger parameter K alone. In fact it is crucially controlled by the injected state and can thus be tuned experimentally. Interestingly, it is even possible to reach conditions such that charge and energy of an injected particle propagate in opposite directions.

In finite size systems, charge partitioning is completely masked by backscattering effects at the non-interacting Fermi liquid leads. We showed that in stark contrast to the charge, energy partitioning provides a measurable characteristic of the tunneling process even in dc setups. Specifically, we proposed realistic geometries in which one is able to probe consequences of energy partitioning.

At higher excitations energies, it is necessary to include curvature effects of the dispersion. Chapter 4 studied the curvature induced energy relaxation of hot particle and hole excitations in quantum wires. The relaxation mechanism is described by a well-defined perturbation theory that relies on three-body processes. These processes show a strong asymmetry for the energy relaxation rates of particle and hole excitations. The hole relaxation is strongly suppressed at low temperatures and ceases completely at $T = 0$. On the other hand, there is no similar limitation for particles and the corresponding energy relaxation rates can become relatively fast (of the order $1/\tau_p \sim \varepsilon^2$, where ε is the excitation energy). In obtaining this result, chapter 4 demonstrated the importance of spin and of the long range Coulomb interaction for three-body relaxation processes. Taking them into

account dramatically increases the energy relaxation rates of particle and hole excitations via $2k_F$ momentum transfer processes. These enhanced relaxation rates provide a quantitative interpretation of a recent experiment by Barak *et al.* (2010b) in terms of three-body processes. Also in line with this experiment, we argued that three-body processes do not transfer a substantial amount of energy between right- and left-moving electrons.

Chapter 5 studied the influence of three-body collisions on the energy relaxation in integer quantum Hall edge states. We specifically addressed different interaction induced edge reconstruction scenarios. For an unreconstructed edge, energy relaxation relies on a chiral three-body relaxation process which is strongly suppressed at low temperatures. Another pronounced difference with scattering in quantum wires is that the Landau level wave functions lead to a suppression of large momentum transfer Coulomb matrix elements such that direct, instead of exchange processes dominate the relaxation.

While unreconstructed edges are expected for steep confinement potentials, a smoother confinement leads to reconstruction effects which were found to strongly increase the energy relaxation rate. Specifically, confinement potentials that are smoother than the repulsive Hartree potential lead to spin reconstruction in $\nu = 2$ quantum Hall edge states, which separates the Fermi momenta of the two spin species by $\sim 1/l_B$ (where l_B is the magnetic length). We showed that the spin reconstructed dispersion leads to an increase of the energy relaxation rate, but still requires finite temperatures.

Softer confinement potentials can also lead to charge reconstruction which we studied in a minimal model of spin polarized edges at filling factor $\nu = 1$. Charge reconstruction introduces additional co- and counter-propagating edge modes. The presence of counter-propagating modes allows for similar relaxation process as in quantum wires, which are not limited to finite temperature. Consequently, we predicted a dramatic increase of the energy relaxation rates in charge reconstructed edges.

The field of one dimensional electron systems out of equilibrium has recently received much theoretical attention. The emerging picture provides an understanding of the low energy behavior, described by bosonization techniques, as well as the high energy limit where curvature effects allow for a perturbative treatment of the electron-electron interaction. An ongoing theoretical challenge is however the intermediate regime, where one has to deal with the strong interactions as well as the finite curvature in a non-equilibrium setting. A promising candidate for this regime is a description in terms of the fermionic quasi-particles[1] of the Luttinger liquid (holons and spinons) [Imambekov *et al.* (2011)] for which moderate curvatures introduce weak interactions. Interestingly, the particle relaxation rates calculated in this thesis coincide with the holon decay rates at the limit of applicability of both theories. It still has to be sorted out whether this is a coincidence or whether there is an underlying connection between the two seemingly different approaches. Another open question is whether our recent understanding of the elementary processes in a Luttinger liquid can be used to construct a full kinetic theory of

[1] Note however that these quasi-particles cannot be represented easily in terms of the original electrons but consist of a fractional combination of right- and left-moving electrons.

the weakly interacting holons and spinons.

An understanding of the kinetics in the strongly interacting regime could lead to an interesting way to probe the properties of one dimensional systems by observing their relaxation behavior. This could be especially useful to discriminate between different reconstruction scenarios of fractional quantum Hall edge states because, while invisible to charge measurement, the neutral modes will contribute to the relaxation behavior.

Another interesting manifestation of the qualitative differences that come along with considering an out of equilibrium setting are nanoelectromechanical systems. There, the non-equilibrium electron current can exert non-conservative forces that act on the mechanical degrees of freedom.

In chapter 6 we provided a scattering theory of current induced forces. Former Green's function approaches could already identify their results for the current induced forces with S-matrix expressions [Bode *et al.* (2011, 2012)]. Chapter 6 showed that the appearance of the S-matrix is not coincidental but follows from a general scattering theory which accounts for slowly time dependent scattering potentials. The advantage of this alternative derivation of the current induced forces is that it gives additional insights into the underlying structure of the theory.

The starting point of the calculation was similar as that of Berry and Robbins (1993) who predicted Lorentz-like forces that act on a heavy particle that is coupled to a closed quantum system. Including a continuous spectrum allows us to obtain also dissipative forces that are mediated by the quantum system. Indeed, the scattering theory provides a well-defined way to extend the discussion to infinite systems owing to the finite time the electron spends in the scattering region. An additional advantage of the derivation of chapter 6 is that it gives an expression for the adiabatic expansion of the full time dependent S-matrix in terms of the frozen scattering states which is useful for applying the approach to concrete examples.

An exciting perspective of current induced forces in nanoelectromechanical systems is the possibility to exert directed forces which lead the way to nano-scale motors or switches. From a theoretical point of view it would also be interesting to study the effect of electron-electron interactions on current induced forces. Especially the strongly correlated one dimensional systems could show a substantial departure from the non-interacting picture.

A Appendix

A.1 The Luttinger Hamiltonian

In this appendix we motivate the Luttinger liquid Hamiltonian starting from the original fermionic Hamiltonian.

A.1.1 Spinless fermions

We start with the Hamiltonian for a spinless system

$$
\begin{aligned}
H &= H_{\text{kin}} + H_{\text{int}} && \text{(A.1)}\\
H_{\text{kin}} &= v_F \int \mathrm{d}x \left(:\psi_R^\dagger(x) \left[\frac{\nabla}{\mathrm{i}}\psi_R(x)\right]: + \psi_L^\dagger(x)\left[\frac{\nabla}{\mathrm{i}}\psi_L(x)\right]: \right) && \text{(A.2)}\\
H_{\text{int}} &= \frac{1}{2}\int \mathrm{d}x \int \mathrm{d}x' V(x-x') : \Big[\rho_R(x) + \rho_L(x) + \psi_L^\dagger(x)\psi_R(x) + \psi_R^\dagger(x)\psi_L(x)\Big] && \text{(A.3)}\\
&\quad \times \Big[\rho_R(x') + \rho_L(x') + \psi_L^\dagger(x')\psi_R(x') + \psi_R^\dagger(x')\psi_L(x')\Big] :
\end{aligned}
$$

In the following we will use the definition of normal ordering

$$
:\psi_1^\dagger\psi_2: = \psi_1^\dagger\psi_2 - \left\langle \psi_1^\dagger\psi_2 \right\rangle \qquad \text{(A.4)}
$$

as well as Eqs. (2.14,2.31) which read

$$
\begin{aligned}
:\psi_{R/L}^\dagger\psi_{R/L}: &= :\rho_{R/L}: = \pm\frac{1}{2\pi}\left(\nabla\theta \pm \nabla\phi\right) && \text{(A.5)}\\
\psi_{R/L}^\dagger(x) &\propto \mathrm{e}^{-\mathrm{i}(\theta(x)\pm\phi(x))}. && \text{(A.6)}
\end{aligned}
$$

The kinetic part can then be bosonized by

$$
\begin{aligned}
&\int \mathrm{d}x :\psi_R^\dagger(x)\left[\frac{\nabla}{\mathrm{i}}\psi_R(x)\right]: \\
&= \frac{1}{2}\int \mathrm{d}x \Big[2\pi :\psi_R^\dagger(x)\Big(:\psi_R^\dagger(x)\psi_R(x):\Big)\psi_R(x): + :\psi_R^\dagger(x)\psi_R(x)(\nabla\theta(x)+\nabla\phi(x)):\Big] && \text{(A.7)}\\
&= \frac{1}{2}\int \mathrm{d}x \Big[2\pi :\psi_R^\dagger(x)\Big(\psi_R^\dagger(x)\psi_R(x)-\langle\rho_R\rangle\Big)\psi_R(x): + :\psi_R^\dagger(x)\psi_R(x)(\nabla\theta(x)+\nabla\phi(x)):\Big] && \text{(A.8)}\\
&= \frac{1}{2}\int \mathrm{d}x \Big[:\psi_R^\dagger(x)\psi_R(x): (\nabla\theta(x)+\nabla\phi(x))\Big] && \text{(A.9)}\\
&= \frac{1}{4\pi}\int \mathrm{d}x \,(\nabla\theta(x)+\nabla\phi(x))^2\,, && \text{(A.10)}
\end{aligned}
$$

where we used the fact that $\psi_R^2 = 0$ and total derivatives drop out. We then find

$$
\begin{aligned}
H_{\text{kin}} &= v_F\int \mathrm{d}x \left(:\psi_R^\dagger(x)\left[\frac{\nabla}{\mathrm{i}}\psi_R(x)\right]: - :\psi_L^\dagger(x)\left[\frac{\nabla}{\mathrm{i}}\psi_L(x)\right]:\right) && \text{(A.11)}\\
&= \frac{v_F}{4\pi}\int \mathrm{d}x \left[(\nabla\theta(x)+\nabla\phi(x))^2 + (\nabla\theta(x)-\nabla\phi(x))^2\right] && \text{(A.12)}\\
&= \frac{v_F}{2\pi}\int \mathrm{d}x \left[(\nabla\phi)^2 + (\nabla\theta)^2\right] && \text{(A.13)}
\end{aligned}
$$

Now we will consider the interaction Hamiltonian. Collecting the terms of momentum transfer close to 0 and $2k_F$ we find

$$
\begin{aligned}
H_{\text{int}} = \frac{1}{2}\int \mathrm{d}x \int \mathrm{d}x' V(x-x'):\Big[&\underbrace{\rho_R(x)\rho_L(x') + \rho_R(x)\rho_R(x')}_{q\sim 0} && \text{(A.14)}\\
&- \underbrace{\psi_R^\dagger(x')\psi_R(x)\psi_L^\dagger(x)\psi_L(x')}_{q\sim 2k_F} + R\leftrightarrow L\Big]:
\end{aligned}
$$

Now we Fourier transform the above expression (with $A(x) = \frac{1}{L}\sum_q \mathrm{e}^{\mathrm{i}qx}A_q$, $A = V, \psi, \rho$) and obtain

$$
\begin{aligned}
H_{\text{int}} &= :\frac{1}{2L^3}\sum_{q,k,k'}\left(V_q - V_{q+k'-k}\right)\psi_{R,k'+q}^\dagger\psi_{R,k'}\psi_{L,k-q}^\dagger\psi_{L,k} && \text{(A.15)}\\
&\quad + \frac{1}{4L^3}\sum_{q,k,k'}\left(V_q - V_{q+k'-k}\right)\psi_{R,k'+q}^\dagger\psi_{R,k'}\psi_{R,k-q}^\dagger\psi_{R,k} + R\leftrightarrow L:\\
&\approx :\frac{1}{2L^3}\sum_{q,k,k'}\left(V_0 - V_{2k_F}\right)\psi_{R,k'+q}^\dagger\psi_{R,k'}\psi_{L,k-q}^\dagger\psi_{L,k}: + R\leftrightarrow L && \text{(A.16)}
\end{aligned}
$$

where we wrote the $\rho_R\rho_R$ term in a symmetric way such that the Pauli principle leads to a vanishing contribution of the $\rho_R\rho_R$ and $\rho_L\rho_L$ terms when approximating V_q as constant. Note however that terms that involve the momentum derivate of the potential (such as V'_{2k_F}) have to be considered when expanding the Hamiltonian to next order in low energies. When including curvature effects of the dispersion one should also include corrections

of the interaction part to be consistent in the low energy expansion [see Rozhkov (2006)]. Here we will focus on the low energy limit and Fourier transforming the above expressions back gives

$$H_{\text{int}} = \int \mathrm{d}x \left(V_0 - V_{2k_F}\right) \left(:\rho_R(x)\rho_L(x): + :\rho_L(x)\rho_R(x):\right), \tag{A.17}$$

such that the full Hamiltonian takes the form

$$H = \frac{1}{2\pi} \int \mathrm{d}x \left[\left(\tilde{v}_F + u\right)\left(\nabla\phi\right)^2 + \left(\tilde{v}_F - u\right)\left(\nabla\theta\right)^2\right] \tag{A.18}$$

with

$$u = \frac{V_0 - V_{2k_F}}{2\pi}. \tag{A.19}$$

By dividing the fermions into right- and left-movers and focusing on the behavior near the Fermi points we effectively took a shortcut to a normalization procedure. As indicated above the Fermi velocity will in general be renormalized to a different value $\tilde{v}_F$ which has to be fixed separately. Fortunately there is a way to determine $\tilde{v}_F$ by requiring Galilean invariance which manifests itself by requireing $cK = v_F$ [Starykh *et al.* (2000)][1]. Bringing the Hamiltonian in the form

$$H = \frac{c}{2\pi} \int \mathrm{d}x \left[\frac{1}{K}\left(\nabla\phi\right)^2 + K\left(\nabla\theta\right)^2\right] \tag{A.20}$$

then determines

$$\frac{1}{K} = \sqrt{\frac{\tilde{v}_F + u}{\tilde{v}_F - u}} \tag{A.21}$$

$$c = \sqrt{\tilde{v}_F^2 - u^2} \tag{A.22}$$

$$cK = \tilde{v}_F - u \tag{A.23}$$

and the Galilean invariance is implemented by

$$\tilde{v}_F = v_F + u \tag{A.24}$$

$$c = v_F\sqrt{1 + 2\frac{u}{v_F}} = v_F\sqrt{1 + \frac{V_0 - V_{2k_F}}{\pi v_F}} \tag{A.25}$$

$$\frac{1}{K} = \sqrt{1 + 2\frac{u}{v_F}} = \sqrt{1 + \frac{V_0 - V_{2k_F}}{\pi v_F}} \tag{A.26}$$

which we used in the main text.

[1] Note that this is indeed required to have an interaction independent definition of the current operator $j(x) = \frac{cK}{\pi}\nabla\theta(x)$.

A.1.2 Spinful fermions

In the spinful case the Hamiltonian consists now of 4 major contributions

$$H = H_\uparrow + H_\downarrow + H_{\uparrow\downarrow} + H_{SG}\,, \tag{A.27}$$

where $H_\uparrow$ and $H_\downarrow$ are the spinless Hamiltonians for each spin species, $H_{\uparrow\downarrow}$ describes the density-density type of interactions between the two spin species and H_{SG} is the sine-Gordon term that describes $2k_F$ scattering with different spins that cannot be casted in a density-density interaction. The additional $H_{\uparrow\downarrow}$ term takes the form

$$H_{\uparrow\downarrow} = \int \mathrm{d}x \int \mathrm{d}x' V(x-x') : \left[\rho_{R\uparrow}(x) + \rho_{L\uparrow}(x)\right]\left[\rho_{R\downarrow}(x') + \rho_{L\downarrow}(x')\right] , \tag{A.28}$$

which is dominated by $V_{q\approx 0}$ momentum transfers. Setting again $V(x-x') = V_0\delta(x-x')$ we find

$$H_{\uparrow\downarrow} = \frac{1}{\pi}\int \mathrm{d}x \frac{V_0}{\pi}\left(\nabla\phi_\uparrow\right)\left(\nabla\phi_\downarrow\right) . \tag{A.29}$$

Now we introduce

$$\phi_{c/s} = \frac{1}{\sqrt{2}}\left(\phi_\uparrow \pm \phi_\downarrow\right) \tag{A.30}$$

$$\theta_{c/s} = \frac{1}{\sqrt{2}}\left(\theta_\uparrow \pm \theta_\downarrow\right) \tag{A.31}$$

which yields

$$H_{\uparrow\downarrow} = \frac{1}{2\pi}\int \mathrm{d}x \frac{V_0}{\pi}\left[\left(\nabla\phi_c\right)^2 - \left(\nabla\phi_s\right)^2\right] . \tag{A.32}$$

From the spinless Hamiltonian we can therefore read off

$$\begin{aligned} & H_\uparrow + H_\downarrow + H_{\uparrow\downarrow} \qquad\qquad (A.33)\\ = \;& \frac{v_c}{2\pi}\int \mathrm{d}x \left[\frac{1}{K_c}\left(\nabla\phi_c\right)^2 + K_c\left(\nabla\theta_c\right)^2\right] + \frac{v_s}{2\pi}\int \mathrm{d}x \left[\frac{1}{K_s}\left(\nabla\phi_s\right)^2 + K_s\left(\nabla\theta_s\right)^2\right] , \end{aligned}$$

with

$$K_c v_c = K_s v_s = v_F \tag{A.34}$$

$$\frac{1}{K_c} = \sqrt{1 + \frac{2V_0 - V_{2k_F}}{\pi v_F}} \tag{A.35}$$

$$\frac{1}{K_s} = \sqrt{1 - \frac{V_{2k_F}}{\pi v_F}} . \tag{A.36}$$

The sine-Gordon term is given by [Giamarchi (2004)]

$$H_{SG} = \frac{V_{2k_F}\Lambda^2}{2\pi^2}\int \mathrm{d}x \cos\left[2\sqrt{2}\phi_s\right] . \tag{A.37}$$

It is again required to do a proper renormalization group analysis to fix the coupling constants [see Giamarchi (2004)]. The result for a spin rotation invariant system is that the coupling constant V_{2k_F} flows to zero such that $K_s^* = 1$ and the sine-Gordon term can be set zero, which gives the result of Eq (2.27) in the main text.

A.2 Energy current correlator

In this appendix we calculate the correlators of Eq. (3.56) using the bosonization technique. As mentioned in the main text we can rewrite the fermionic field operators as

$$\psi_R^\dagger \sim \mathrm{e}^{-\mathrm{i}(Q_+\theta_+ + Q_-\theta_-)} = \mathrm{e}^{-\mathrm{i}(Q_+A_+\nabla\theta_+ + Q_-A_-\nabla\theta_-)}, \tag{A.38}$$

where we defined the auxiliary operators $A_\pm = \nabla^{-1}$ which help to calculate the expectation values

$$\begin{aligned} &\Big\langle \psi_R(x',t')\psi_R^\dagger(x,t)\nabla\theta_\pm(x,t) + \psi_R(x',t')\nabla\theta_\pm(x,t)\psi_R^\dagger(x,t)\Big\rangle \qquad (A.39)\\ =\ & \frac{2\mathrm{i}}{Q_\pm}\frac{\partial}{\partial A_\pm}\bigg|_{A_\pm=\nabla^{-1}} \Big\langle \psi_R(x',t')\psi_R^\dagger(x,t)\Big\rangle . \end{aligned}$$

Note that $A_\pm$ and ∇ only act on x and not on x'. Now we also define

$$\psi_R^\dagger(x) \sim \mathrm{e}^{-\sum_{q>0,\pm}\left[M_q^\pm(x)\beta_{\pm q} - M_q^{\pm\dagger}(x)\beta_{\pm q}^\dagger\right]} = \mathrm{e}^{-\sum_{q>0,\pm}\left[\pm A_\pm \mathrm{i}q\left(M_q^\pm(x)\beta_{\pm q} + M_q^{\pm\dagger}(x)\beta_{\pm q}^\dagger\right)\right]}, \tag{A.40}$$

with $M_q^\pm(x) = \sqrt{\frac{2\pi}{LqK}}Q_\pm \mathrm{e}^{\mathrm{i}\left(\pm qx - \omega_q t\right)}$. Therefore we can use $A_\pm M_q^\pm = \frac{1}{\pm \mathrm{i}q}M_q^\pm$ and $A_\pm M_q^\dagger = \frac{-1}{\pm \mathrm{i}q}M_q^{\pm\dagger}$. Since bosonic operators with positive and negative momenta commute we find that

$$\begin{aligned} &\Big\langle \psi_R(x,t)\psi_R^\dagger(0,0)\Big\rangle \qquad (A.41)\\ \propto\ & \prod_\pm \Big\langle \mathrm{e}^{\sum_{q>0}\left[M_q^\pm(x)\beta_{\pm q} - M_q^{\pm\dagger}(x)\beta_{\pm q}^\dagger\right]}\mathrm{e}^{-\sum_{q>0}\pm A_\pm \mathrm{i}q\left[M_q^\pm\beta_{\pm q} + M_q^{\pm\dagger}\beta_{\pm q}^\dagger\right]}\Big\rangle\\ =\ & \prod_\pm \Big\langle \mathrm{e}^{\sum_{q>0}\left(\left[M_q^\pm(x) \mp A_\pm \mathrm{i}qM_q^\pm\right]\beta_{\pm q} - \left[M_q^{\pm\dagger}(x) \pm A_\pm \mathrm{i}qM_q^{\pm\dagger}\right]\beta_{\pm q}^\dagger\right)}\Big\rangle \qquad (A.42)\\ & \times \mathrm{e}^{\sum_{q>0} -\frac{1}{2} \pm A_\pm \mathrm{i}q\left(M_q^\pm(x)M_q^{\pm\dagger} + M_q^{\pm\dagger}(x)M_q^\pm\right)}\\ =\ & \mathrm{e}^{F_+(x,t)}\mathrm{e}^{F_-(x,t)}, \qquad (A.43) \end{aligned}$$

where we defined the fields $F_\pm(x,t)$ similar to the book of Giuliani and Vignale (2005). Now we use the independent boson theorem

$$\Big\langle \mathrm{e}^{\sum_i\left(x_ib_i + y_ib_i^\dagger\right)}\Big\rangle = \mathrm{e}^{\frac{1}{2}\sum_i\left\langle\left(x_ib_i + y_ib_i^\dagger\right)^2\right\rangle} \tag{A.44}$$

to calculate

$$\begin{aligned} F_\pm &= \frac{1}{2}\sum_{q>0}\left(-\left[M_q^\pm(x) \mp A_\pm \mathrm{i}qM_q^\pm\right]\left[M_q^{\pm\dagger}(x) \pm A_\pm \mathrm{i}qM_q^{\pm\dagger}\right]\right)\left(\left\langle \beta_{\pm q}\beta_{\pm q}^\dagger\right\rangle + \left\langle \beta_{\pm q}^\dagger\beta_{\pm q}\right\rangle\right) \\ &\quad -\frac{1}{2}\sum_{q>0}\pm A_\pm \mathrm{i}q\left(M_q^\pm(x)M_q^{\pm\dagger} + M_q^{\pm\dagger}(x)M_q^\pm\right). \end{aligned} \tag{A.45}$$

Consequently we can then calculate the desired derivative with respect to the auxiliary operators

$$\begin{aligned} \left.\frac{\partial}{\partial A_\pm}\right|_{A_\pm=\nabla^{-1}} F_\pm &= \frac{1}{2}\sum_{q>0}\left(\pm \mathrm{i}qM_q^\pm\left[M_q^{\pm\dagger}(x) - M_q^{\pm\dagger}\right] - \left[M_q^\pm(x) - M_q^\pm\right] \pm \mathrm{i}qM_q^{\pm\dagger}\right) \qquad \text{(A.46)} \\ &\quad \times\left(\left\langle \beta_{\pm q}\beta_{\pm q}^\dagger\right\rangle + \left\langle \beta_{\pm q}^\dagger\beta_{\pm q}\right\rangle\right) \mp \frac{1}{2}\sum_{q>0}\mathrm{i}q\left(M_q^\pm(x)M_q^{\pm\dagger} + M_q^{\pm\dagger}(x)M_q^\pm\right) \\ &= \pm\sum_{q>0}\mathrm{i}q\left\{-M_q^\pm(x)M_q^{\pm\dagger}\left(n_B(\omega_q)+1\right) + M_q^{\pm\dagger}(x)M_q^\pm n_B(\omega_q)\right\}, \qquad \text{(A.47)} \end{aligned}$$

where $\left\langle \beta_q^\dagger\beta_q\right\rangle = n_B = \left(\mathrm{e}^{\omega_q/T}-1\right)^{-1}$. Finally we obtain

$$\begin{aligned} &\left\langle \psi_R(x,t)\psi_R^\dagger(0,0)\nabla\theta_\pm(0,0) + \psi_R(x,t)\nabla\theta_\pm(0,0)\psi_R^\dagger(0,0)\right\rangle \qquad \text{(A.48)} \\ &= \pm\frac{4\pi}{LK}Q_\pm\sum_{q>0}\left\{\mathrm{e}^{\mathrm{i}\left(\pm qx-\omega_q t\right)}\left(n_B(\omega_q)+1\right) - \mathrm{e}^{-\mathrm{i}\left(\pm qx-\omega_q t\right)}n_B(\omega_q)\right\}\left\langle \psi_R(x,t)\psi_R^\dagger(0,0)\right\rangle. \end{aligned}$$

Now note that

$$\begin{aligned} &\nabla\theta_\pm(x,t)\psi_R^\dagger(x,t)\psi_R(x',t') + \psi_R^\dagger(x,t)\nabla\theta_\pm(x,t)\psi_R(x',t') \qquad \text{(A.49)} \\ &= \left(\psi_R^\dagger(x',t')\psi_R(x,t)\nabla\theta_\pm(x,t) + \psi_R^\dagger(x',t')\nabla\theta_\pm(x,t)\psi_R(x,t)\right)^\dagger. \end{aligned}$$

The other correlator of Eq. (3.56) can therefore be obtained by complex conjugation of Eq. (A.48) with exchange of $\psi_R^\dagger \leftrightarrow \psi_R$. The latter also leads to a minus sign in front of the $\partial/\partial A_\pm$ which now acts on ψ. Other minus signs in the exponent due to $\psi_R^\dagger \leftrightarrow \psi_R$ drop out because of the quadratic form of the independent boson theorem. We therefore conclude

$$\begin{aligned} &\left\langle \nabla\theta_\pm(0,0)\psi_R^\dagger(0,0)\psi_R(x,t) + \psi_R^\dagger(0,0)\nabla\theta_\pm(0,0)\psi_R(x,t)\right\rangle \qquad \text{(A.50)} \\ &= \mp\frac{4\pi}{LK}Q_\pm\sum_{q>0}\left\{\mathrm{e}^{-\mathrm{i}\left(\pm qx-\omega_q t\right)}\left(n_B(\omega_q)+1\right) - \mathrm{e}^{\mathrm{i}\left(\pm qx-\omega_q t\right)}n_B(\omega_q)\right\}\left\langle \psi_R^\dagger(0,0)\psi_R(x,t)\right\rangle. \end{aligned}$$

A.3 Three-body amplitude

In this appendix we calculate the three-body amplitude of Lunde *et al.* (2007). To also suit the case of quantum Hall systems we will generalize the derivation of Lunde *et al.* (2007) and also keep the dependence of $V_q(k_1-k_2)$ in terms of the initial momenta. Specifically

we use

$$V = \frac{1}{2L} \sum_{k_1 k_2 q \sigma_1 \sigma_2} V_q(k_1 - k_2) a^\dagger_{k_1+q\sigma_1} a^\dagger_{k_2-q\sigma_2} a_{k_2\sigma_2} a_{k_1\sigma_1} \,. \tag{A.51}$$

We then calculate the expectation value of the three-body matrix element of Eqs. (4.8,5.8) in the main text. The three-body state can be written in second quantization as $|123\rangle = a^\dagger_{k_1\sigma_1} a^\dagger_{k_2\sigma_2} a^\dagger_{k_3\sigma_3} |0\rangle$. Applying the fermionic commutation relations $\{a_i, a_j^\dagger\} = \delta_{ij}$ we obtain

$$G_0 V|123\rangle = \frac{1}{2L} \sum_q \sum_{(abc)\in\mathcal{P}(123)} \frac{V_q(k_a - k_b)\mathrm{sign}(abc)}{\epsilon_{k_b} + \epsilon_{k_a} - \epsilon_{k_b-q} - \epsilon_{k_a+q} + \mathrm{i}0^+} a^\dagger_{k_a+q\sigma_a} a^\dagger_{k_b-q\sigma_b} a^\dagger_{k_c\sigma_c} |0\rangle \,, \tag{A.52}$$

where $\mathcal{P}(123)$ describes the possible permutations of the indices and $\mathrm{sign}(abc)$ is positive (negative) for cyclic (anti-cyclic) ordering. Multiplying by $\langle 1'2'3'|V$ we then obtain

$$\begin{aligned}\langle 1'2'3'|VG_0V|123\rangle_c \;=\; & \frac{1}{(2L)^2} \sum_{\substack{(abc)\in\mathcal{P}(123)\\(a'b'c')\in\mathcal{P}(1'2'3')}} \sum_{qq'} \frac{V_q(k_a - k_b) V_{q'}(k_{a'} - k_{b'}) \mathrm{sign}(abc)\mathrm{sign}(a'b'c')}{\epsilon_{k_b} + \epsilon_{k_a} - \epsilon_{k_b-q} - \epsilon_{k_a+q} + \mathrm{i}0^+} \\ & \times \left\langle 0 \left| a_{k_{c'}\sigma_{c'}} a_{k_{b'}-q'\sigma_{b'}} a_{k_{a'}+q'\sigma_{a'}} a^\dagger_{k_a+q\sigma_a} a^\dagger_{k_b-q\sigma_b} a^\dagger_{k_c\sigma_c} \right| 0 \right\rangle_c \end{aligned} \tag{A.53}$$

Now we exclude effective two-particle processes. This means that in the possible pairings of creation operators in Eq. (A.53) it is not allowed that an initial state k_c scatters directly into a state $k_{c'}$ (without involving a momentum transfer q). Therefore we obtain nonzero contributions for

$$\begin{aligned} & \langle 1'2'3'|VG_0V|123\rangle_c \\ = \;& \big(\delta_{k_c,k_{a'}+q'}\delta_{k_b-q,k_{c'}}\delta_{k_a+q,k_{b'}-q'} - \delta_{k_c,k_{a'}+q'}\delta_{k_b-q,k_{b'}-q'}\delta_{k_a+q,k_{c'}} \qquad (A.54) \\ & -\delta_{k_c,k_{b'}-q'}\delta_{k_b-q,k_{c'}}\delta_{k_a+q,k_{a'}+q'} + \delta_{k_c,k_{b'}-q'}\delta_{k_b-q,k_{a'}+q'}\delta_{k_a+q,k_{c'}}\big) \\ = \;& \big(\delta_{q,k_b-k_{c'}}\delta_{q',k_c-k_{a'}} - \delta_{q,k_{c'}-k_a}\delta_{q',k_c-k_{a'}} - \delta_{q,k_b-k_{c'}}\delta_{q',k_{b'}-k_c} + \delta_{q,k_{c'}-k_a}\delta_{q',k_{b'}-k_c}\big) \\ & \times\delta_{k_a+k_b+k_c,k_{a'}+k_{b'}+k_{c'}} \,, \qquad (A.55) \end{aligned}$$

where we omitted the Kronecker-deltas that involve the spin indices for better readability. After renaming of indices we finally obtain

$$\begin{aligned}\langle 1'2'3'|VG_0V|123\rangle_c = & \sum_{\substack{(abc)\in\mathcal{P}(123)\\(a'b'c')\in\mathcal{P}(1'2'3')}} \frac{\tilde{V}_{k_{c'}-k_c}(k_c - k_b)\tilde{V}_{k_{a'}-k_a}(k_{b'} - k_{a'})\mathrm{sign}(abc)\mathrm{sign}(a'b'c')}{\epsilon_{k_b} + \epsilon_{k_c} - \epsilon_{k_{c'}} - \epsilon_{k_b+k_c-k_{c'}} + \mathrm{i}0^+} \\ & \times \frac{1}{(2L)^2} \delta_{k_a+k_b+k_c,k_{a'}+k_{b'}+k_{c'}} \delta_{\sigma_{a'},\sigma_a} \delta_{\sigma_{b'},\sigma_b} \delta_{\sigma_{c'},\sigma_c} \end{aligned} \tag{A.56}$$

in terms of the symmetrized potentials $\tilde{V}_q = V_q + V_{-q}$.

Bibliography

M. Abramowitz and I. A. Stegun, *Handbook of Mathematical Functions: With Formulas, Graphs, and Mathematical Tables*. Dover Publications (1964).

C. Altimiras, H. le Sueur, U. Gennser, A. Anthore, A. Cavanna, D. Mailly, and F. Pierre, *Chargeless heat transport in the fractional quantum Hall regime*. arXiv:1202.6300 (2012).

C. Altimiras, H. le Sueur, U. Gennser, A. Cavanna, D. Mailly, and F. Pierre, *Non-equilibrium edge-channel spectroscopy in the integer quantum Hall regime*. Nature Physics **6**, 34 (2010a).

C. Altimiras, H. le Sueur, U. Gennser, A. Cavanna, D. Mailly, and F. Pierre, *Tuning Energy Relaxation along Quantum Hall Channels*. Physical Review Letters **105**, 226804 (2010b).

D. N. Aristov, *Luttinger liquids with curvature: Density correlations and Coulomb drag effect*. Physical Review B **76**, 085327 (2007).

O. M. Auslaender, H. Steinberg, A. Yacoby, Y. Tserkovnyak, B. I. Halperin, K. W. Baldwin, L. N. Pfeiffer, and K. W. West, *Spin-Charge Separation and Localization in One Dimension*. Science **308**, 88 (2005).

O. M. Auslaender, A. Yacoby, R. de Picciotto, K. W. Baldwin, L. N. Pfeiffer, and K. W. West, *Experimental Evidence for Resonant Tunneling in a Luttinger Liquid*. Physical Review Letters **84**, 1764 (2000).

O. M. Auslaender, A. Yacoby, R. de Picciotto, K. W. Baldwin, L. N. Pfeiffer, and K. W. West, *Tunneling Spectroscopy of the Elementary Excitations in a One-Dimensional Wire*. Science **295**, 825 (2002).

J. E. Avron, A. Elgart, G. M. Graf, and L. Sadun, *Optimal Quantum Pumps*. Physical Review Letters **87**, 236601 (2001).

D. A. Bagrets, I. V. Gornyi, A. Mirlin, and D. G. Polyakov, *Relaxation processes in a disordered Luttinger liquid*. Semiconductors **42**, 994 (2008).

D. A. Bagrets, I. V. Gornyi, and D. G. Polyakov, *Nonequilibrium kinetics of a disordered Luttinger liquid*. Physical Review B **80**, 113403 (2009).

G. Barak, L. N. Pfeiffer, K. W. West, B. I. Halperin, and A. Yacoby, *Spin reconstruction in quantum wires subject to a perpendicular magnetic field*. arXiv:1012.1845 (2010a).

G. Barak, H. Steinberg, L. N. Pfeiffer, K. W. West, L. I. Glazman, F. von Oppen, and A. Yacoby, *Interacting electrons in one dimension beyond the Luttinger-liquid limit*. Nature Physics **6**, 489 (2010b).

Y. Barlas, Y. N. Joglekar, and K. Yang, *Charge and spin reconstruction in quantum Hall strips*. Physical Review B **83**, 205307 (2011).

S. D. Bennett, J. Maassen, and A. A. Clerk, *Scattering Approach to Backaction in Coherent Nanoelectromechanical Systems*. Physical Review Letters **105**, 217206 (2010).

S. D. Bennett, J. Maassen, and A. A. Clerk, *Erratum: Scattering Approach to Backaction in Coherent Nanoelectromechanical Systems [Phys. Rev. Lett. 105, 217206 (2010)]*. Physical Review Letters **106**, 199902 (2011).

E. Berg, Y. Oreg, E. Kim, and F. von Oppen, *Fractional Charges on an Integer Quantum Hall Edge*. Physical Review Letters **102**, 236402 (2009).

M. V. Berry and J. M. Robbins, *Chaotic Classical and Half-Classical Adiabatic Reactions: Geometric Magnetism and Deterministic Friction*. Proceedings of the Royal Society of London. Series A: Mathematical and Physical Sciences **442**, 659 (1993).

A. Bid, N. Ofek, H. Inoue, M. Heiblum, C. L. Kane, V. Umansky, and D. Mahalu, *Observation of neutral modes in the fractional quantum Hall regime*. Nature **466**, 585 (2010).

Y. N. Y. Blanter, *Quantum Transport*. Cambridge University Press (2010).

M. Bockrath, D. H. Cobden, J. Lu, A. G. Rinzler, R. E. Smalley, L. Balents, and P. L. McEuen, *Luttinger-liquid behaviour in carbon nanotubes*. Nature **397**, 598 (1999).

N. Bode, S. Viola Kusminskiy, R. Egger, and F. von Oppen, *Scattering Theory of Current-Induced Forces in Mesoscopic Systems*. Physical Review Letters **107**, 036804 (2011).

N. Bode, S. Viola Kusminskiy, R. Egger, and F. von Oppen, *Current-induced forces in mesoscopic systems: A scattering matrix approach*. Beilstein Journal of Nanotechnology **3**, 144 (2012).

P. W. Brouwer, *Scattering approach to parametric pumping*. Physical Review B **58**, R10135 (1998).

M. Büttiker, *Scattering theory of current and intensity noise correlations in conductors and wave guides*. Physical Review B **46**, 12485 (1992).

A. M. Chang, L. N. Pfeiffer, and K. W. West, *Observation of Chiral Luttinger Behavior in Electron Tunneling into Fractional Quantum Hall Edges*. Physical Review Letters **77**, 2538 (1996).

Y. Chen, T. Dirks, G. Al-Zoubi, N. O. Birge, and N. Mason, *Nonequilibrium Tunneling Spectroscopy in Carbon Nanotubes*. Physical Review Letters **102**, 036804 (2009).

D. B. Chklovskii, B. I. Shklovskii, and L. I. Glazman, *Electrostatics of edge channels*. Physical Review B **46**, 4026 (1992).

H. G. Craighead, *Nanoelectromechanical Systems*. Science **290**, 1532 (2000).

S. Das and S. Rao, *Spin-Polarized Scanning-Tunneling Probe for Helical Luttinger Liquids*. Physical Review Letters **106**, 236403 (2011).

C. de C. Chamon and X. G. Wen, *Sharp and smooth boundaries of quantum Hall liquids*. Physical Review B **49**, 8227 (1994).

J. Dempsey, B. Y. Gelfand, and B. I. Halperin, *Electron-electron interactions and spontaneous spin polarization in quantum Hall edge states*. Physical Review Letters **70**, 3639 (1993).

V. V. Deshpande, M. Bockrath, L. I. Glazman, and A. Yacoby, *Electron liquids and solids in one dimension*. Nature **464**, 209 (2010).

E. V. Deviatov, A. Lorke, G. Biasiol, and L. Sorba, *Energy transfer along the reconstructed quantum Hall edge*. arXiv:1101.4006 (2011).

P. A. M. Dirac, *A theory of electrons and protons*. Proceedings of the Royal Society A: Mathematical, Physical and Engineering Sciences **126**, 360 (1930).

M. Dolev, Y. Gross, R. Sabo, I. Gurman, M. Heiblum, V. Umansky, and D. Mahalu, *Characterizing Neutral Modes of Fractional States in the Second Landau Level*. Physical Review Letters **107**, 036805 (2011).

O. Entin-Wohlman, A. Aharony, and Y. Levinson, *Adiabatic transport in nanostructures*. Physical Review B **65**, 195411 (2002).

R. Fazio, F. W. J. Hekking, and D. E. Khmelnitskii, *Anomalous Thermal Transport in Quantum Wires*. Physical Review Letters **80**, 5611 (1998).

M. Galperin, M. A. Ratner, and A. Nitzan, *Molecular transport junctions: vibrational effects*. Journal of Physics: Condensed Matter **19**, 103201 (2007).

B. Gelfand, J. Dempsey, and B. Halperin, *Effects of electron-electron interactions on the ground state of quantum Hall edge states*. Surface Science **305**, 166 (1994).

T. Giamarchi, *Quantum Physics in One Dimension*. Oxford University Press (2004).

G. Giuliani and G. Vignale, *Quantum Theory Of The Electron Liquid*. Cambridge University Press (2005).

I. S. Gradshteyn and I. M. Ryzhik, *Table of integrals, series, and products*. Elsevier/Academic Press, seventh edition (2007).

G. Granger, J. P. Eisenstein, and J. L. Reno, *Observation of Chiral Heat Transport in the Quantum Hall Regime*. Physical Review Letters **102**, 086803 (2009).

M. Grayson, D. C. Tsui, L. N. Pfeiffer, K. W. West, and A. M. Chang, *Continuum of Chiral Luttinger Liquids at the Fractional Quantum Hall Edge*. Physical Review Letters **80**, 1062 (1998).

E. Grosfeld and S. Das, *Probing the Neutral Edge Modes in Transport across a Point Contact via Thermal Effects in the Read-Rezayi Non-Abelian Quantum Hall States*. Physical Review Letters **102**, 106403 (2009).

D. B. Gutman, Y. Gefen, and A. D. Mirlin, *Tunneling spectroscopy of Luttinger-liquid structures far from equilibrium*. Physical Review B **80**, 045106 (2009).

D. B. Gutman, Y. Gefen, and A. D. Mirlin, *Bosonization of one-dimensional fermions out of equilibrium*. Physical Review B **81**, 085436 (2010a).

D. B. Gutman, Y. Gefen, and A. D. Mirlin, *Bosonization out of equilibrium*. Europhysics Letters **90**, 37003 (2010b).

F. D. M. Haldane, *'Luttinger liquid theory' of one-dimensional quantum fluids. I. Properties of the Luttinger model and their extension to the general 1D interacting spinless Fermi gas*. Journal of Physics C: Solid State Physics **14**, 2585 (1981).

B. I. Halperin, *Quantized Hall conductance, current-carrying edge states, and the existence of extended states in a two-dimensional disordered potential*. Physical Review B **25**, 2185 (1982).

A. Imambekov and L. I. Glazman, *Phenomenology of One-Dimensional Quantum Liquids Beyond the Low-Energy Limit*. Physical Review Letters **102**, 126405 (2009a).

A. Imambekov and L. I. Glazman, *Universal Theory of Nonlinear Luttinger Liquids*. Science **323**, 228 (2009b).

A. Imambekov, T. L. Schmidt, and L. I. Glazman, *One-Dimensional Quantum Liquids: Beyond the Luttinger Liquid Paradigm*. arXiv:1110.1374 (2011).

Y. Jompol, C. J. B. Ford, J. P. Griffiths, I. Farrer, G. A. C. Jones, D. Anderson, D. A. Ritchie, T. W. Silk, and A. J. Schofield, *Probing Spin-Charge Separation in a Tomonaga-Luttinger Liquid*. Science **325**, 597 (2009).

C. L. Kane and M. P. A. Fisher, *Thermal Transport in a Luttinger Liquid*. Physical Review Letters **76**, 3192 (1996).

C. L. Kane, M. P. A. Fisher, and J. Polchinski, *Randomness at the edge: Theory of quantum Hall transport at filling ν=2/3*. Physical Review Letters **72**, 4129 (1994).

T. Karzig, L. I. Glazman, and F. von Oppen, *Energy Relaxation and Thermalization of Hot Electrons in Quantum Wires*. Physical Review Letters **105**, 226407 (2010).

T. Karzig, A. Levchenko, L. I. Glazman, and F. von Oppen, *Relaxation and edge reconstruction in integer quantum Hall systems*. (to be published) (2012).

T. Karzig, G. Refael, L. I. Glazman, and F. von Oppen, *Energy Partitioning of Tunneling Currents into Luttinger Liquids*. Physical Review Letters **107**, 176403 (2011).

M. Khodas, M. Pustilnik, A. Kamenev, and L. I. Glazman, *Fermi-Luttinger liquid: Spectral function of interacting one-dimensional fermions*. Physical Review B **76**, 155402 (2007).

B. J. Kim, H. Koh, E. Rotenberg, S. Oh, H. Eisaki, N. Motoyama, S. Uchida, T. Tohyama, S. Maekawa, Z. Shen, and C. Kim, *Distinct spinon and holon dispersions in photoemission spectral functions from one-dimensional $SrCuO_2$*. Nature Physics **2**, 397 (2006).

C. Kim, A. Y. Matsuura, Z. Shen, N. Motoyama, H. Eisaki, S. Uchida, T. Tohyama, and S. Maekawa, *Observation of Spin-Charge Separation in One-Dimensional $SrCuO_2$*. Physical Review Letters **77**, 4054 (1996).

M. Kindermann and C. W. J. Beenakker, *Quantum theory of electromechanical noise and momentum transfer statistics*. Physical Review B **66**, 224106 (2002).

D. L. Kovrizhin and J. T. Chalker, *Equilibration of integer quantum Hall edge states*. Physical Review B **84**, 085105 (2011a).

D. L. Kovrizhin and J. T. Chalker, *Relaxation in driven integer quantum Hall edge states*. arXiv:1111.3914 (2011b).

L. D. Landau, *The Theory of a Fermi Liquid*. Soviet Physics JETP **3**, 920–925 (1957).

L. D. Landau and E. M. Lifshitz, *Quantum Mechanics: Non-Relativistic Theory*. Pergamon Press (1977).

R. Landauer, *Spatial Variation of Currents and Fields Due to Localized Scatterers in Metallic Conduction*. IBM Journal of Research and Development **1**, 223 (1957).

R. Landauer, *Electrical resistance of disordered one-dimensional lattices*. Philosophical Magazine **21**, 863 (1970).

B. Lassagne, Y. Tarakanov, J. Kinaret, D. Garcia-Sanchez, and A. Bachtold, *Coupling Mechanics to Charge Transport in Carbon Nanotube Mechanical Resonators*. Science **325**, 1107 (2009).

H. le Sueur, C. Altimiras, U. Gennser, A. Cavanna, D. Mailly, and F. Pierre, *Energy Relaxation in the Integer Quantum Hall Regime*. Physical Review Letters **105**, 056803 (2010).

S. Lee, S. Ryu, C. Nayak, and M. P. A. Fisher, *Particle-Hole Symmetry and the ν=5/2 Quantum Hall State*. Physical Review Letters **99**, 236807 (2007).

A. Levchenko, T. Micklitz, J. Rech, and K. A. Matveev, *Transport in partially equilibrated inhomogeneous quantum wires*. Physical Review B **82**, 115413 (2010).

A. Levchenko, T. Micklitz, Z. Ristivojevic, and K. A. Matveev, *Interaction effects on thermal transport in quantum wires*. Physical Review B **84**, 115447 (2011a).

A. Levchenko, Z. Ristivojevic, and T. Micklitz, *Interaction-induced corrections to conductance and thermopower in quantum wires*. Physical Review B **83**, 041303 (2011b).

M. Levin, B. I. Halperin, and B. Rosenow, *Particle-Hole Symmetry and the Pfaffian State*. Physical Review Letters **99**, 236806 (2007).

I. P. Levkivskyi and E. V. Sukhorukov, *Energy relaxation at quantum Hall edge*. Physical Review B **85**, 075309 (2012).

J.-T. Lü, M. Brandbyge, and P. Hedegåard, *Blowing the Fuse: Berry's Phase and Runaway Vibrations in Molecular Conductors*. Nano Letters **10**, 1657 (2010).

A. Lunde, K. Flensberg, and L. I. Glazman, *Three-particle collisions in quantum wires: Corrections to thermopower and conductance*. Physical Review B **75**, 245418 (2007).

A. M. Lunde, S. E. Nigg, and M. Büttiker, *Interaction-induced edge channel equilibration*. Physical Review B **81**, 041311 (2010).

J. M. Luttinger, *An Exactly Soluble Model of a Many-Fermion System*. Journal of Mathematical Physics **4**, 1154 (1963).

D. L. Maslov and M. Stone, *Landauer conductance of Luttinger liquids with leads*. Physical Review B **52**, R5539 (1995).

D. C. Mattis and E. H. Lieb, *Exact Solution of a Many-Fermion System and Its Associated Boson Field*. Journal of Mathematical Physics **6**, 304 (1965).

P. A. Mello, N. Kumar, and N. K. Kumar, *Quantum transport in mesoscopic systems: complexity and statistical fluctuations : a maximum-entropy viewpoint*. Oxford University Press (2004).

T. Micklitz and A. Levchenko, *Thermal conductance and energy relaxation rate in quantum wires due to three-particle collisions*. arXiv:1005.0154 (2010).

T. Micklitz and A. Levchenko, *Thermalization of Nonequilibrium Electrons in Quantum Wires*. Physical Review Letters **106**, 196402 (2011).

T. Micklitz, J. Rech, and K. A. Matveev, *Transport properties of partially equilibrated quantum wires*. Physical Review B **81**, 115313 (2010).

M. V. Moskalets, *Scattering Matrix Approach to Non-Stationary Quantum Transport*. Imperial College Press (2011).

M. V. Moskalets and M. Büttiker, *Adiabatic quantum pump in the presence of external ac voltages*. Physical Review B **69**, 205316 (2004).

M. V. Moskalets and M. Büttiker, *Magnetic-field symmetry of pump currents of adiabatically driven mesoscopic structures*. Physical Review B **72**, 035324 (2005a).

M. V. Moskalets and M. Büttiker, *Magnetic-field symmetry of pump currents of adiabatically driven mesoscopic structures*. Physical Review B **72**, 035324 (2005b).

D. Mozyrsky, M. B. Hastings, and I. Martin, *Intermittent polaron dynamics: Born-Oppenheimer approximation out of equilibrium*. Physical Review B **73**, 035104 (2006).

R. G. Pereira, J. Sirker, J. Caux, R. Hagemans, J. M. Maillet, S. R. White, and I. Affleck, *Dynamical Spin Structure Factor for the Anisotropic Spin-1/2 Heisenberg Chain*. Physical Review Letters **96**, 257202 (2006).

R. G. Pereira, J. Sirker, J. Caux, R. Hagemans, J. M. Maillet, S. R. White, and I. Affleck, *Dynamical structure factor at small q for the XXZ spin-1/2 chain*. Journal of Statistical Mechanics: Theory and Experiment **2007**, P08022 (2007).

L. N. Pfeiffer, H. Stormer, K. Baldwin, K. West, A. Goni, A. Pinczuk, R. Ashoori, M. Dignam, and W. Wegscheider, *Cleaved edge overgrowth for quantum wire fabrication*. Journal of Crystal Growth **127**, 849 (1993).

K. Pham, M. Gabay, and P. Lederer, *Fractional excitations in the Luttinger liquid*. Physical Review B **61**, 16397 (2000).

F. Pistolesi, Y. M. Blanter, and I. Martin, *Self-consistent theory of molecular switching*. Physical Review B **78**, 085127 (2008).

V. V. Ponomarenko, *Renormalization of the one-dimensional conductance in the Luttinger-liquid model*. Physical Review B **52**, R8666 (1995).

R. E. Prange and S. M. Girvin, *The Quantum Hall effect*. Springer-Verlag (1987).

J. Rech and K. A. Matveev, *Resistivity of Inhomogeneous Quantum Wires*. Physical Review Letters **100**, 066407 (2008).

J. Rech, T. Micklitz, and K. Matveev, *Conductance of Fully Equilibrated Quantum Wires*. Physical Review Letters **102** (2009).

L. Rijkels and G. E. W. Bauer, *Hysteresis and defects of spin-polarized edge states in the integer quantum Hall regime*. Physical Review B **50**, 8629 (1994).

M. L. Roukes, *Nanoelectromechanical systems face the future*. Physics World **14**, 25 (2001).

A. V. Rozhkov, *Class of exactly soluble models of one-dimensional spinless fermions and its application to the Tomonaga-Luttinger Hamiltonian with nonlinear dispersion*. Physical Review B **74**, 245123 (2006).

I. Safi and H. J. Schulz, *Transport in an inhomogeneous interacting one-dimensional system*. Physical Review B **52**, R17040 (1995).

K. V. Samokhin, *Lifetime of excitations in a clean Luttinger liquid*. Journal of Physics: Condensed Matter **10**, L533 (1998).

S. D. Sarma and A. Pinczuk, *Perspectives in Quantum Hall Effects: Novel Quantum Liquids in Low-Dimensional Semiconductor Structures*. John Wiley & Sons (2008).

T. L. Schmidt, A. Imambekov, and L. I. Glazman, *Fate of 1D Spin-Charge Separation Away from Fermi Points*. Physical Review Letters **104**, 116403 (2010a).

T. L. Schmidt, A. Imambekov, and L. I. Glazman, *Spin-charge separation in one-dimensional fermion systems beyond Luttinger liquid theory*. Physical Review B **82**, 245104 (2010b).

P. Segovia, D. Purdie, M. Hengsberger, and Y. Baer, *Observation of spin and charge collective modes in one-dimensional metallic chains*. Nature **402**, 504 (1999).

O. A. Starykh, D. L. Maslov, W. Häusler, and L. I. Glazman, *Gapped Phases of Quantum Wires*. Lecture Notes in Physics **544**, 37 (2000).

G. A. Steele, A. K. Hüttel, B. Witkamp, M. Poot, H. B. Meerwaldt, L. P. Kouwenhoven, and H. S. J. van der Zant, *Strong Coupling Between Single-Electron Tunneling and Nanomechanical Motion*. Science **325**, 1103 (2009).

H. Steinberg, G. Barak, A. Yacoby, L. N. Pfeiffer, K. W. West, B. I. Halperin, and K. L. Hur, *Charge fractionalization in quantum wires*. Nature Physics **4**, 116 (2008).

T. H. Stoof and G. E. W. Bauer, *Density-functional theory of quantum wires and dots in a strong magnetic field*. Physical Review B **52**, 12143 (1995).

S. Takei, M. Milletari, and B. Rosenow, *Nonequilibrium electron spectroscopy of Luttinger liquids*. Physical Review B **82**, 041306 (2010).

S. Teber, *Bosonization approach to charge and spin dynamics of one-dimensional spin- 1/2 fermions with band curvature in a clean quantum wire*. Physical Review B **76**, 045309 (2007).

S. Tomonaga, *Remarks on Bloch's Method of Sound Waves applied to Many-Fermion Problems*. page 544 (1950).

Y. Tserkovnyak, B. I. Halperin, O. M. Auslaender, and A. Yacoby, *Interference and zero-bias anomaly in tunneling between Luttinger-liquid wires*. Physical Review B **68**, 125312 (2003).

K. v. Klitzing, G. Dorda, and M. Pepper, *New Method for High-Accuracy Determination of the Fine-Structure Constant Based on Quantized Hall Resistance*. Physical Review Letters **45**, 494 (1980).

J. Voit, *Charge-spin separation and the spectral properties of Luttinger liquids*. Physical Review B **47**, 6740 (1993).

J. Voit, *One-dimensional Fermi liquids*. Reports on Progress in Physics **58**, 977 (1995).

C. Wu, B. A. Bernevig, and S. Zhang, *Helical Liquid and the Edge of Quantum Spin Hall Systems*. Physical Review Letters **96**, 106401 (2006).

A. Yacoby, H. L. Stormer, N. S. Wingreen, L. N. Pfeiffer, K. W. Baldwin, and K. W. West, *Nonuniversal Conductance Quantization in Quantum Wires*. Physical Review Letters **77**, 4612 (1996).

Z. Yao, H. W. C. Postma, L. Balents, and C. Dekker, *Carbon nanotube intramolecular junctions*. Nature **402**, 273 (1999).

Acknowledgements

This thesis would not have been possible without the support of many people for which I am truly grateful.

First of all, I want to thank my PhD advisor Felix von Oppen. He showed me the conceptual beauty of condensed matter physics and was one of the main reasons why I entered this intriguing field. I especially want to thank him for his enduring council and guidance throughout the course of this thesis. In many valuable discussions I was fascinated by his intuitive way of thinking about physics. I am also grateful for the opportunity to participate in the „Low dimensional electron systems"- research program in Santa Barbara, which he offered me at the beginning of my thesis.

I also want to thank Piet Brouwer for co-refereeing my thesis and as director of the Dahlem Center of Complex Quantum Systems that provided a remarkable environment for the studies during my PhD. I especially appreciated his great insights during countless discussion in our „dice seminar" (journal club).

Furthermore, I want to thank my co-workers that contributed to the work of this thesis with their knowledge and valuable discussion. They are: Leonid Glazman (Yale), Gil Refael (Caltech), Alex Levchenko (Michigan), Florian Wendler (TU), Mark Thomas (FU), Silvia Viola Kusminskiy (FU), and Gergely Zaránd (Budapest). Moreover, I acknowledge many great discussions with Tobias Micklitz (FU), Falko Pientka (FU) and especially Niels Bode (FU) who was always willing to listen to all kinds of problems that I encountered during my studies.

I want to thank all members of the AG von Oppen and AG Brouwer and especially my officemates Silvia and Alexandra for their support and for making the last three years a great time inside and outside the physics department. Moreover, I want to thank Brigitte Odeh for administrative support.

I also acknowledge funding by Deutsche Forschungsgesellschaft under Schwerpunkt-programm 1243.

Last but not least I want to deeply thank my family and friends for their company and support which goes far beyond the last three years. I especially want to thank Fritzi for her love and understanding that carried me during my studies.

Publications

- *Energy Relaxation and Thermalization of Hot Electrons in Quantum Wires*,
  Torsten Karzig, Leonid I. Glazman, and Felix von Oppen,
  Physical Review Letters **105**, 226407 (2010).
- *Energy Partitioning of Tunneling Currents into Luttinger Liquids,*
  Torsten Karzig, Gil Refael, Leonid I. Glazman, and Felix von Oppen,
  Physical Review Letters **107**, 176403 (2011).
- *Relaxation and edge reconstruction in integer quantum Hall systems*,
  Torsten Karzig, Alex Levchenko, Leonid I. Glazman, and Felix von Oppen,
  arXiv:1206.0261.